CHALMERS
UNIVERSITY OF TECHNOLOGY

System-Level Architecture Definition and IWM Study for an Electrical Off-Road Emergency Vehicle Platform Prototype

REPORT

Master's thesis in Automotive Engineering

GERARD CABANA BATLLAURA

DEPARTMENT OF MATERIAL AND INDUSTRIAL SCIENCE
CHALMERS UNIVERSITY OF TECHNOLOGY

Gothenburg, Sweden 2026
www.chalmers.se

MASTER'S THESIS IMSX30

System-Level Architecture Definition and IWM Study for an Electrical Off-Road Emergency Vehicle Platform Prototype

GERARD CABANA BATLLAURA

CHALMERS
UNIVERSITY OF TECHNOLOGY

Department of Material and Industrial Science
Specialization in Automotive Engineering
Chalmers University of Technology
Gothenburg, Sweden 2026

System-Level Architecture Definition and IWM Study for an Electrical Off-Road Emergency Vehicle Platform Prototype

Supervisor: Dag Henrik Bergsjö

Master's Thesis 2026
Department of Material and Industrial Science
Chalmers University of Technology
SE-412 96 Gothenburg
Telephone +34 677 112 429

System-Level Architecture Definition and IWM Study for an Electrical Off-Road Emergency Vehicle Platform Prototype

GERARD CABANA BATLLAURA
Department of Material and Industrial Science
Chalmers University of Technology

Abstract

The focus in this work is to identify an early-stage development architecture for an electric off-road vehicle, specifically for the use of emergency and defensive forces. An IWM propulsion system for this vehicle would also be a prospective option for this type of vehicle.

To start with a benchmarking with similar vehicles to provide realistic design parameters and architectural constraints. Based on this evaluation, I developed a concept around the automobile and the wheel system. The study is complemented by simplified analytical calculations and numerical methods such as structural, CFD, and thermal.

The results suggest major limitations of the IWM concept in this case. These issues mainly stem from tight packaging space, high torque demands, and a lower cooling capacity compared to conventional systems.

Based on this evaluation, a distributed electric drive architecture using multiple outboard motors is a more effective solution. This work establishes a solid architectural baseline and provides the data needed for early decision-making in future vehicle development.

Acknowledgements

I would like to express my sincere gratitude to everyone who has supported and helped me, both directly and indirectly, throughout this master's thesis.

I am especially thankful to my supervisor, Dag Henrik, for giving me the opportunity to be part of such an interesting project and for allowing me to work alongside other students with the same motivation and willingness to learn.

I would also like to thank all the members of the project team for their constant willingness to collaborate, help, and create a friendly working environment, which has made a significant difference and supported me throughout the project.

Finally, I would like to thank Shenade for the support and guidance provided on technical and analytical aspects. Your help has been essential, and this thesis would not have been the same without it.

CONTENTS

LIST OF FIGURES

LIST OF TABLES

ACRONYMS

IWM	In-Wheel Motor
CFD	Computational Fluid Dynamics
CAD	Computer-Aided Design
FEA	Finite Element Analysis
EV	Electric Vehicle
GVW	Gross Vehicle Weight
CG	Centre of Gravity
FR	Total resistive force (N)
Rdyn	Dynamic wheel radius (m)
Frr	Rolling resistance force (N)
Fd	Aerodynamic drag force (N)
Fhc	Hill-climbing force (N)
Fi	Inertial force (N)
T	Wheel torque (Nm)
Nm	Newton meter
kW	Kilowatt
UGV	Unmanned Ground Vehicle

1. INTRODUCTION

1.1 Context

The automotive industry continues on as a cornerstone of the global economy, contributing to approximately 7% of Europe's overall GDP, according to recent surveys from 2024 and 2025 [1]. Even with its rather recent history, with Karl Benz's first gasoline vehicle invented in only 1886 [2], the automotive sector has seen many changes. These include strengthening the internal combustion engine, which has gone on to find commonplace on assembly lines, and later including electronics and digital systems [3].

At present, the sector is undergoing one of the most complex transitions in its history. It is not facing a single challenge, but rather multiple simultaneous processes of change, in a phase defined by the integration of software, vehicle electrification, restructuring of supply chains, and implementation of strict climate policies [4].

Figure 1 clearly shows that electrification, which has gone on to become a major trend in the sector, and has turned into a core strategic necessity for maintaining a competitive edge, as well as following environmental rules. As a result, regulation EU 2019/631, requires manufacturers to reduce CO2 emissions by at least 55% by 2030, compared to 2021 [5]. Incorporating electric vehicles into business production lines, have been found to be one of the main ways to meet these regulations, and to avoid financial penalties.

As a result, the challenges arising from this transition significantly raise barriers to entry in the sector, particularly in a context shaped by growing international competition. Notably, Chinese manufacturers have made a strong entry, with their sales volumes in Europe increasing by 44% year on year in 2025 [6].

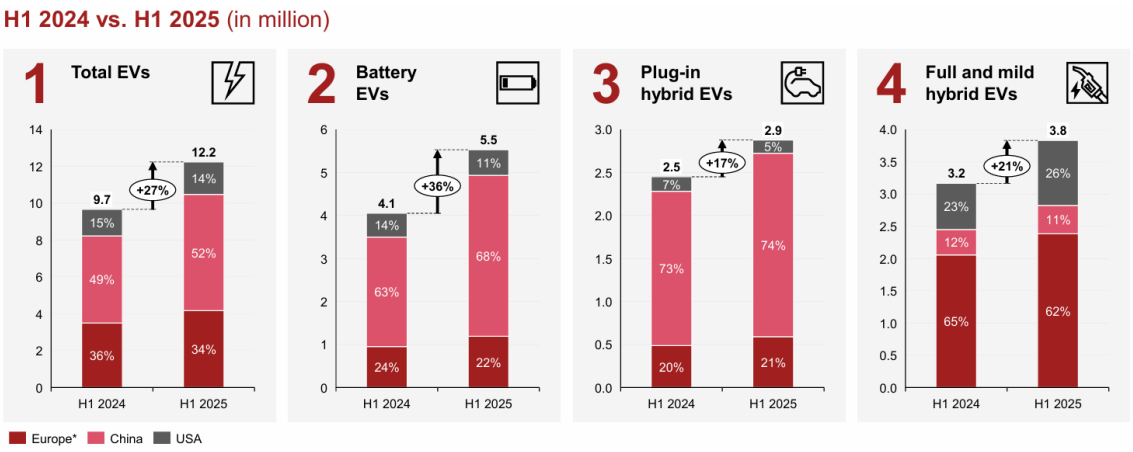

Fig. 1. Electric vehicles growth H1 2024 vs H1 2025 [69]

1.2 Project Motivation

While section 1.1 highlights the significant complexities and barriers for new entries into the automotive industry, another sector, for many reasons, is currently experiencing significant demand for monetary investments, innovation, and continuous development; the defence industry. This sector finds itself at a time when global monetary involvement is required. A worldwide pattern points to moving towards a time of economic, political and safety falling apart, reminiscent of the Cold War era. Escalating global tensions between Russia's push into Ukraine, persistent instability across the Middle East, and growing friction between China and the United States have all collectively caused a significant surge in global defence spending, seen in an 8.1% rise during 2024, ending up at a record amount of $2 trillion [7] .

That is why the defence industry is also driving the development of new vehicles and systems, and is beginning to initiate, whenever possible, real energy transition. 'Electrification is seen … as an extension of the renewed modernisation of the Department', and the US Army had announced, via its Electric Light Reconnaissance Vehicle plan, the inclusion of 'hybrid tactical vehicles by 2035 and fully electric versions by 2050,' establishing a clear, official plan for the electrification of ground platforms, according to a report by the RAND Corporation [8]. This is driven both by the global and regional trends associated with global demand for military vehicles; as of 2023, the global military vehicle electrification market was worth USD 4.02 billion and is anticipated to exceed USD 13.13 billion by 2032 at a compound annual growth rate (CAGR) of 14.1% [9]. That is, in part because there is a growing need for ground vehicles which are more efficient, quieter and less dependent on complex logistics. Operationally, National Defense Magazine states that the United States Army is actively prototyping electric and hybrid vehicles and expects that hybrid tactical vehicles will be launched by the 2030s and fully electric vehicles by 2040 [10]. Meanwhile, the United States Marine Corps takes the longer view, where energy infrastructure is still a factor in their deployment contexts.

Collectively, these inputs indicate that ground electrification is occurring, in part, for tactical (reduced thermal and acoustic), logistical (fewer fuel convoys), and strategic (greater energy resilience) reasons. This modernised shift toward electric military platforms is closely linked to the increasing uptake of autonomous mobility. Just as unmanned aerial systems have increased significantly (see Figure 2 of Military Drone Transfers), armed forces are beginning to adopt autonomous and electrified ground vehicles, integrating sensors, state-of-the-art energy storage systems, and mobile microgrids to aid in distributed and more resilient operations.

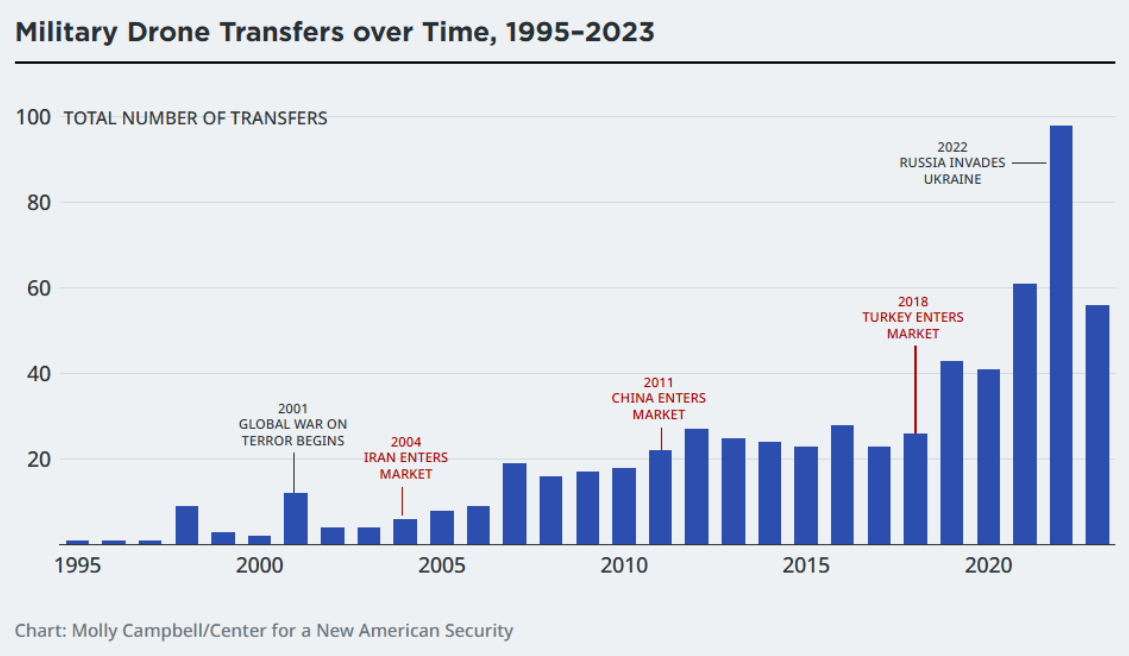

Fig. 2. Military Drone transfer 1995-2023 [70]

Based on the analysis carried out, it becomes clear that while the automotive sector presents high barriers to entry due to its level of maturity and intense competition, the defense domain is currently undergoing a phase of technological expansion driven by investment, electrification, and the development of autonomous systems. For this reason, this project focuses on this sector, using as a case study the conceptual approach of Eira Systems AB and the design of an off-road autonomous vehicle. This approach makes it possible to assess technological feasibility in an environment where there is growing demand for innovation, and where trends in electrified and autonomous mobility still offer significant room for development.

1.3 Thesis Overview

This thesis is centred on the early concept development of an off-road, self-driving electric vehicle prototype designed to be adaptable for emergency and defence purposes. The project is undertaken by a broader multidisciplinary university initiative bringing together students from various engineering fields, and there is, at present, no defined mechanical architecture or validated system layout that exists for the proposed system. The primary goal is to build a coherent, system-level mechanical and structural architecture that can be relied on as a technical base for future implementation. This will be facilitated by analysing comparative vehicles under benchmarking analysis, specifying the geometric and dynamic parameters and sizing of initial design of key subsystems, including chassis layout, wheels, braking elements, and rear axle configuration. Such simplified analytical calculations, which are based on vehicle dynamics and drivetrain methodologies, will be adopted wherever suitable, with supportive engineering assumptions that are reasonable. A simple 3D model of the vehicle layout will be put together, not for in-depth validation, but for visualisation of the design. Furthermore, the study will evaluate the possibility of implementing in wheel motor propulsion technologies in the class of vehicles. It will also involve a calculation of the necessary wheel torque under severe operating conditions, unsprung mass effects analysis, and qualitative airflow characteristics with comparison between

conventional and integrated wheel concepts. Ultimately, the thesis seeks to provide a technically supported architectural baseline for the project, while offering engineering expertise on technology selection, to support informed decision making, as the project goes towards later design stages.

1.4 Problem Statement

Early stage development of the autonomous off road electric vehicles is still heavily technically uncertain, as the full architecture of the system and its mechanical construction is undecided. As part of the multidisciplinary university initiative, the prototype remains in the conceptual phase, due to the mission profile not fully consolidated yet, system requirements only partially defined, and no validated structural or propulsion configuration.

This lack of definition can result in design choices that do not fully match up, as work gets done at much later stages, thus the risk of inefficient designs, redesigns, or problems involving subsystem integration. Furthermore, the complexity of the issues is brought forward by potential solutions, such as in-wheel motor propulsion. While these systems can have benefits in terms of packaging, efficiency, or controllability, their acceptability for demanding off-road applications remains unclear.

For a practical basis of such a concept, they should be examined with respect to the required wheel torque, effects on the unsprung mass, thermal behaviour, as well as integration limitations. To solve this, a clear mechanical system framework must be determined, which is facilitated through initial sizing of designs and an intuitive analytical evaluation. This is the focus and main technical problem of this thesis: to minimise early uncertainty and to build a solid engineering basis for future design development.

1.5 Objectives

This thesis will provide a cohesive system-level mechanical architecture for an autonomous off-road electric vehicle concept and assess the possibilities of introducing in-wheel motor propulsion. As the project is exploratory and in its early stages, the detailed objectives are outlined as follows:

1- Define the mission context of operation and establish initial engineering objectives at a systems level.
2- Benchmark similar vehicle platforms to obtain geometric, mass, and mobility parameter ranges.
3- Draw out an initial architectural envelope and determine key mechanical subsystems for vehicle-level integration.
4- Conduct preliminary sizing and conceptual design of the base wheel-end frame arrangement (tires, brakes, and components), using simple CAD layout illustration.

5- The feasibility of integrating in-wheel motors in the system is assessed using:

5.1 Motor torque requirement calculation of wheels.

5.2 Unsprung mass comparison.

5.3 Qualitative airflow assessments.

5.4 Thermal behaviour analysis during braking.

6- Create an architectural concept baseline ready in advance for subsequent system-based implementation for a conceptual design to drive additional system-level development.

Secondary goals should be considered if project time permits; include:

7- Model and visualise the extended chassis layout of structure and subsystem assembly for the extended chassis and design in general.

This prioritisation reflects intent to priorities architectural definition and propulsion feasibility assessment as main engineering contributions of the thesis, however, it acknowledges that early-stage conceptual development inevitably needs the flexibility of iterative modification to accommodate new understandings.

2. CONCEPTUAL DESIGN AND VEHICLE ARCHITECTURE FRAMEWORK

2.1 Product Development Processes

” Each great product is a product of an idea, but not every idea is a great product.” That’s where the product development process comes in. This approach transforms raw concepts into market-ready solutions [11].
Product development is a complex process that shapes a company’s financial success. The cross functional work with marketing, design, and manufacturing must be closely coordinated in order to meet customer satisfaction and ensure profitability. the process is complex due to several factors, including product quality, cost development, time, expense, and the capabilities that the product will build, and must collectively be managed, and assess the overall performance of a team or an organisation. At its core, the product development process is a structured sequence of activities that takes market opportunities and converts them into commercial products.
While there are intellectual or organizational dimensions to a lot of these, a well laid out process delivers certain clear advantages as it provides quality by setting out predefined stages and checkpoints, which allows for cross functional coordination, time to plan a milestone and timeline, supports project progress, and develops the system for continuous improvement [12].

This process is typically scaffolded into stages ranging from conception and concept ideation through to detailed design, production preparation, and to final launch (see Fig 3). Throughout these activities, the team lowers uncertainty, reinforces core functions, and gradually converges

toward a solution that is both technically and commercially viable. Essentially, product development is a process of gathering information, decision making, mitigating potential risk and ultimately, producing something that can be manufactured for a given purpose and be accepted in the market.

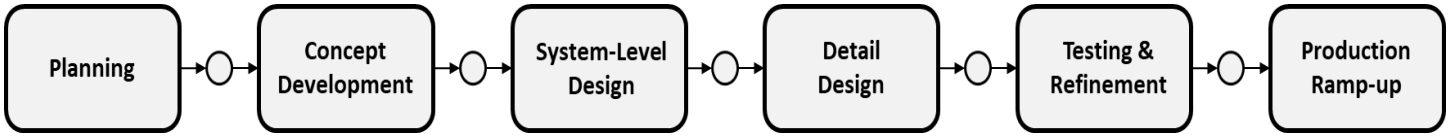

Fig. 3. The product development process [12]

When applied to the automotive industry, particularly to vehicles, these concepts highlight their complex nature and interconnected systems. Vehicles form part of a broader automotive ecosystem, shaped by technological shifts such as digitalisation, autonomy, and electrification. As a result, development projects are becoming increasingly complex, while also being expected to be delivered faster and at a lower cost [13].

Automotive product development is, therefore, a structured but highly complex process that transforms abstract concepts into operational vehicles. Systems engineering is critical for bringing mechanical, electrical, and software subsystems together within the vehicle structure, resulting in the coordination of several stakeholders (e.g., design, engineering, supply chain, and regulatory functions), which becomes one of the most challenging aspects of the developmental process [14].

Such complexity emphasises the importance of having a clearly articulated system architecture in the initial design phases. The product development in early phases is essential as it determines how the system as a whole, develops, because foundational structure and main functional decisions appear at conceptual design activities [12]. The significance of these concepts is also evident in industrial conceptual development frameworks like ISO 26262, which explicitly distinguishes the concept and system definition phases from later development stages, highlighting their relevance in risk identification and architectural planning [15].

Decisions made during these early stages have a strong influence on how the product evolves throughout its development lifecycle. It is commonly estimated that more than 80% of a product's cost is effectively committed during the initial design phases, despite the limited information available at that stage [16]. Moreover, early architectural choices strongly influence system behaviour and subsequent design flexibility, as the product structure and subsystem interactions begin to take shape during the conceptual definition phase. Similarly, these phases are characterised by high uncertainty due to incomplete information, evolving requirements, and the exploratory nature of concept generation, making structured decision making essential to guide development [12].

2.2 Concept Development and System-Level Design

The product development process is the sequence of steps a company uses to conceive, design, and bring a product to market [12]. It can be understood as the process of identifying needs and challenges, then generating, testing, and refining ideas to address them typically through a

product, but also through a service or strategy [17]. During the concept development phase, the needs of the target market are identified, alternative product ideas are generated and evaluated, and one or more concepts are selected for further development. A concept is understood as a description of a product's form, function, and features, and is typically accompanied by a set of specifications and a competitive analysis. [12]. Figures 4 and 5 illustrate the steps of the development process, with Figure 4 presenting the main, high-level groups, and Figure 5 providing a more detailed view.

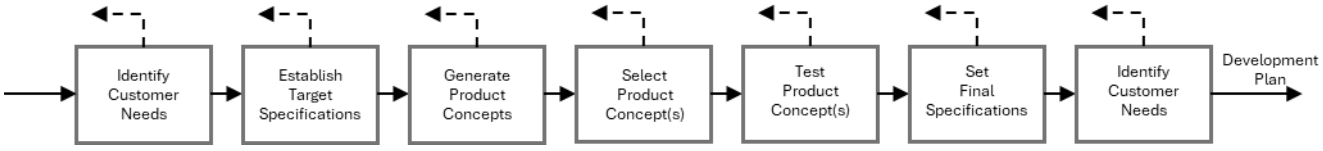

Fig. 4. Front-end activities comprising the concept development phase [12]

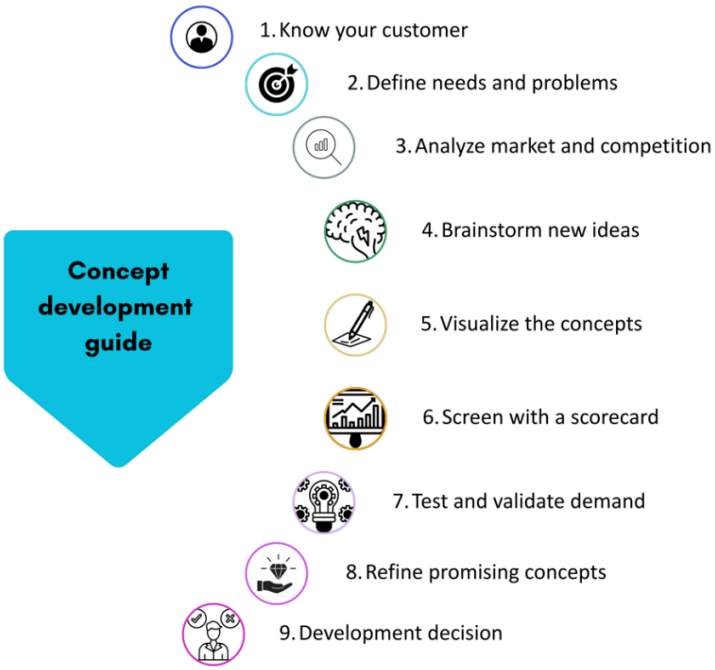

Fig. 5. 9-step concept development process (adapted from [17])

Concept development typically follows one of two broad approaches to innovation: one being market pull, and the other being the technology push. Innovation with technology is driven by the availability of a new technological capability that firms then need to seek out appropriate applications and markets for its use. In this case, the technology is determining the course of development, as the product concept is being built around its integration. The product development process itself can still be followed; however, it usually starts by matching available technology to opportunities within the market, and carries a relatively higher risk if the technology does not provide clear competitive advantages and or real user needs [12].

Market pull development is based on identifying user requirements or market requirements in which the engineering team must create or modify technologies that solve these needs. Specifically, technology push seeks solutions that a technology itself could address, and market-

pull seeks solutions to an existing need [18] . The touchscreen smartphone interface is a classic example of technology push innovation. Although there was no prior interest or demand for it, it completely revolutionised the mobile phone industry.
On the other hand, the shift from analogue to digital cameras reflects market pull logic; the consumer's market demands on smartphones are more compact and immediate in image feedback, which is the basis of technological innovation [18].
From a general innovation point of view, market pull strategies are motivated by customer insights and market trends, which tend to reduce uncertainty and better align demand with consumer needs. Technology push innovation comes from new scientific and engineering discoveries and can result in original product introductions that do not come with immediate market acceptance, resulting in increased uncertainty, but potentially leading to more disruption. To be able to optimise the results of such development [19], organisations usually blend both perspectives to match technological capability within the market opportunity. This thesis, therefore, adopts a market pull lens, where an automotive concept derives from the critical needs of defence and emergency mobility rather than new enabling technologies.

System-level design is another key aspect within concept development, as it bridges the gap between conceptual solutions into structure engineering architectures. This stage of the design phase includes defining the product architecture, decomposing the product into subsystems and components, and performing preliminary design of key elements. Initial considerations regarding production and final assembly are also typically addressed at this stage. The outputs commonly include a geometric layout of the product, functional specifications for each subsystem, and an initial process flow representation for assembly activities [12] .

As illustrated in Figure 6, system-level design represents a central step in the development of complex engineered systems, which aligns with the context of this thesis. Vehicles can be considered highly complex systems composed of interacting subsystems before detailed design can proceed.

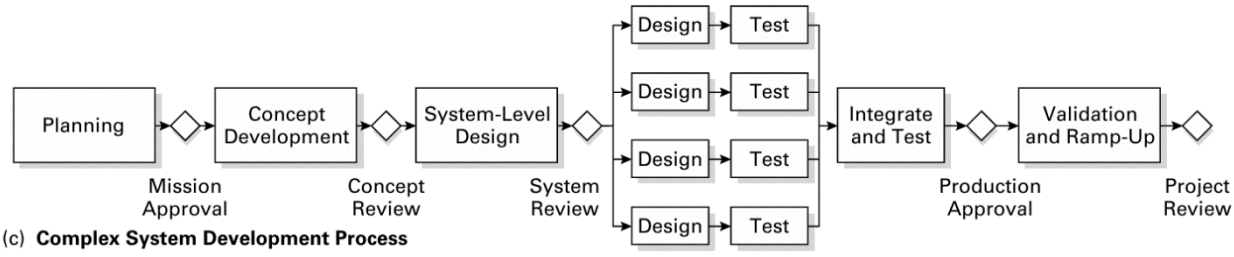

Fig. 6. Complex System Development Process [12]

Within a larger systems engineering context, system design is the practice of designing an architecture, modules, components, and interfaces of a system to help you deliver what you need for a system to get what you want. This phase will also set the stage for development and testing by conceptualizing and translating user requirements into an integrated technical blueprint of what a user needs. Intersections among the system components interactivity is particularly critical to know, as it is because it allows the purposes and constraints to be recognized and applied in a collaborative manner among different branches. Hence, system-level design is inherently interdisciplinary and fundamental in the design of software systems as the ultimate goal; this is in order for an overall architecture to be consistent, scalable, and congruent with functional expectations [20].

One other result of this system-level design process is the overall product architecture to be unified by the identification of subsystem interactions and structural organization. The functional components are then represented from one and the same physical elements as those, and the interfaces between subsystems are determined, enabling coordination in an app development process and also to remain compatible as we progress through the design [12]. Design for systems can be seen as the definition of the architecture, the components, the modules, the interfaces, etc., to provide a technical guide towards the implementations and the integration [21]. Since more complex engineered systems are complex and usually contain multiple subsystems and technologies, strict control over their boundaries and interactions is required to ensure overall functionality and control system complexity [22].

As a general rule of thumb, interdependencies arising from subsystem interfaces imply that design changes can propagate over a given system which supports the need for explicit interface definition and architectural coordination within early stages of development [22]. Indeed, system architecture is both a logical relation between the functional elements and their spatial ordering in the physical reality to provide links between ideas of a structure and geometric layout. At the same time, initial layouts and parameter estimations map functional structures into location and let us evaluate (and further improve) architecture before the detailed plans take shape [12].

Given that there could be myriad architectural alternatives, the system-level design must by definition consider tradeoff analysis between alternative aims, like performance and cost, schedule, reliability, and integration constraints. Trade-off studies are an essential tool that allows decision-making at multiple levels across the system lifecycle [23], as they facilitate structured comparative comparisons of alternatives and evaluation of system-level impacts. We see such alternatives as combinations of related subsystems that form their own systems, where the choice of design has a tangible effect on the system as a whole and how it develops. Exploring trade-offs allows engineers to understand the relations between requirements, design decisions, and impacts, thus laying a framework for future engineering work with complex products such as vehicles [23].

As for system-level design in early project phases, another characteristic is the uncertainty that is there. At this stage, very little detail in terms of behaviour, technical feasibility or performance outcomes for subsystems is generally known, rendering models highly abstract and unable to provide comprehensive detail about the system, particularly within architectural configurations. Reframing the design process as such yields an intrinsically iterative process where the parameters are evaluated, refined, and iteratively narrowed with subsequent iteration and evaluation [24]. In fact, it is important to recognize and address this uncertainty to inform pragmatic development decisions during difficult projects, like vehicles, where inter-system interactions play a significant part in the overall performance. This situation captures the essence of the current research project which consists of designing a new vehicle system early in its development, i.e., without a design baseline in place. The resultant work is a matter of dealing with uncertainty and limited data availability, and involving informed engineering assumptions along the architectural definition.

2.3 Product Architecture

Product architecture refers to the way in which the functional elements of a product are assigned to its physical building blocks and how these blocks interact through defined interfaces. A product

can be understood both in functional terms, referring to the components and assemblies implementing those functions. The architecture represents the structural scheme linking these perspectives by organising components into major grouping and defining their interactions, enabling coordinated development across teams and subsystems [12].

From a broader industry perspective, product architecture describes the high-level structure of a product and how its parts relate to one another to deliver overall functionality [25]. Importantly, this concept differs from detailed physical design or geometric layout. While layout focuses on dimensions, positioning, and physical embodiment, architecture captures the logical organisation and relationships between system elements providing a conceptual framework that guides subsequent design decisions rather than specific exact implementation [26]. As such, architectural definition precedes and informs detailed design activities by establishing how the system is decomposed and structured at the higher level of abstraction.

The evolution of product architecture can be linked to the broader technological maturation process illustrated in Figure 7, where early development stages are characterised by exploration and architectural uncertainty, followed by the emergence of dominant design configurations as products mature. This transition provides context for understanding how architectural structuring and modularisation decisions develop over time.

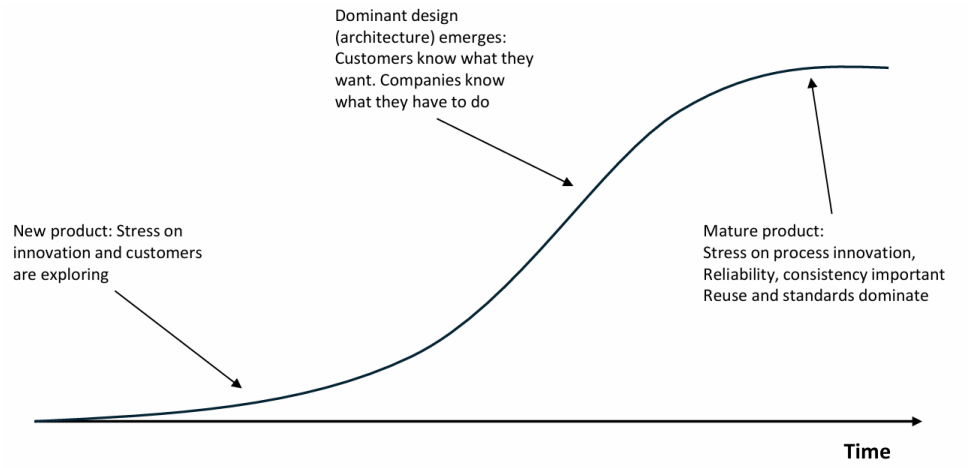

Fig. 7. Architecture and the "S-curve" [71]

The most notable distinction in product architecture typology is in regard to its modularity, which is generally categorised into modular and integral architecture [27]. Modularity is not an absolute feature, most types of products have mixed levels of modularity or integrality depending on the degree to which functionality of their design is distributed to existing physical constructions. In the Modular architecture, there are chunks with only one or a few functional elements and they interact using a simple, defined interface; for these reasons, one of the factors that determines whether or not an element of the system can be designed, changed or reworked relatively independently of the overall system, without the need for large-scale redesign. This separation supports flexibility, standardisation, and interchangeability, as well as adaptability, maintenance, and scalable product development [12] .

On the other hand, an integral architecture aggregates functional realization in a number of pieces or unites multiple pieces to support certain functionalities, with tightly matched interactions and strong interdependence between multiple components. Although such integration may optimise performance, efficiency, packaging or material usage, it can reduce flexibility, with changes to one element potentially requiring more extensive system redesign and thus making maintenance or lifecycle adaptation more complex [28]. Comparative studies in automotive modularity also reveal that modular architectures value interface standardisation and organisational-level design flexibility, whereas integral architectures prioritise technical optimisation and system-level performance integration [29].

The modular architectures can be grouped as slot, bus, and sectional type, each in reference to the interface organisation structure yet based upon the fundamental principle of one-to-one functional mapping and well-defined interactions [12]. These distinctions further support the impact architectural decisions have on system behaviour, scalability, and construction plans, which reiterates their importance for early design stages.

Product architecture is an early design decision that goes beyond simply defining the structure of a system and has long-term implications for system development. Architectural decisions affect manufacturability, product variety, supply chain organisation, and the versatility in design evolution and modification [12]. Architecture determines how functions are distributed and how subsystems interact, and, as such, it constrains downstream decisions at design, testing, and integration levels. Therefore, other architectural designs will frequently have to be benchmarked against trade-offs in terms of performance, flexibility, cost and difficulty of development. This value is further emphasized in the present literature of architectural decision-making practices where early comparison among architectural choices is proved to influence technical and development results, reiterating the importance of structured assessment at concept stages [30]. In these early-stage, sparsely supported projects, architectural assumptions lead ongoing engineering and, once set, architectural structures persist because they dictate interfaces and component dependencies, thus the sooner that systems can be chosen based on architectural knowledge the more expensive and time consuming design will be when new systems are re-designed in the downstream. Vehicle design is a particularly constrained example of product architecture because subsystems share a strong coupling. With packaging constraints, the load paths, thermal behaviour and placement of elements, drivetrain, suspension and structural design are influenced directly on one another making subsystem independent development impossible [12].

Because of this interdependence, the introduction of new technologies (such as electrification, autonomous sensing or wheel-integrated propulsion) influences the entire vehicle layout rather than the components, hence architectural definition becomes a decisive tool in the acceleration process of innovation in automotive systems [31], [32].

Therefore, the suitability of a vehicle architecture depends heavily on the operational environment and mission profile, which must be understood before detailed design choices can be made.

2.4 Off-Road and Military Emergency Vehicle Requirements

Ground transport platforms used in emergency and military contexts operate under fundamentally different conditions to those experienced by conventional passenger vehicles. According to military evacuation doctrine, casualty transport is a time-critical activity that is often performed

in uncertain and potentially hostile environments. In such conditions, accessibility and survivability take precedence over comfort or efficiency [33]. However, recent operational reports from modern conflicts suggest that the conditions encountered are even more challenging: evacuation often takes place in areas with uneven terrain, limited infrastructure, and constant surveillance. This forces the use of any available vehicle rather than specialised ambulances, provided they are prepared for such conditions [34]. Consequently, such vehicles must be understood not as conventional transport products, but as elements embedded within a broader operational system where environmental and tactical factors directly influence the definition of the engineering problem and the resulting design requirements.

As illustrated in Figure 8, evacuation is often carried out using any available vehicle capable of reaching the casualty location, rather than a dedicated medical platform. This prioritises accessibility and mobility over optimised medical transport.

Fig. 8. Casualty evacuation using a non-specialized off-road vehicle near the front line in Ukraine. Source: (Yasuyoshi Chiba AFP / Getty Images (2023))

Following these operational reasons, vehicles for highly demanding environments will not match the performance of the ordinary road vehicle. Instead of comfort, efficiency or top speed, military and emergency vehicles are usually defined with the mobility indicators gained from the performance of operational capability and therefore evaluated on a performance basis so that the outcome in hostile conditions with regard to military/emergency response is the functional performance of the vehicle as much or more than mobility performance. In other words, their vehicle sizes do not really depend much on maximum velocity and installed power but solely on their ability to traverse challenging situations.

The most commonly used metrics in literature and technical specifications can be grouped into three categories, namely negotiation of the terrain to navigate the ground, handling of the obstacles by an object on the ground of vehicle and traction of the engine, and the endurance (the ability to operate and survive) of an instrument. Table 1 summarizes these different categories of metrics and makes a few general observations.

TERRAIN NEGOTIATION CAPABILITY	VEHICLE GROUND INTERACTION	OPERATIONAL USABILITY
Gradeability	Ground pressure	Manoeuvrability
Step climbing	Vehicle mass	Turning radius

trench/gap crossing	Power-to-weight ratio	Braking distance
Fording depth	Tire contact patch	Operational range
Ground clearance		
Lateral stability (side slope)		

Table 1. Mobility performance metric groups used for operational vehicle characterization

Figures 9 and 10 illustrate, respectively, an example of contact area measurement used in mobility characterization and typical technical data describing terrain negotiation capabilities in comparable vehicles.

Fig. 9. Area used in Canadian mobility characterization [72]

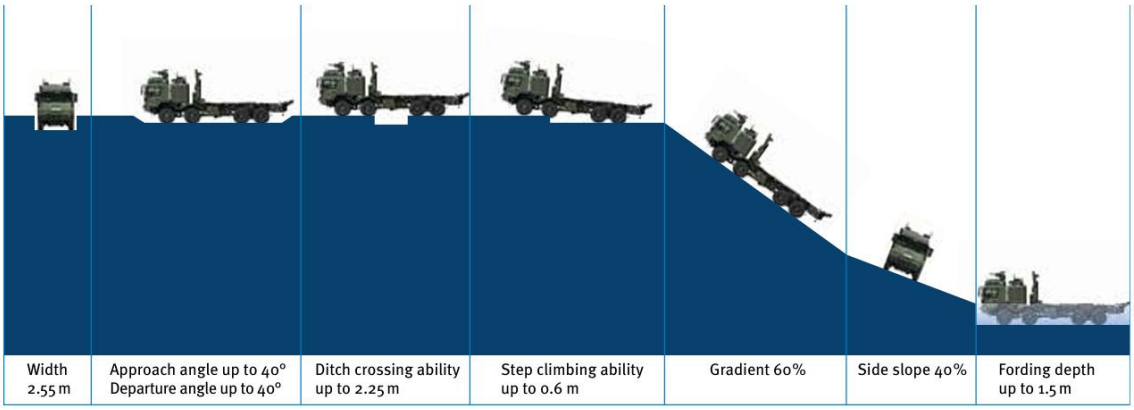

Fig. 10. Example of technical data on terrain-negotiation capabilities for the Rheinmetall MAN HX series [73]

These parameters play a fundamental role in defining the operational capability of such platforms.

For this reason, Chapter 4 of this work includes a benchmarking study of comparable vehicles in order to establish realistic parameter ranges and preliminary architectural constraints for the proposed prototype.

Modern operational environments impose constraints that go beyond pure mobility performance. Ground vehicles operating near conflict areas must move under constant surveillance threat, including aerial observation and indirect fire risk, as observed in recent field evacuation experiences in Ukraine [34] . This exposure to detection and hostile engagement limits the possibility of remaining stationary and forces continuous repositioning during missions.

Consequently, mobility becomes directly linked to survivability rather than only to transport efficiency [35].

Additionally, operational conditions are inherently uncertain. Terrain type, slope and soil consistency may change continuously, which directly affects vehicle mobility performance in off-road environments [36]. At the same time, payload mass varies depending on transported personnel and equipment, and military mobility standards therefore require vehicles to operate effectively across multiple loading conditions [37]. As a result, vehicles cannot be designed for a single operating point but must maintain functionality across a wide range of loads and ground conditions, requiring high low-speed torque availability, robust suspension behaviour and tolerance to traction variability.

Beyond mobility, detectability becomes a design driver. Tactical platforms aim to reduce acoustic and thermal signatures to avoid identification by hostile sensors, which has motivated increasing interest in electrified propulsion and integrated drivetrains. In hybrid and electric military prototypes tested by the U.S. Army's Rapid Capabilities and Critical Technologies Office, silent mobility "silent watch" capability are highlighted as critical advantages, enabling vehicles to move and operate with reduced engine noise in tactical scenarios [38]. Such characteristics not only decrease the risk of detection but also support reduced fuel consumption and greater electrical power availability on-board.

Finally, the rise of the remote and unmanned ground-sector system aims to decrease staff exposure and provides a compelling case for more reliable autonomous and tele-operated vehicles operating in volatile conditions (UGV logistics and evacuation research). The anticipated expansion of the military vehicle sector with respect to figure 11 is projected to reach 2x the size of the market size from today to 2031.

This forecast also accounts for military electric vehicles, which are also growing significantly. These operational factors directly translate to engineering requirements: high reliability under continuous operation, elevated torque at low speed, tolerance to mass variability, controlled thermal dissipation, and architectures compatible with autonomous operation.

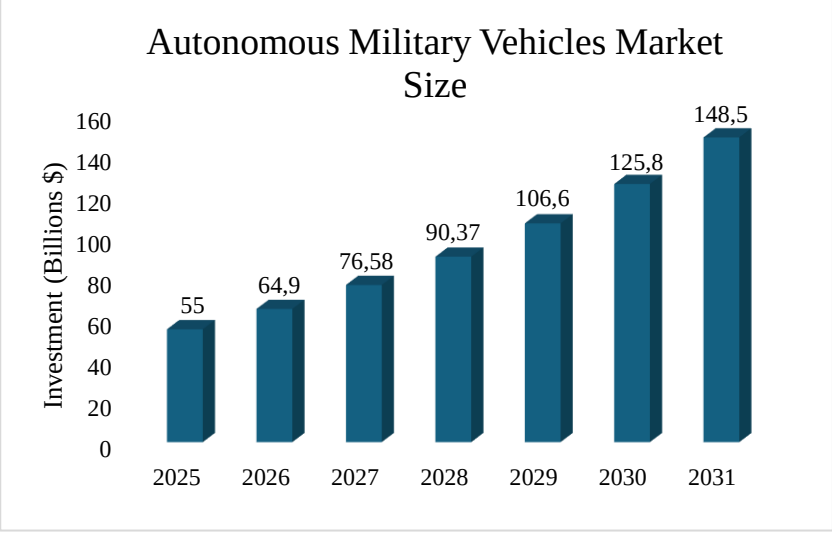

Fig. 11. Autonomous Military Vehicles market Size (adapted from[74])

The operational scenarios outlined in have engineering implications as well. Vehicles working under difficult conditions need to be structures that are well-structured. As discussed elsewhere in this paper it is known that for evacuation vehicles it is frequently a matter of structural robustness in a field environment while load will always depend on force of a lot on impact but load and uneven ground rather than lightness and therefore its operation [35].

Mobility requirements also decide powertrain design. Off-road mobility literature shows that performance on soft soil and obstacle negotiation is based on wheel torque available at very low rate but not speed, thus traction strength in tactical vehicles is the fundamental consideration [36], when deciding whether a vehicle works in a fast vehicle or not.

From a chassis perspective, maintaining ground contact in the course of irregular terrain requires large diameter tires and high compliance suspension systems to cope with terrain variability and load redistribution [39].

Finally, survivability of the vehicle is vital to model. Recent military applications focus on smaller acoustic signatures and silent use through electrified propulsion and therefore layout should accommodate distributed electronics and autonomous or remote operation [35].

2.5 System-Level Vehicle Parameter Definition in Early Design

2.5.1 Simplified Vehicle Representation in Early Design

Vehicles are complex systems made of multiple interacting parts, including mechanical, electrical, and software components. In systems engineering, a system is simply a group of elements organized to perform specific functions under set requirements and constraints. Because vehicles are so complex, you need a structured approach to model and analyse them during the development process [40].

During the early stages of vehicle concept development, the complete system configuration is usually not yet defined. In projects involving the development of new vehicle platforms, such as the prototype addressed in this work, many subsystems, dimensions, and component layouts may still be unknown. Consequently, the design process initially focuses on defining global vehicle characteristics, such as overall dimensions, general architecture, and preliminary subsystem arrangements. Detailed component integration and final packaging decisions are usually only addressed in later development stages, once the overall concept has been established. As many subsystem characteristics, dimensions and mass properties are uncertain at this stage, detailed physical modelling of the vehicle is generally not possible. Instead, simplified system representations are used to capture the vehicle's dominant characteristics while keeping modelling complexity manageable. In the context of conceptual vehicle development, this simplified representation is typically achieved by describing the vehicle through a limited set of first-order parameters that approximate its overall behaviour and support early architectural reasoning.

2.5.2 Categories of Vehicles Parameters

In the early stages of designing a simple representation of the vehicle, the parameters describing the system can be grouped into several categories according to the physical aspects they represent. Engineers usually describe the vehicle by various constraints associated with dimensional aspects, subsystem configuration, and performance parameters, and compare architecture alternatives during the vehicle concept generation phase. Being in this project, currently with no references and bases, we need to start making initial parameters or estimates of what these parameters are to start providing some guidance in the project's path.

From the perspective of early-stage vehicle architecture construction, four key groupings of parameters are established. These groups summarize the primary features of the vehicle system, making it manageable to describe their behavior rather than needing a detailed physical design.

- ***Geometric parameters***

Geometric parameters define the primary dimensions of the vehicle while providing a basic layout. Common examples include wheelbase, track width, overhangs, and ground clearance. These will be of primary importance to vehicle stability, packaging constraints, terrain negotiability, and how these parameters will influence vehicle behavior, which is especially critical for off-road vehicle applications.

- ***Mass properties***

Mass-related parameters give the size and distribution of the vehicle weight. This consists of the total mass of the vehicle, payload capacity, mass distribution, and estimated center of gravity height. These parameters, even if only approximately defined, provide some initial indication of traction ability and vehicle load transfer patterns.

- ***Operational parameters***

Operational parameter values are the vehicle's expected utilization and mission envelope. Here we would like to include payload requirements, operating speed range, and obstacle negotiation capability. These parameters combine vehicle operational mission with architectural design decisions.

- ***Derived parameters***

Derived parameters are quantities obtained from geometric and mass characteristics, which are used to estimate the performance characteristics of a vehicle. Examples are wheel torque requirements, ground contact pressure, and gradeability capability. While these parameters are generally estimated through simplistic analytical relationships, they offer useful information on system feasibility in early designs.

At the present development stage, many of these parameters remain unknown. Instead, they are estimated through the development and characterization of models built on similar vehicles or engineering assumptions, or simple calculations. As a result, the vehicle architecture can be explored with these approximations that take into account the uncertainty of early design phases.

Category	*Example parameters*	*Engineering relevance*
Geometric	Wheelbase, track width, overhangs, ground clearance	Stability, packaging and terrain negotiability
Mass	Vehicle mass, payload, CG height	Load transfer and traction capability
Operational	Payload requirements, speed range, obstacle capability	Mission envelope
Derived	Wheel torque, contact pressure, gradeability	Performance estimation

Table 2. Illustrative examples of parameter categories used in early vehicle modelling

2.5.3 Influence on Architectural Decisions

In addition to being basic descriptor details of the vehicle system, the first-order parameters mentioned above play an essential role in guiding architectural decisions during early stages of the design process. Even when only approximately estimated, these parameters are key to foundational parts of the vehicle configuration, i.e., structural arrangement, running gear architecture and propulsion concepts.

Consequently, they allow for an initial analytical overview for testing alternative vehicle architectures prior to detailed subsystem design. For design-related vehicle models, various decisions on architecture are driven to some degree by the parameter set used to represent the system. The possibility for suspension construction and packaging limitations are made with geometric parameters like wheelbase, track width and ground clearance. The mass parameters affect the load-transfer behaviour and the suspension style, structural requirement and tyre selection accordingly. Operational parameters regarding mission profile and terrain capability create the predicted performance envelope and thus affect drivetrain configuration and vehicle mobility properties.

In these early stage steps these parameters are introduced only as modelling abstractions to model the vehicle at system level. Precise physical definitions, measurement conventions and geometric interpretation are deliberately deferred to the methodology section, in which they are directly established as analytical variables to benchmark and architecturally examine. This allows architectural solutions to be explored at an early stage, considering the technical uncertainties involved with concept vehicle development. In this regard, even broader preliminary evaluation of new propulsion concepts (e.g., IWM) can also be done to gauge their compatibility with the proposed vehicle architecture.

2.6 In-Wheel Motor

As discussed in the previous section, the early stages of vehicle development provide an opportunity to explore emerging or novel technologies that may influence the configuration of the system architecture. In projects where the vehicle platform is still in a conceptual definition phase, preliminary evaluations of innovative subsystems can be carried out to assess their potential compatibility with the proposed architecture.

This is the case for the propulsion system known as the *in-wheel motor* (IWM), hereafter referred to as IWM throughout this work, in which the electric motors are integrated within the wheel rather than connected through a conventional drivetrain. Although this architecture offers several potential advantages in terms of packaging flexibility, drivetrain simplification, and torque control, it also introduces technical challenges related to torque delivery, available space for components and their integration, and thermal management.

Due to these challenges and the limited number of commercial implementations, IWM technology remains an active area of research and development. Consequently, assessing its feasibility within the context of the vehicle's architectural requirements requires a preliminary review and analysis to determine how to approach the topic and where to focus the study to make it as efficient and useful as possible for the project.

For this reason, this section introduces the fundamental and generic principles of IWM based on the information currently available, in order to discuss the core concept, its advantages and limitations, and the architectural implications associated with its integration into the vehicle design.

2.6.1 Concept and Technological Overview

New drivetrain architectures have emerged within the vehicle industry due to continuing electrification, which has been developed to enhance efficiency, simplify mechanics and expand range.

In conventional electric cars the electric motor is placed in the body of the vehicle and supplies the power to the wheels directly via mechanical elements, including the transmission, differentials and driveshafts. There is another way in which the electric traction motor is embedded inside the wheel assembly, referred to as the in-wheel motor (IWM), and works in the same way. In this type of arrangement, propulsion torque is transmitted immediately to the wheels with no intermediate mechanical transmission mechanisms, revolutionizing conventional vehicle drivetrains [41]. Hence the gearbox, driveshafts and differentials in the drivetrain can be excluded which in turn simplifies the drivetrain system with better decision makers for design.

Figure 12 demonstrates the comparison between a central-motor EV system and an IWM drive EV in simple schematic form, to visually highlight the key differences and trade-offs.

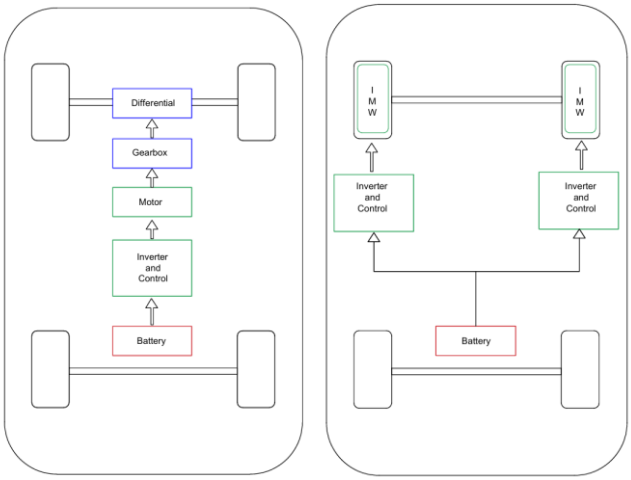

Fig. 12. Comparision between central-motor EV and IWM architecture (adapted from[43])

Depending on the vehicle layout, in-wheel motors (IWMs) can be configured into different drivetrain configurations. Electric vehicles can provide two IWMs on the front or rear axle for either front-wheel or rear-wheel drive setups. Alternatively, a motor is put in each wheel, allowing a fully distributed four-wheel-drive design with independent torque control. These configurations can yield a high flexibility of design in the vehicle's drivetrain system [41].

2.6.2 Advantages and limitations

The in-wheel motor (IWM) system provides a number of benefits in contrast to classical centrally driven propulsion systems. With propulsion embedded directly in the wheel, mechanical elements (e.g. gearboxes, driveshafts, and differentials) can be removed, making for an easier drive vehicle with decreased mechanical losses and enhanced efficiencies.

In addition, there can be independent drive for each wheel, allowing for dynamic strategies in the form of torque vectoring, which enhances traction performance under specific road conditions. Lack of mechanical transmission modules leads to reduce the need for maintenance and flexibility in packaging materials, which opens up further space for components like battery systems and passenger compartments [41].

The inherently distributed design of those in-wheel motor systems create more flexibility and control with a relatively distributed structure and can be most promising for upcoming EV platforms [42].

Even so, alongside the above challenges, the IWM systems bring with them some major barriers to be solved, preventing their wide implementation. One major disadvantage is the expansion of unsprung mass, owing to the fact that the motor is incorporated into the wheel assembly, leading to inferior ride comfort, poorer suspension performance, and overall vehicle dynamics [41].

Furthermore, without mechanical reduction systems, direct-drive configurations would allow a motor to produce a very high torque when it travels slowly, introducing real limitations to motor

layout, adding to the dimensions and complexity of the system, and also affecting its overall performance.

Thermal management also is a significant concern. The confined area between the wheel hub and the car means that conventional air-cooling systems are often too limited as well as the exposure to airflow, so advanced options like liquid cooling are required. The wheel also exposes the motor to unpleasant conditions; these include vibration, shock, water and debris, which introduce design complexity and durability demands [41].

However, since in-wheel motor (IWM) technology offers powerful potential with respect to drivetrain simplification and vehicle control, its application demands consideration of these shortfalls when assessing its incorporation into a vehicle design. Thus, these important factors will be studied experimentally and with a prototype level approach, to learn about these challenges both qualitatively and quantitatively, and to compare these challenges with regular systems.

2.6.3 System configurations

Based on the number and layout of motors in the vehicle, IWM systems can be implemented in different drivetrain configurations. Rather than focusing on only one electric motor in the vehicle for each wheel, which propulsion would be produced by a single key motor, the IWM systems can be distributed, so that even the external car may take multiple wheels for it at once, depending on the drivetrain design and its needs. The simplest configuration is where the electric motor is integrated directly into the wheel hub, and torque is delivered straight to the wheel, and mechanical transmission systems like gearboxes, differentials, or driveshafts are not required. This simplifies the design, and the system can be much easier to handle as the power is sent directly into the wheels [41].

Many more advanced configurations include power electronics in the wheel assembly, giving together a complete drive. In a similar style, inverter units and control assemblies are mounted alongside the motor, minimizing and thus reducing wiring length, electrical losses, and total system volume. But in this operation, thermal and protective factors like external elements, which contribute to working time temperature fluctuation, damping, and vibration [43], are required for the components, adding to the heat management problems.

Thermal cooling is a crucial feature of the IWM-based design due to the small space of the wheel. Several cooling options have been suggested: air, oil, and liquid cooling systems. Of these, liquid cooling is the most commonly used method in high-performance applications to provide a high heat dissipation capacity and ensure the motor operates safely under demanding load conditions. The general IWM system architecture has been described as illustrated in Figure 13 and concerns the electrical elements of the motor.

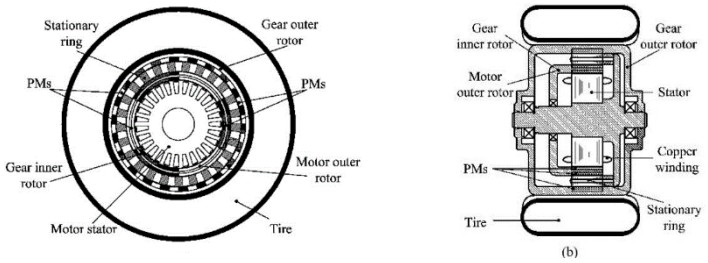

Fig. 13. General architecture of IWM drivetrain systems [75]

So, on the highest level of integration, some idea is to have the electric motor combined with additional subsystems (braking, suspension) integrated in the wheel module. The architecture complexity targets maximizing packaging efficiency and simplifying the process of vehicle assembly, but it also brings significant challenges in structural design, system reliability, and mass. Different IWM models from Michelin and Continental are presented in Figures 14 and 15 and each of them has its own characteristics and the different types of design they are used for. These are just some examples of the complexity of prototypes and the variety of solutions looked at, therefore there isn't a single standardized system that each manufacturer follows or adopts.

Fig. 15. Example of IWM integration concept from Micheline [75]

Fig. 14. Example of IWM integration concept from Continental [76]

As can be seen, Michelin integrated both the braking and suspension systems, making the design extremely complex. Continental, on the other hand, included only the braking system specifically a drum brake which at first glance does not appear to be the most optimal solution in terms of thermal performance.

2.6.4 Architectural implications and Technology Maturity

The application of IWM systems has important impacts on vehicle structure, with respect to packaging, suspension configuration and system integration. Adding the motor in the wheel is an additional increase in unsprung mass to the vehicle which is one of the most recognized drawbacks of such a system. Higher unsprung mass negatively impacts suspension performance, riding comfort and overall vehicle handling and remains one of the major obstacles to the widespread adoption of IWM systems [44].

Other than aerodynamic limitations, there are a number of engineering problems that the majority are still in the prototype or experimental stage at the IWM application stages. These are the need to produce high torque at low rotational speeds without mechanical reduction, constraints in torque density for certain vehicle applications and the stringent thermal management demands arising from the physical constraint in the wheel hub [45].

Moreover, the direct exposure of a motor to heavy operating conditions like vibrations, impacts, water, and debris makes it even more difficult that over a vehicle's lifetime we can depend on it for reliability. The combined effects of these factors with cost and integration issues make it hard to see how, for large scale industrial adoption in-wheel motor technology that may lead to its advantages.

However, all these difficulties aside, early conceptual studies are still necessary to assess the feasibility of this kind of technology to be used in specific vehicle architectures. For example, if the vehicle concept is developed theoretically as a system, early modeling, simulation, and packaging could enable quantitative and qualitative insight about how in-wheel motor could work. This research aims to respond to that question and assess the feasibility of it within a vehicle proposal and then help shape future development decisions.

3. METHODOLOGY

3.1 Methodology Approach

Once the fundamental theoretical concepts have been introduced, this section describes the methodological approach followed in this project.

First, since the project starts from a conceptual stage with no clearly defined prior references, a benchmarking study is carried out on vehicles with features similar to the prototype to be developed. Based on this analysis, the main dimensions, geometric parameters, and configurations of these vehicles are gathered, using the information available from manufacturers.

Based on the collected data, a set of design parameters and ranges can be established (in the form of reference dimensions) to determine the main dimensions of the vehicle. The ranges are set based on technical criteria that will include design and construction, and using choices such as decision matrices derived from product planning techniques in the way of product planning.

Once the overall architecture is defined, the design of the wheel systems is developed, considering both a conventional setup and a solution based on an in-wheel motor (IWM). Both systems are modeled using CAD tools, taking a catalog tire as a reference, which sets the main geometric constraints of the assembly.

A theoretical calculation of the wheel torque is carried out, using vehicle dynamics equations to estimate the requirements under different operating conditions and to assess the feasibility of the IWM system.

Finally, numerical simulations analyze the developed models. These include structural, thermal, and fluid dynamics analyses to compare both solutions. This process yields quantitative results to support decision-making.

In addition, a preliminary system-level model of the vehicle architecture is developed, integrating the defined dimensions and the main components of the overall setup. This model makes it possible to visually and spatially validate the proposed configuration, helping with packaging analysis and ensuring the overall design is consistent.

More detailed information and the full process are presented in Sections 4 and 5 of this work. The data collected from the benchmarking of all the vehicles can be found in Appendix A.

3.2 Benchmarking and Parameter Definition

A benchmarking study is carried out using existing vehicles with similar features and applications to establish a consistent basis for the conceptual definition of the vehicle. Most of the selected vehicles have dimensions and weights close to those of the target prototype to be developed. The benchmarking process focuses on identifying and collecting key parameters that describe the vehicle at a system level.

These include geometric properties (wheelbase, track width, overall dimensions, wheel size) along with the details of vehicle configuration and vehicle design. The availability of data for the analysed vehicles depends on public sources, since there is not always a complete report from companies of a detailed part of a technical and structural design. Figure 16 shows what dimensions correspond to some of the parameters considered and analysed during the benchmarking.

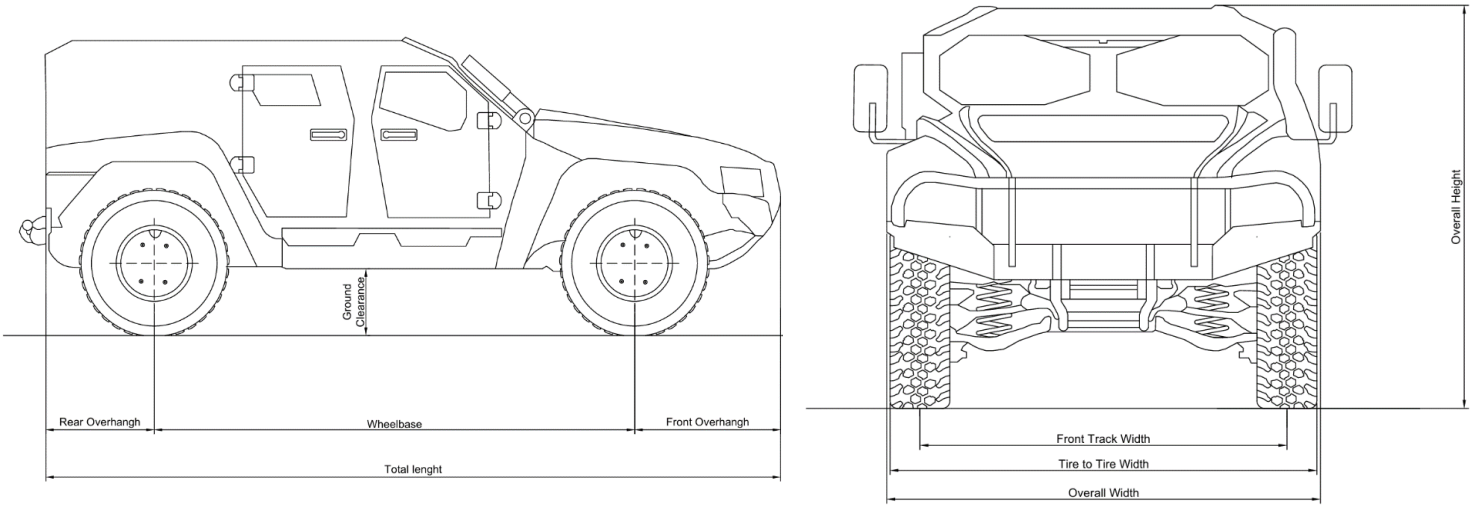

Fig. 16.Main geometric parameters used for vehicle definition

The collected information is organized and analyzed with the aim of defining representative ranges for the main design parameters. These ranges are used as reference values during the conceptual development process, supporting the definition of the vehicle architecture and ensuring good consistency with current solutions and models on the market.

To keep everything clear and well structured, the extracted data is arranged in tables, making it easier to compare different vehicle models and, as a result, supporting analysis and decision-making.

3.3 Decision Matrices for Concept Selection

During the conceptual design phase, several alternatives need to be evaluated under uncertainty and with limited information. In addition to engineering judgment and team decisions, structured methods are used to support a more objective selection process.

Table 3 shows an example of the parameter structure used during the benchmarking process.

In this project, decision matrices are used as a methodology, following the approach proposed in the work of Karl T. Ulrich and Steven D. Eppinger [12]. Two methods are especially useful in the early stages to rule out concepts or options that are not relevant.

	MODEL:
MASS & GEOMETRIC PARAMETERS	Wheelbase (mm)
	Track Width (mm)
	Total length (mm)
	Width (mm)
	Ground clearance (mm)
	Tare mass (kg)
	GVW (kg)
	Payload (kg)
	Overall height (mm)
MOBILITY AND PERFORMANCE	Max speed (km/h)
	Gradeability (%)
	Side Slope (°)
	Max Torque (Nm)
	Approach/Departure Angle (º)
RUNNING GEAR & STRUCTURAL CONFIGURATION	Suspension Type (F/R)
	Axle Type
	Tyre Size
	Brake Type
	Chassis type

Table 3. Templated used for recollecting the benchmarking data

The screening matrix allows a quick comparison between different alternatives against a reference solution, using simple rating criteria. After that, a concept scoring matrix is applied, where each alternative is evaluated based on weighted criteria. This is more detailed and helps us in the final decision of which is the most suitable one. Such matrices allow for several criteria with different kinds of considerations. To name the most concrete ones, there are packaging constraints, system requirements, performance, and ease of integration. This mechanism is structured into a clear choice procedure. The matrices mentioned above are illustrated in Figures 17 and 18. For more details, we will discuss how our criteria are determined (and if those criteria were successful as well as we could not find any positive answer as these scores were good) in chapter 4.

	Concepts						
Selection Criteria	**A Master Cylinder**	**B Rubber Brake**	**C Ratchet**	**D (Reference) Plunge Stop**	**E Swash Ring**	**F Lever Set**	**G Dial Screw**
Ease of handling	0	0	–	0	0	–	–
Ease of use	0	–	–	0	0	+	0
Readability of settings	0	0	+	0	+	0	+
Dose metering accuracy	0	0	0	0	–	0	0
Durability	0	0	0	0	0	+	0
Ease of manufacture	+	–	–	0	0	–	0
Portability	+	+	0	0	+	0	0
Sum +'s	2	1	1	0	2	2	1
Sum 0's	5	4	3	7	4	3	5
Sum –'s	0	2	3	0	1	2	1
Net Score	2	–1	–2	0	1	0	0
Rank	1	6	7	3	2	3	3
Continue?	Yes	No	No	Combine	Yes	Combine	Revise

Fig. 17. Concept Screening Matrix [12]

		Concept							
		A (Reference) Master Cylinder		**DF Lever Stop**		**E Swash Ring**		**G+ Dial Screw+**	
Selection Criteria	**Weight**	**Rating**	**Weighted Score**	**Rating**	**Weighted Score**	**Rating**	**Weighted Score**	**Rating**	**Weighted Score**
Ease of handling	5%	**3**	0.15	3	0.15	4	0.2	4	0.2
Ease of use	15%	**3**	0.45	4	0.6	4	0.6	3	0.45
Readability of settings	10%	2	0.2	**3**	0.3	5	0.5	5	0.5
Dose metering accuracy	25%	**3**	0.75	3	0.75	2	0.5	3	0.75
Durability	15%	2	0.3	5	0.75	4	0.6	**3**	0.45
Ease of manufacture	20%	**3**	0.6	3	0.6	2	0.4	2	0.4
Portability	10%	**3**	0.3	3	0.3	3	0.3	3	0.3
	Total Score	2.75		3.45		3.10		3.05	
	Rank	4		1		2		3	
	Continue?	No		Develop		No		No	

Fig. 18. Concept Scoring Matrix [12]

3.4 Vehicle and Wheel System Design

Once the main architectural parameters have been defined, the conceptual design phase is performed by developing representative models of the vehicle and the wheel system. The goal of this stage is not to obtain a detailed design, but to create simplified and consistent geometries that allow comparison and analysis between the two different configurations.

Once the team has decided which type of wheel will be used, the design process is based on selecting a model from a commercial catalog. This model serves as the main reference to define the wheel dimensions and the available packaging space. This approach ensures that all subsequent designs remain realistic and consistent in terms of dimensions. Figure 19 shows the catalog image from which the tire and rim data used in the design were taken.

COMMERCIAL DESCRIPTION	Load/speed index	CAI *MSPN*	M+S	POR	Measuring Recommended Rim	Optional Rim	Mass (+/- 3%) **kg** *lbs*	Tread depth **mm** *32nd*	Overall width (+/- 3mm) **mm** *inch*	Overall diameter (+/- 4mm) **mm** *inch*	Static laden radius **mm** *inch*	Rolling circumference (+/- 0.5%) **mm** *inch*
X FORCE ZL™ 14.00 R 20 TL*	**168/165K**	**249003**	√	√	**10.00W**	**9.0** **10.0** **10.00**	**105,0** *231,5*	**22.3**	**386** *15*	**1258** *50*	**578** *23*	**3832** *151*

Running conditions	Maximum load & pressure per tyre				Maximum speed		Footprint	
	kg *lbs*		**bar** *psi*		**km/h** *mph*		**cm²** *sq. in*	
Road	**5600**	*12346*	**8.6**	*125*	**110**	*68*	**983**	*152*
Cross Country	**5600**	*12346*	**6.2**	*90*	**70**	*43*	**1240**	*192*
Mud and Sand	**5600**	*12346*	**4.1**	*59*	**30**	*19*	**1657**	*257*

Fig. 19. Selected tyre and rim specifications from commercial catalogue used as design reference

Thus, two systems are proposed based on this reference. On the one hand, a customized IWM architecture has been developed; on the other hand, a standard wheel system with brake disc and caliper is utilized.

The second alternative is a baseline solution for further comparison while providing a standard and widely used reference model where the results of the IWM prototype analysis can be compared. The CAD models are designed according to the geometric features critical for the analysis and functional volumes required for the analysis. The level of detail is carefully restricted so that model complexity is balanced by analyses, because braking simulations can be quite high-demanding.

A simpler vehicle layout model is also designed to act as a global reference for system integration. This design provides a general chassis configuration based on the specified dimensions. This allows for better knowledge on packaging restrictions and where component distribution occurs and also the feasibility of both designs. The analyses and numerical evaluations are based on these models.

3.4.1 Catia V5

CATIA V5 is a computer-aided design (CAD) tool primarily used in the automotive and aerospace industries to design complex engineering products. It is part of an integrated software suite for the entire product lifecycle from early concept design to manufacturing and analysis. The software is organized into workbench modules focused on specific design tasks. In this project, the modelling process is mostly executed through the Part Design and Assembly Design workbenches. Parametric 3D components can be generated by operations such as extrusions, cuts, and revolutions using the Part Design workbench. On the other hand, the Assembly Design workbench defines the spatial constraints and relationships between individual components so they may be brought together into a complete system [46].

These tools enable consistent and flexible geometries, all of which are ideal for developing the simplified models needed during the initial conceptual design stage. The workbenches are listed in Figure 20 in CATIA V5, highlighting those related to mechanical design.

Many different workbenches are available as shown. Nonetheless, as mentioned above, most of this work mainly deals with Part Design and Assembly Design, which are widely used, together with Generative Shape Design.

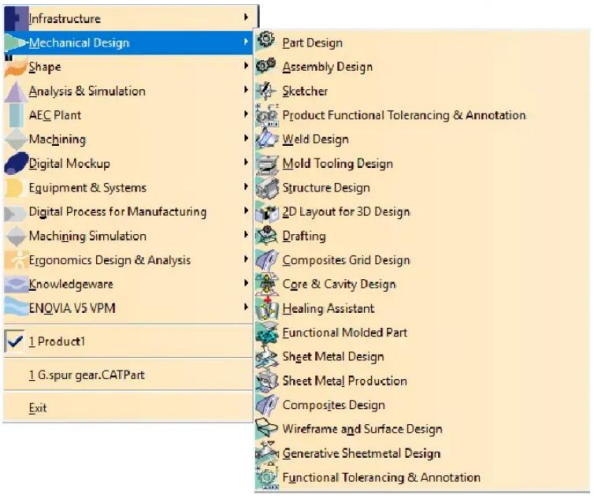

Fig. 20. CATIA V5 interface area

3.5 Theoretical Torque Calculation

A theoretical calculation of the required wheel torque is done of the proposed models and 3D design is done, hence a clear indication of the geometry for some simulation on the proposed model to proceed.

The goal of this calculation is to estimate the demand for torque under various operating conditions including the worst cases in this case. The obtained values are not only used to evaluate the feasibility of the In-Wheel Motor (IWM) configuration but also are used to construct a theoretical reference for other propulsion system options. Since we use estimated vehicle mass and operating conditions as inputs, the calculations can be applied to the other drivetrain configurations since they reflect the torque that is required at the wheel level.

3.5.1 General Torque Formulation

To determine the total torque required at the wheel under a given condition, the main equation used is Equation 1, shown below:

$$T_{Total\ wheels} = F_R \cdot R_{dyn} \quad \text{Eq. 1}$$

Where:

F_R = Sum of the resistive forces

R_{dyn} = Dynamic wheel radius

This simplified model is intended for an initial estimation of the required torque and does not take into account traction limits, load transfer effects, or tire and terrain interaction.

3.5.2 Resistive Forces Model

As shown in the previous equation, the calculation of the total resistive force is required in order to determine the torque demand at the wheels. These forces represent the opposition to motion and therefore directly influence the torque required to overcome different operating conditions.

Equation 2 presents the resistive forces considered in this study. These forces are commonly used in vehicle longitudinal dynamics models to estimate traction requirements.

$$F_R = F_{rr} + F_d + F_{hc} + F_i \quad \text{Eq. 2}$$

Where:

F_{rr} = rolling resistance force

F_d = aerodynamic drag force

F_{hc} = hill-climbing force

F_i = inertial force

The detailed formulation and calculation procedure for each of these forces are presented in Chapter 5, where the methodology is applied to the defined operating scenarios.

3.5.3 Assumptions and conditions

To estimate the torque, several conditions and assumptions need to be set for consistency throughout the analysis. These are necessary within the context of the vehicle development as most parameters are currently not yet fully defined and are thus assumed as target values or working ranges. The calculations are based on a fairly general estimate of vehicle mass for the intended uses. Although this value may change as the design evolves, it provides a consistent reference to evaluate traction requirements, since at this stage it is considered the target mass for the vehicle.

Different operating scenarios are considered to obtain a wide range of demand for the vehicle. These include steady-state conditions as well as dynamic cases involving acceleration and resistance due to terrain conditions.

Special attention is given to demanding scenarios that represent worst-case conditions. This makes it possible to identify the highest torque requirements in situations that may occur, even if they are not the most common.

The analysis assumes standard vehicle longitudinal dynamics, where the main resistive forces are taken into account. Some simplifications are applied to keep a good balance between model accuracy and its use at a conceptual level.

The application of this methodology to representative operating scenarios is presented in Chapter 5.

3.6 Simulation Tools and Approach

3.6.1 Ansys Workbench

This work implemented simulations using ANSYS Workbench, which is included in the ANSYS software suite. ANSYS is a common engineering simulation tool to provide a computer with the capability to analyse and predict how systems and products will behave under realistic operating conditions long before building them. It is grounded in the numerical approaches using finite element analysis (FEA) and computational fluid dynamics (CFD) and allows structural, thermal, and fluid flow characteristics to be explored in one environment. ANSYS Workbench serves as an integrated platform that unifies different kinds of analysis within the same interface to facilitate integration between geometry, physical models, and results.

Such multiphysics nature is particularly important for interactions between different physical effects in this study, as in this work [47].

3.6.2 Selection Simulation Modules

Figure 21 shows the analysis systems available in the version of ANSYS 2024 R1 used in this project.

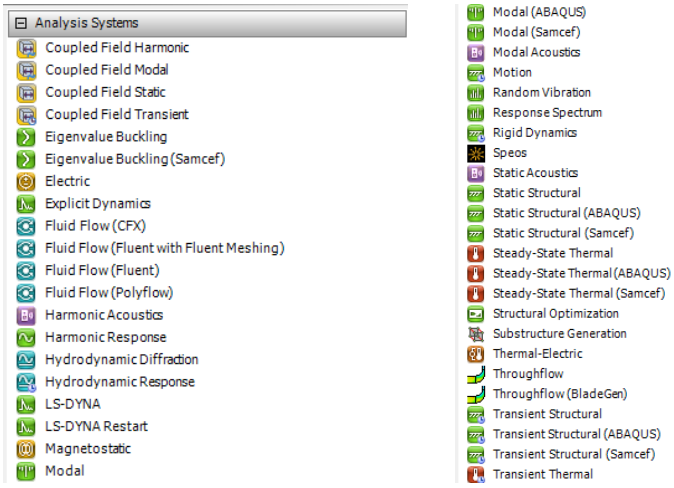

Fig. 21. Simulation modules of Ansys Workbench environment

As can be seen, the ANSYS Workbench platform includes many different modules, each designed to perform specific types of analysis.

3.6.2.1 Static Structural

The Static Structural module is used in the first analysis carried out in ANSYS. It determines displacements, stresses, strains, and forces in structures or components caused by loads that do not generate significant inertia or damping effects. Steady loading and response conditions are taken into account, which imply that the applied loads and the structural response change slowly over time [48].

Structural module can be seen using Figure 22. It is divided into several main parts. Firstly, the Geometry section introduces the 3D model. Then the Meshing section (to define parameters of the mesh size and characteristics). Fig. 22. Structure of the Static Structural analysis system in ANSYS Workbench. Figure 6. Structure of the Static Structural analysis system for ANSYS Workbench.

Finally, the Setup section applies loads, forces, and boundary conditions to the model. The next section delves into what each of these submodules is doing, as most of the ANSYS modules follow a similar pattern.

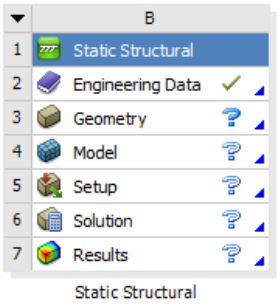

Fig. 22. Structure of the Static Structural analysis system within Ansys workbench

3.6.2.2 Coupled Field Transient Mode

These works are carried out using the Coupled Field Transient module in ANSYS for braking simulation and heat evaluation. This module covers an interplay of multiple physics interactions. Such analysis makes possible simultaneous simulations of multiple physical effects, which can be applied at once; e.g., structural and thermal behaviour in a single model. That is, it offers a thermo-mechanical analysis of the response to mechanical contact, where the mechanical contact directly affects heat generation in the system [49].

The transient formulation can be used to study time-dependent behaviour, reflecting how displacement, stress, and strain affect the adaptation towards changing loads and thermal conditions over time. This is particularly significant for applications that use different properties (i.e., mechanical behaviour) of the object, because both the IWM and the conventional system studied in this work experience differences in their temperature.

Figure 23 presents a sketch of the framework of Coupled Field Transient module in ANSYS Workbench. Like a lot of other modules, it is arranged as a series of steps that specifies the workflow through the simulated method.

The **Engineering Data module** is used to define the material properties required for the simulation, including both mechanical and thermal parameters.

The **Geometry module** contains the 3D model to be analyzed. This model can be imported or created externally using CAD software.

The **Model module** provides access to the pre-processing interface, where the physics of the model is defined, following the structure shown on the right side of the image. This includes material assignment, definition of coordinate systems, connections between components, and mesh generation for the analysis.

The **Setup module** is used to define the analysis conditions, such as loads, boundary conditions, and thermal inputs, as well as the type of simulation and time-dependent parameters.

The **Solution module** controls the numerical solving process, where the simulation is executed based on the defined model and conditions.

Finally, the **Results module** allows post-processing and visualization of the outputs, including variables such as stress, displacement, temperature distribution, and deformation, among others.

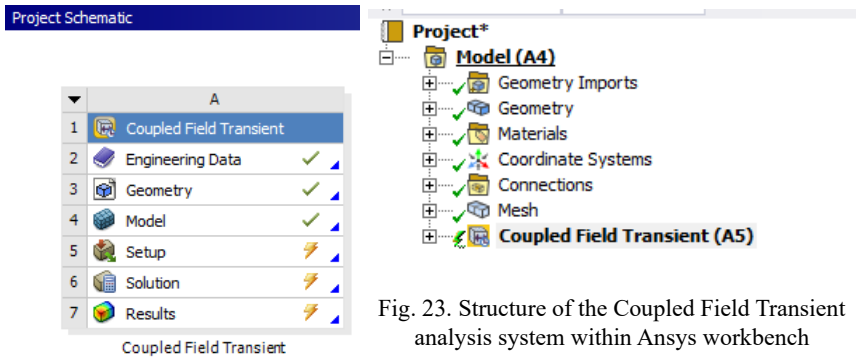

Fig. 23. Structure of the Coupled Field Transient analysis system within Ansys workbench

3.6.2.3 Steady-State & Transient Thermal

As discussed, the Coupled Field mode is the most realistic option, but it also demands the most computing power. Because of this, the simulations might crash. Modeling contact, friction, and multiple forces at the same time is incredibly heavy. A standard laptop, like the one used for this project, will likely struggle to handle it.

That is why you need a backup plan. Anticipating these failures early saves you from wasting valuable project time.

If the Coupled Field simulation fails, you can move to Steady-State and Transient Thermal modes. Still, we are able to track how heat moves through the system.

The Steady-State model does not change over time and if so, then that model will be the first way when you check if the setup is working right or the setup needs improvement. Once you can locate the steady-state results, you change to the Transient mode and so on. This step applies heat over time, showing you how the system actually responds to changing thermal loads. Figure 24 shows the steady-state and transient thermal structures.

The specific heat loads, boundary conditions, and final simulation results are detailed in Chapter 5.

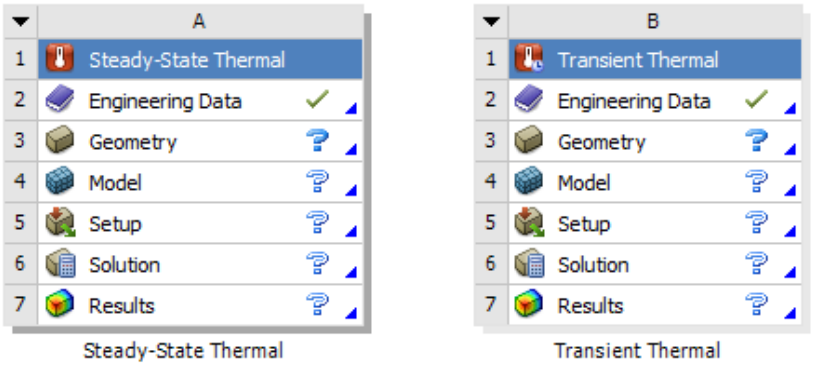

Fig. 24. Structure of the Steady-State and Transient analysis systems within Ansys Workbench

3.6.2.4 Fluid Flow (Fluent) Module

Apart from the thermo-mechanical analysis in the study, a computational fluid dynamics (CFD) simulation will then be performed to investigate how those flow lines affect both 3D models.

Keep in mind that CFD-based calculations on 3D models are really complicated to get exact and realistic results. In the present study, because this model is a custom design and the project is academic, the goal is not to get exact results but rather to understand how the flow behaves around the models and to identify the main differences between them.

he analysis will be carried out in ANSYS Fluent, a general-purpose CFD tool extensively applied in engineering to simulate fluid flow, heat transfer, and related physical phenomena.

CFD is the numerical analysis of equations that deal with fluid mechanics, such as the conservation of mass, momentum, and energy. And then we can predict how the flow behaves under various operating conditions.

ANSYS Fluent provides an integrated environment for performing simulation including pre-processing, solving, and post-processing with the complete simulation in one interface. This enables the study of intricate flow conditions like those associated with turbulence, heat transfer, and multiphase flows, which is particularly well suited to the investigation of cooling performance and airflow behaviour in engineering systems [50].

Figure 25 illustrates the Fluid Flow (Fluent) module architecture of ANSYS Workbench. It is apparent that it follows a workflow similar to the previous coupled field analysis and a consistent sequence of geometry, mesh, setup, solution, and results.

More emphasis is placed on the geometry and mesh definition in this instance, as it is pivotal for defining the boundary conditions in the system and thus, producing reliable CFD results. The specific simulation process and configuration are laid out next in the development section of the work.

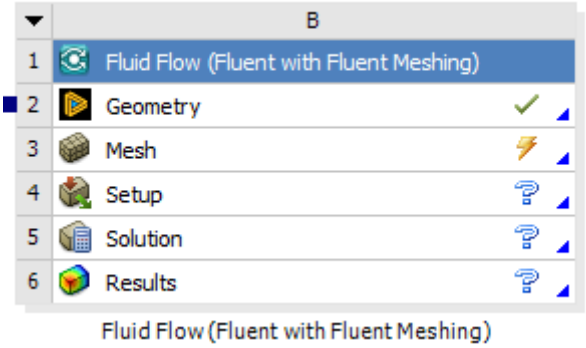

Fig. 25. Ansys Workbench project schematic for Fluid Flow (Fluent) analysis

4. SYSTEM-LEVEL VEHICLE ARCHITECTURE DEFINITION

4.1 Baseline Vehicle Architecture Definition

As discussed in the previous chapter, the intended functions and objectives of the new prototype are clearly oriented toward the development of a modular off-road vehicle platform. At this early stage of development, defining a preliminary vehicle architecture is essential in order to establish dimensional and functional boundaries aligned with the initial design direction.

While benchmarking (introduced in Section 3.4) provides a structured method for building the architecture foundation of the vehicle, a set of preliminary assumptions was established prior to this analysis. These assumptions were made on the basis of the general engineering judgement and domain knowledge and are solely illustrative reference ranges to guide early conceptual framing.

The parameters we present below do not represent final design targets. We provide an initial architecture envelope that will be further tested out using benchmarking performance and trade-offs in the remainder of this chapter.

The baseline parameter set used to define preliminary vehicle architecture is presented in Table 4.

Parameter	***Value***
GVW	up to 10,000 kg
Minimum mass	~3,500 kg
Payload per wheel	~2,500 kg
Wheelbase	3.0–3.5 m
Track width	~2.0 m
Total length	5–6 m
Ground clearance	0.35–0.40 m

Max speed	~120 km/h
Power per wheel	100–200 kW (estimate)
Torque levels	~20000 Nm (estimate)

Table 4. Initial baseline parameter set

4.2 Benchmarking Results and Trend Analysis

Once the methodology, parameters, and vehicle categories considered in the benchmarking study were defined, the collected data were structured to enable statistical comparison and trend identification.

As an illustrative example, Table 5 presents the extracted data corresponding to one of the nineteen reference vehicles analysed. The dataset includes key dimensional, mechanical, and performance parameters that form the basis for the comparative analysis.

MODEL: PLASAN SANDCAT		
MASS & GEOMETRIC PARAMETERS	Wheelbase (mm)	3180
	Track Width (mm)	1885
	Total length (mm)	5295
	Width (mm)	1995
	Ground clearance (mm)	260
	Tare mass (kg)	6350
	GVW (kg)	8845
	Payload (kg)	2495
	Overall height (mm)	2390
MOBILITY AND PERFORMANCE	Max speed (km/h)	120
	Gradeability (%)	60
	Side Slope (°)	39
	Max Torque (Nm)	895
	Approach/Departure Angle (º)	35/36
RUNNING GEAR & STRUCTURAL CONFIGURATION	Suspension Type (F/R)	Semi-elliptic leaf spring + hydraulic shock absorbers (F&L)
	Axle Type	Rigid Axle
	Tyre Size	285/70 R19.5
	Brake Type	Four-wheel wheel ventilated disk
	Chassis type	Commercial ladder-frame Ford F-550

Table 5. Example of benchmark vehicle parameter dataset

These data are processed and animated using visual representations to indicate the dominant patterns and establish reference values to the framework for the basic geometry of the prototype vehicle. Benchmarking results for all reference cars are shown in Appendix A.

Based on the parameters and characteristics presented in Table 5 collected for each benchmark vehicle, the most representative variables are selected. This analysis should help find an average value range and design trends to characterize the baseline vehicle architecture.

We will review comparisons of the mass and the key dimensions from the wheelbase perspective to the Gross Vehicle Weight (GVW). We also present a supplementary graphical analysis based on running gear, mobility, and overall size of the body.

4.2.1 Primary architecture dimension trends

To establish baseline architectural dimensional tendencies, key relationships between vehicle mass and primary geometric parameters are analysed. Particular attention is given to the influence of gross vehicle weight on longitudinal layout definition.

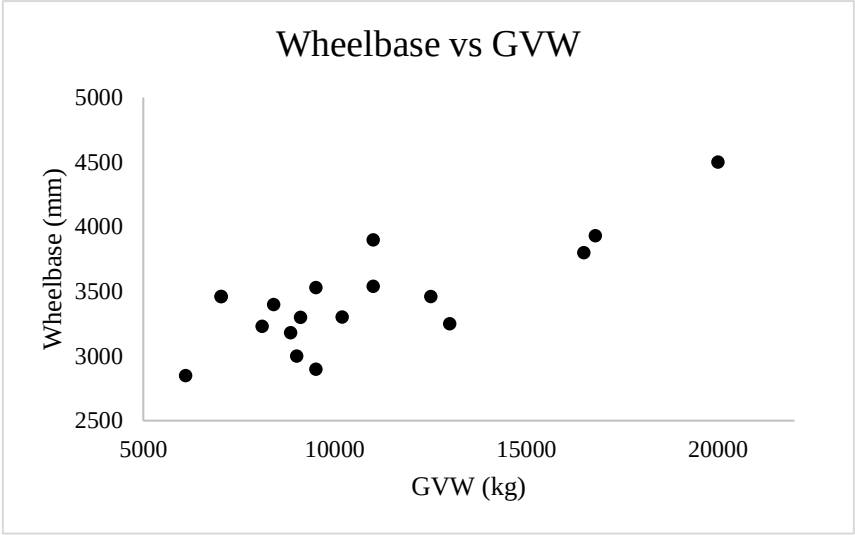

Fig. 26. Wheelbase vs Gross Vehicle Weight

Benchmarking results displayed in Figure 26 demonstrate a distinct accumulation of vehicles in the gross vehicle weight interval (8000-11000 kg), with the corresponding wheelbase values generally ranging from 3000 and 3500 mm.

This trend suggests a common scaling behaviour for the longitudinal layout packaging and serves as a reference envelope for the baseline architecture definition. After assessing the longitudinal dimensional scaling, lateral architectural tendencies are evaluated through the relationship between track width and gross vehicle weight in Figure 27.

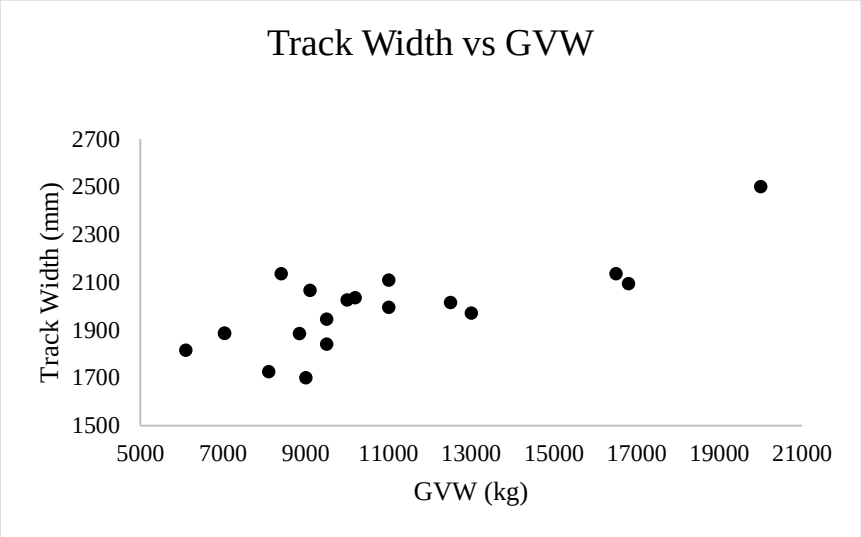

Fig. 27. Track Width vs GVW

The benchmarked platforms do not show a linear relationship between the gross vehicle weight and track width. However, there is sharp clustering around the 8.5-11 tonne GVW range, where most vehicles' track width lies about 1800 mm to 2100 mm. For this reason, track width is mainly associated with stability (packaging and transportability), not vehicle load. Platforms larger than 15 tonnes GVW have high track widths and in this way shift to being heavy-duty vehicle architecture fit for different operational requirements. Having investigated lateral dimensional variations, the envelope of the complete vehicle is considered overall given the total length of the vehicle and its gross weight.

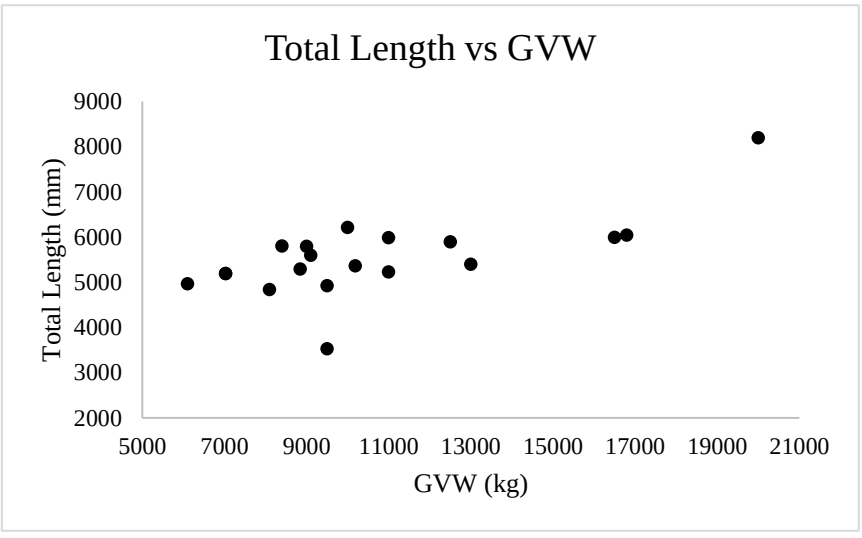

Fig. 28. Total Length vs GVW

As noted in Figure 28, there is no linear relationship between GVW and vehicle length, and the packaging requirements and mission specification are more important than mass alone. Only a

few outliers are specific vehicles, being outside the typical dimensional range for the benchmark system.

To compare the previous mass assumption of a typical off-road vehicle, we see that the vehicles of the same weight range generally have spans between 5000 and 62000 mm in length, the largest configuration for our off-road systems. The relationship between vehicle mass and other primary parameters is evaluated, where proportional geometric tendencies are examined. The relationship between wheelbase and total vehicle length provides insight into structural layout distribution and overhang proportions across the benchmark platforms as we can see in the Figure 29.

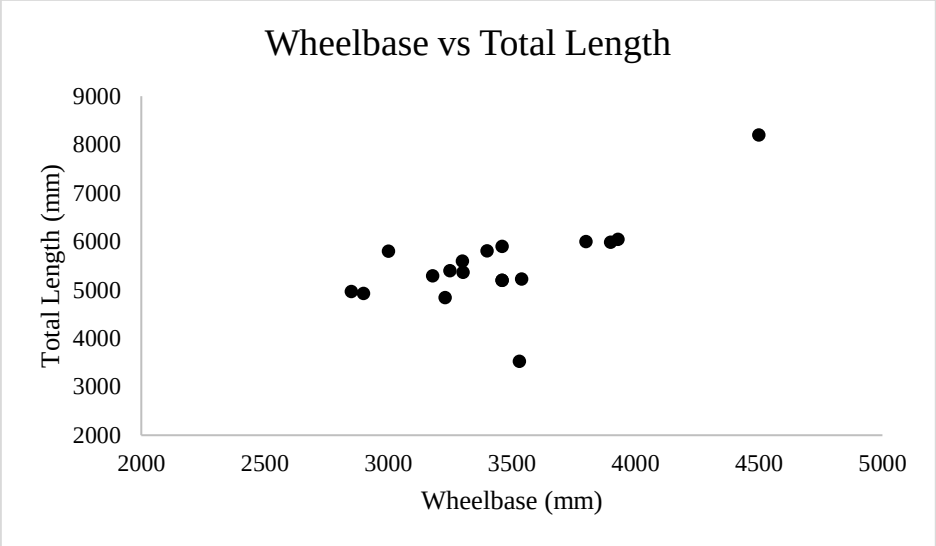

Fig. 29. Wheelbase vs Total Length

The relationship of wheelbase with total vehicle length had been examined to find out the proportional architectural patterns between their corresponding off-road vehicles. This comparison allows analysis of structural packaging distribution and overhang proportions, which are considered influencing not just vehicle stability, manoeuvrability, yet obstacle negotiation capability.

Clearly, the overall vehicle length is positively correlated with the wheelbase, reflecting typical behaviour based on architectural scale for stability and load distribution. The majority of the studied vehicles concentrate in the wheelbase range of 3000-3500 mm with total vehicle lengths between 4800 mm and 5900 mm.

This is the dominant proportional envelope of medium weight off-road platforms. This clustering enables further considerations of the proportional proportions during the later architectural definition process in accordance with existing design procedures in the target segment.

4.2.2 Mobility Capability Indicators

After establishing baseline dimensional trends, mobility-related characteristics are evaluated. Ground clearance is analysed as a primary indicator of off-road capability, directly affecting terrain negotiation and obstacle clearance.

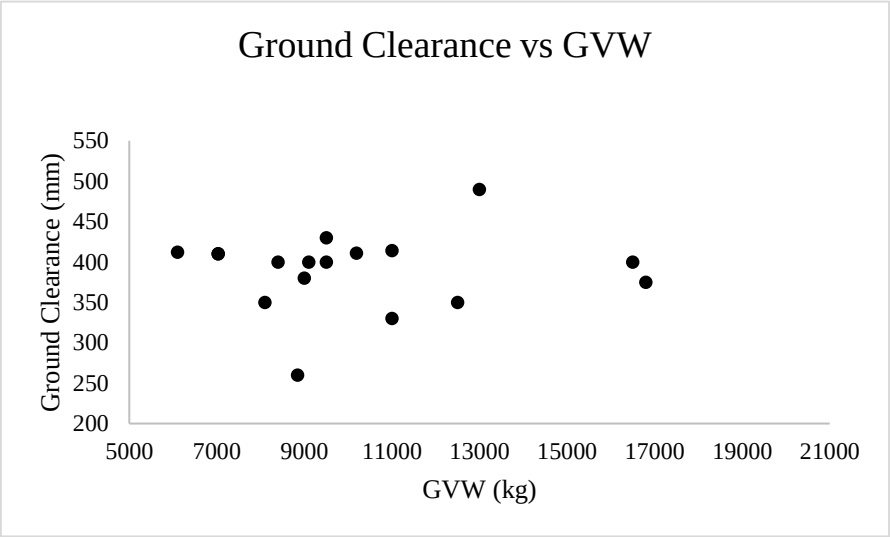

Fig. 30. Ground Clearance vs GVW

No strong correlation could be found between the gross vehicle weight and ground clearance in the benchmarking results. More so, there is a general rule that ground clearance is a design parameter that is largely independent of vehicle mass.

The majority of tested vehicles stay within a ground clearance range of approximately 380-430 mm (see fig. 28), showing the general compromise adopted between off-road capability, vehicle stability, and packaging constraints. There are a small portion of outliers with significantly higher or lower values that indicate special mission requirements over the general trend of platform design for that particular domain.

4.2.3 Running gear Architecture Trends

After evaluating dimensional and mobility characteristics, this benchmarking analyzes running gear architecture characteristics. These subsystems significantly affect vehicle durability, mobility performance, maintenance requirements, and integration complexity.

his analysis examines suspension architecture distribution and tyre configuration trends across the benchmarked platforms to find which design practices are dominant among similar off-road vehicles. Selection of suspension architecture has major implications for mobility, structural robustness, and integration complexity. The suspension type distribution across the benchmark dataset is then investigated as a way of exploring prevalent design tendencies of similar off-road platforms, as visualized in Figure 31.

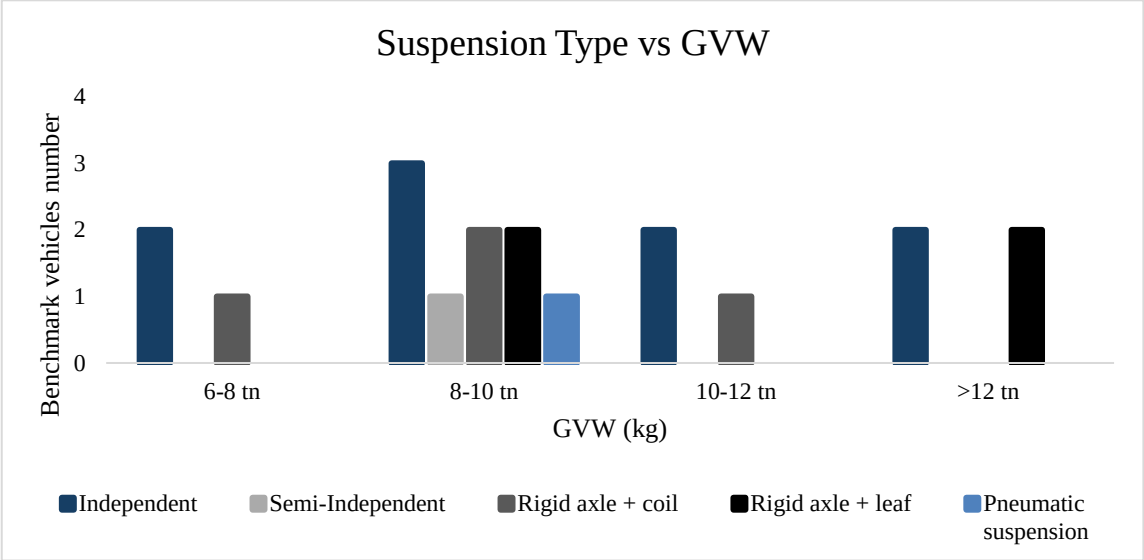

Fig. 31. Suspension Type vs GVW

The benchmarking results show a relationship between vehicle mass and suspension architecture selection. Independent suspension systems are widely employed in vehicles below approximately 9-10 tonnes GVW, primarily owing to their advantages for both comfort in motoring and mobility performance.

Meanwhile, rigid axle with coil springs and leaf springs are also widely present in this range. With an increase in mass, the rigid axle systems become more frequent in the benchmarked platforms. Pneumatic suspension shows infrequent presence in the dataset, implying low usage in off-road military vehicles wherein durability and simplicity are prioritized in driving technology.

According to initial estimation of mass assumption given above, independent suspension and rigid axle design can be considered as potential options for the proposed architecture. Subsequent steps will therefore require a more extensive trade-off analysis to accommodate the issues around mobility, durability, complexity, and integration. Tyre size distribution was explored in order to aid in defining the running gear architecture between benchmarked vehicles since these types of tyres are crucial for mobility performance, load capacity, and the integration of wheel-end components. The different tires in analysed vehicles are plotted in Figure 32.

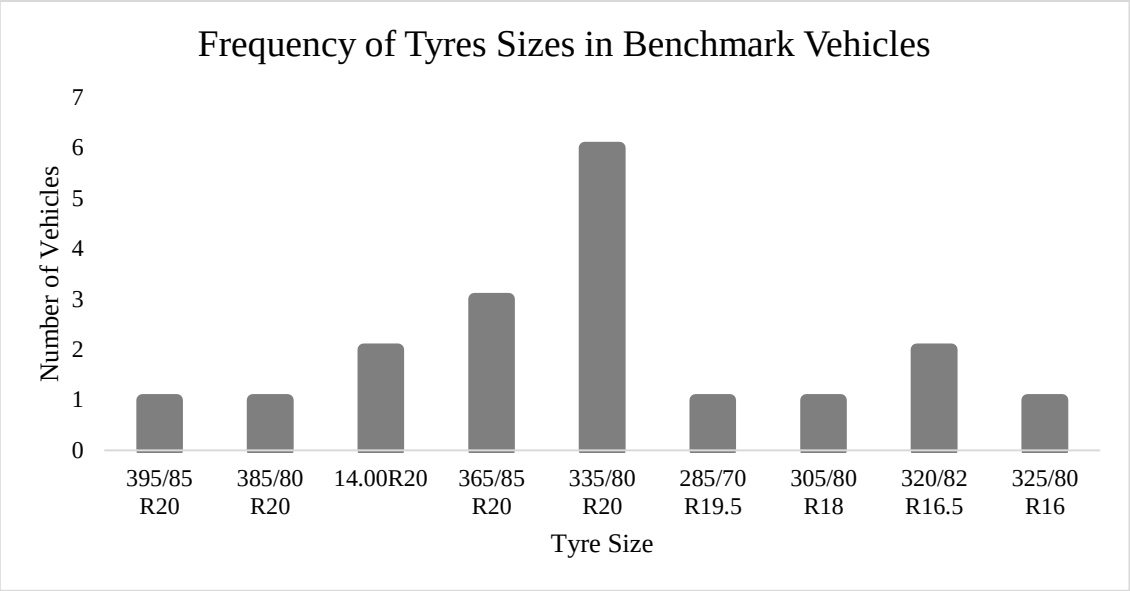

Fig. 32. Frequency of Tyre Sizes in analysed vehicles

The benchmarking reveals a clear dominance of 20-inch wheel diameters among similar military off-road vehicles. Although we notice a variety of tyre width and profile combinations, the vast majority of platforms use a few standardized R20 tyre design choices.

It appears that the 20-inch wheel diameter strikes a typical engineering trade-off between load capacity, durability, and terrain adaptability to have it considered as a good baseline assumption in the architectural definition stage.

4.2.4 Powertrain Demands Indicators

To understand the propulsion demands associated with increasing vehicle mass, the relationship between gross vehicle weight and required drivetrain torque was analysed across the benchmark set, and the results are shown in Figure 33.

This comparison provides a first-order indication of traction requirements relevant for preliminary powertrain concept evaluation.

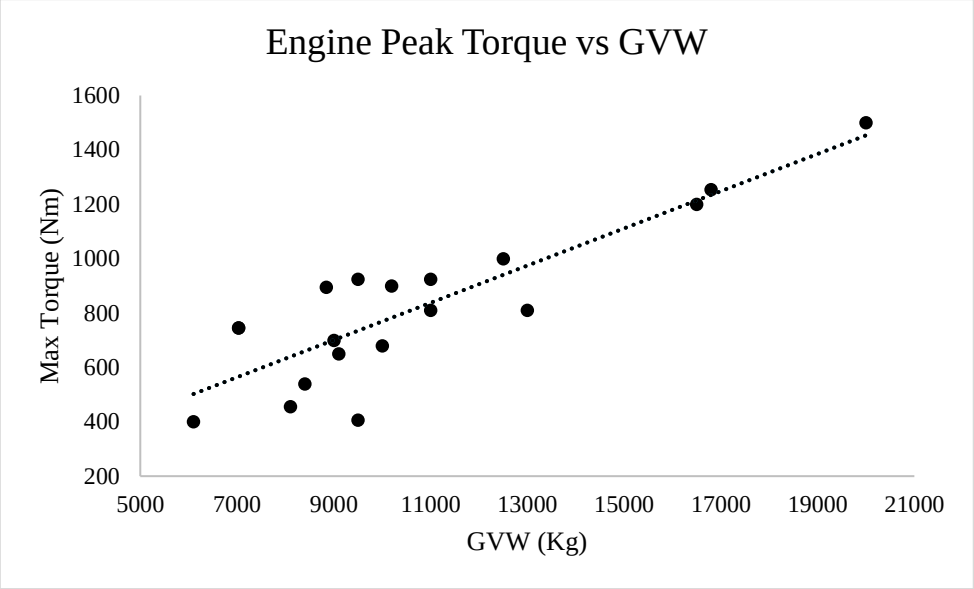

Fig. 33. Engine Peak torque as a function of GVW

The benchmarks reveal a strong positive correlation between vehicle gross weight and the required maximum drivetrain torque. Heavy-weight platforms, as expected, require more torque to maintain tractive performance, especially in off-road conditions. Torque values are usually between 500 Nm and 900 Nm for medium-weight platforms in the benchmark dataset, which is the most commonly detected cluster among comparable vehicles.

This range should serve as an initial reference for sizing purposes and underscores the large torque requirements that are anticipated when assessing alternative drivetrain concepts such as wheel integrated electric motors. Note that the reported torque values correspond to a peak engine output value provided by manufacturers.

Because transmission and differential torque multiplication gives the actual torque at the wheel much higher. Unlike in theoretical models, detailed drivetrain ratio data is not traditionally available and thus not covered in this benchmark analysis.

Nevertheless, even accounting for this limitation, the size of the observed engine torque values highlights one of the fundamental constraints of wheel-integrated powertrain offerings: similar torque levels placed directly at the wheel are capable of imposing significant restrictions on motor packaging, thermal management and structural robustness.

4.3 Concept Evaluation and Trade-Off Analysis

Following the benchmarking analysis presented in *section 4.2*, a set of architectural parameters and system configurations were identified as relevant for defining the baseline vehicle concept.

The purpose of this section is to structure together these alternatives, and narrow them down to the range of possible design choices and to choose preliminary system configurations. There are two evaluation methods depending on the nature of each parameter (in our example they will be:

- Quantitative range definition directly based on benchmarking trends, like dimensions or packaging indicators. ·
- Concept comparison using decision matrices introduced in section 3.5.

We use selection and weighted scoring matrices only in key architectural decisions where trade-offs between performance, complexity, durability, and integration exist. The parameters that would have statistically well-studied clustering are defined from benchmark ranges alone.

4.3.1 Dimensional Envelope Definition

The dimensional envelope of the vehicle was defined based on the trends observed in the benchmarking analysis. Unlike discrete architectural concepts, dimensional parameters represent continuous design variables and therefore do not require formal concept selection matrices. Instead, representative value ranges were identified from the clustering behaviour of comparable platforms.

These ranges provide the geometric boundary conditions for the subsequent architecture definition and ensure consistency with established vehicle proportions within the analysed segment. Table 6 shows the preliminary dimensional envelope definition.

Parameter	***Selected Range***	***Basis***
Wheelbase	3000–3500 mm	Wheelbase vs GVW values
Track width	1800–2100 mm	Stability / packaging trends
Total length	5000–6200 mm	Length vs GVW distribution
Ground clearance	380–430 mm	Mobility capability common range
GVW	7000–10000 kg	Benchmark overlap

Table 6. Benchmark-derived dimensional ranges

The identified ranges do not represent final design values but define a feasible solution space within which subsequent architecture decisions will be made. The final parameter selection will be carried out in Section 4.4 once system-level trade-offs have been evaluated.

4.3.2 Suspension Architecture Evaluation

As identified in the benchmarking results, the suspension and axle architectures commonly adopted in comparable off-road vehicles include independent suspension, semi-independent

configurations, rigid axle with coils springs, rigid axle with leaf springs, and pneumatic suspension systems.

Due to the presence of multiple viable alternatives with different performance and integration trade-off, the selection of baseline architecture cannot rely solely on statistical observation. Therefore, a structured concept evaluation is performed using the screening and weighted scoring matrices described in Section 3.5.

Table 7 presents the evaluation criteria and assigned weights used to compare the candidate suspension concepts.

Criteria	***Weight***
Off-road mobility	20
Load capability	15
Durability	15
Mechanical simplicity	10
Maintenance	10
Integration complexity	10
Cost	20

Table 7. Suspension Architecture evaluation criteria

Once the selection of criteria and their weights has been defined, we can start the evaluation using the screening matrix (see Table 8).

Criteria	***Independent***	***Rigid + Coil***	***Rigid + Leaf***	***Pneumatic***
Off-road mobility control	+	0	−	+
Load capability	0	+	+	0
Durability	+	+	+	−
Unsprung mass impact	+	0	−	−
Packaging flexibility	+	0	−	−
Maintenance complexity	−	0	+	−
Integration complexity	+	0	−	−
Cost suitability	−	0	+	−
Sum +	5	2	4	1
Sum −	2	0	4	6
Net Score	**3**	**2**	**0**	**-5**

Table 8. Suspension evaluation, screening matrix

Based on the screening matrix results, we have rejected the rigid + leaf and pneumatic systems. We will now carry out the final analysis between the independent and the rigid + coil suspension systems, using the weighted matrix shown in *Table 9.*

The remaining suspension concepts are evaluated using a weighted scoring matrix. A qualitative 1-5 rating scale was adopted, where 1 represents very poor performance and 5 represents excellent performance relative to each evaluation criterion. Ratings are assigned based on engineering judgment supported by benchmarking observations and known characteristics of each architecture.

		Independent suspension		***Rigid + Coil Suspension***	
Criteria	**Weight**	Weight	Score	Weight	Score
Mobility control	0.20	5	1.00	3	0.60
Load capability	0.20	3	0.60	5	1.00
Durability	0.15	4	0.60	5	0.75
Unsprung mass	0.15	5	0.75	3	0.45
Packaging flexibility	0.10	4	0.40	3	0.30
Maintenance simplicity	0.10	3	0.30	4	0.40
Cost suitability	0.10	3	0.30	4	0.40
TOTAL SCORE			**3.95**		**3.9**

Table 9. Weighted suspension matrix

The scores also emphasize several important performance variations between the two ideas. Mobility control ratings for independent suspension were higher, owing to better wheel articulation and better terrain conformity seen on benchmark platforms. It also performed better in relation to unsprung mass effects, which enhance ride dynamics and obstacle negotiation capabilities.

By contrast, the rigid axle with coil springs scored higher on load carrying capacity and durability, reflecting its structural simplicity and proven use in heavy-duty applications. These two opposing aspects account for the close total scoring results obtained by these two concepts.

From the weighted idea scoring it shows that independent suspensions score as best in scale overall, because they allow superior mobility control and reduced unsprung mass, which are critical for off-road performance. In contrast, the rigid axle with coil springs shows high load capacity, durability and cost-effectiveness, and hence an extreme similarity between the previous two.

The minor difference in design indicates both architectures are not completely dominating the design domain. Instead, the two offer advantages in varying performance domains. Therefore, the results suggest an application of hybrid suspension design where independent suspension is used

on the front axle to provide for higher steering and mobility performance and a rigid coil-spring axle is connected at the rear to increase load capacity and structural integrity.

4.3.3 Running Gear Configuration

This subsection analyses the vehicle running gear elements arrangement based on the benchmarking observations and the engineering feasibility. Axle layout philosophy, tyre standardisation, and braking architecture trends were addressed as a means to test and develop homogeneous system assumptions for the basic vehicle definition.

4.3.3.1 Axle Configuration Philosophy

Results of benchmarking suggest that both independent and rigid axle arrangements are used most frequently, according to the requirements of the mission and load. Referring to the suspension concept chosen in Section 4.3.2, a mixed axle philosophy is adopted.

- Independent front axle to enhance steering precision and terrain adaptability.
- Rigid rear axle increases load capacity and structural robustness. Independent front axle to enhance steering precision and terrain adaptability.

4.3.3.2 Tyre Standardization Context

Benchmark analysis showed strong industry convergence towards 20-inch wheel diameters for comparable vehicle classes.

In the present project, tyre size selection is constrained by project-level standardization requirements, resulting in the adoption of 14.00 R20 tyres as the baseline reference.

This constraint is treated as a boundary condition rather than an outcome concept evaluation, and is therefore propagated into subsequent architecture definition steps.

4.3.3.3 Brake Architecture Assumptions

The benchmarking dataset shows near-universal adoption of ventilated disc braking systems across comparable vehicle platforms, regardless of axle architecture.

As can also be observed in the data tables presented in Appendix A, the large majority of analysed vehicles employ disc brakes systems with hydraulic actuation. This reinforces the observed industry convergence towards this solution within the considered vehicle class.

Given this clear trend and the absence of competing viable alternatives within the benchmark set, disc brake systems are assumed as the baseline braking architecture for the conceptual vehicle definition. Detailed sizing and actuation strategy are considered outside the scope of this system-level study.

4.3.3.4 Wheel-End Integration Assumptions

At this stage, the wheel-end is treated as a modular mechanical interface integrating:

- Brake system
- Bearings
- Hub structure
- Future drivetrain interface

No detailed geometric design is performed; however, maintaining packaging neutrality is important to preserve compatibility with the wheel-integrated powertrain concept evaluated later in this thesis.

4.3.4 Summary of Selected Parameter Ranges

These benchmarking trends, the observed dimensional clusters, and the concept evaluation matrices presented in the previous sections suggest setting out a range of feasible parameter ranges and architectural options.

At this stage, the objective is not to define final vehicle values, but to delimit the technically viable solution space within which the baseline architecture will be selected in the following chapter. These ranges correspond to configurations found in similar off-road platforms practiced by the industry to ensure that preliminary mission and performance assumptions for the project are satisfied.

Table 10 presents the viable dimensional envelopes, system configurations, and component architectures derived from the benchmarking and trade-off analyses. These ranges and options constitute the engineering design space used to guide the baseline mechanical architecture definition.

PARAMETER	VIABLE RANGE / OPTIONS	BASIS
GVW	7000 - 10000 kg	Project definition
WHEELBASE	3000 – 3500 mm	Benchmark overlap
TRACK WIDTH	1800 – 2150 mm	Stability clustering
TOTAL LENGTH	5000 – 6200 mm	Dimensional trends
GROUND CLEARANCE	380 – 430 mm	Mobility benchmarking
TYRES	14.00 R20	Supervisor input / industry prevalence
SUSPENSION ARCHITECTURE	Independent / Rigid axle (coil)	Matrix evaluation

AXLE TYPE	Independent front / Rigid rear viable	Trade-off outcome
BRAKE TYPE	Hydraulic ventilated discs	Industry convergence
CHASSIS CONCEPT	Ladder frame compatible	Platform benchmarking

Table 10. Viable Dimensions Envelope

The results demonstrate that multiple architectural solutions remain technically viable within the defined parameter space. Instead of focusing on a single optimal configuration, the trade-off analysis illustrates mobility performance vs. structural robustness vs. integration complexity vs. cost.

As a result, the subsequent chapter moves from defining solution-space to choosing a representative baseline mechanical architecture, in which particular parameter values and configurations are selected in order to facilitate the development of conceptual vehicle layouts and further engineering exploration.

4.4 Selected Baseline Mechanical Architecture

4.4.1 Selection Rationale

Following the benchmarking analysis and the definition of feasible parameter ranges presented in Sections 4.2 and 4.3, a representative baseline mechanical architecture is established in order to enable conceptual vehicle layout development and preliminary system integration work.

The selected values should not be interpreted as a final design specification. Due to the early stage of the project and the limited availability of detailed system constraints, the parameters defined in this section serve as engineering reference targets required to progress with conceptual modelling and evaluation activities.

When the dimensional values chosen are selected, they will be representative points in a range of what can be produced on the basis of the available feasible ranges instead of statistical averages. These design goals can be made to create a more coherent vehicle architecture to build on in the future in a way that can be improved in later development phases.

Therefore, the resulting configuration should be considered by the reader as a conceptual baseline architecture that is subject to change when subsystems are defined and packaging and operational requirements are determined. The parameter ranges established earlier will remain the primary validity envelope within which future iterations should remain aligned.

4.4.2 Baseline Dimensional Definition

The baseline dimensional parameters selected for the conceptual vehicle architecture are summarized in Table 11. These representative values define the geometric reference envelope used for subsequent layout development and system positioning.

PARAMETER	BASELINE VALUE	UNIT	BASIS
GROSS VEHICLE WEIGHT (GVW)	7000 - 10000	kg	Benchmarking range
MAX PAYLOAD PER WHEEL	2500	kg	Benchmarking range
WHEELBASE	3250	mm	Benchmarking clustering (section 4.2.1)
TRACK WIDTH	2150	mm	Benchmarking clustering (section 4.2.1)
TOTAL VEHICLE LENGTH	5500	mm	Benchmarking range (Section 4.2.1)
GROUND CLEARANCE	400	mm	Benchmarking range (4.2.2)
TYRE SIZE	14.00 R20		Project constraints / Industry standard
MAAXIMUM SPEED	110	km/h	Benchmarking range

Table 11.Baseline dimensional parameters for the conceptual vehicle architecture

4.4.3 Baseline Running Gear Architecture

The baseline running gear architecture selected for the conceptual vehicle definition is summarized in Table 12. These configurations establish the mechanical reference framework supporting vehicle mobility, load transfer, and structural integration within the conceptual layout.

SUBSYSTEM	SELECTED BASELINE CONFIGURATION	ALTERNATIVE CONSIDERED	SELECTION BASIS
SUSPENSION ARCHITECTURE	Independent front + Rigid axle (coil) rear	Fully independent / Fully rigid axle	Trade-off matrix results (Section 4.3.2)
AXLE CONFIGURATION	Mixed architecture (Independent + Rigid)	Solid axle both ends	Load capability vs mobility balance
BRAKE SYSTEM	Hydraulic ventilated disc brakes	Pneumatic disc systems	Industry convergence (Benchmark Appendix A)
CHASSIS TYPE	Ladder frame structure	Monocoque / Hybrid frame	Benchmark prevalence + packaging flexibility
DRIVETRAIN LAYOUT	4x4 wheel-driven architecture	6x6 o distributed layouts	Project definition

Table 12.Baseline running gear architecture selected for conceptual vehicle definition

Figures 34 and 35 show the side and front views of the vehicle, including some of the key dimensions defined through benchmarking and the applied decision criteria. It should be emphasized that the body representation used in these figures corresponds to the Thales Hawkei vehicle, one of the platforms analysed during the benchmarking process.

These figures do not aim to define the future body design of the prototype, nor the corresponding approach and departure angles, as these are strongly dependent on the body geometry. At this early stage of the project, defining the body structure is neither feasible nor within the scope of this work. The selected model has been used solely at a conceptual level to illustrate the defined geometric parameters.

Nevertheless, it is possible that at later stages these angles may need to be estimated and defined on a hypothetical basis in order to perform certain dynamic calculations that require them.

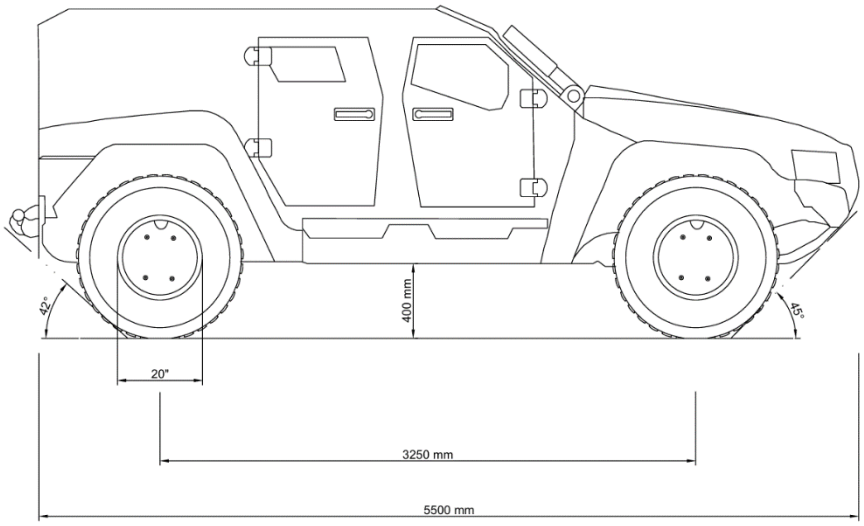

Fig. 34. Side view of benchmark-based vehicle dimensions

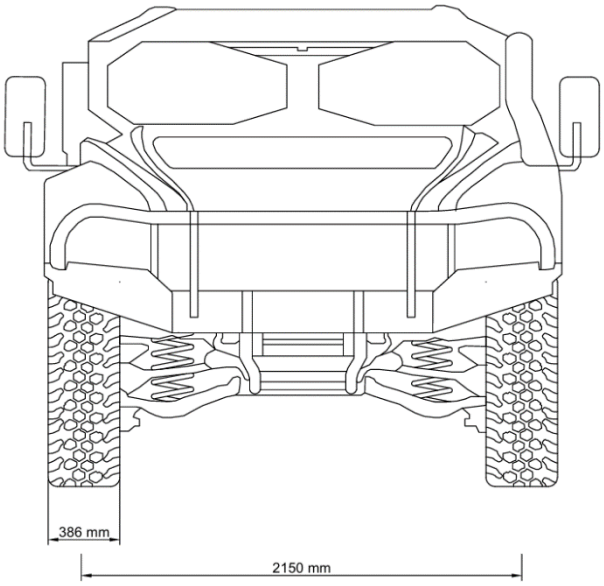

Fig. 35. Front view of benchmark-based vehicle dimensions

This baseline architecture defines the mechanical and dimensional foundations you need to develop your conceptual layout. We excluded details like mass distribution and structural packaging for now. You will determine those parameters once you decide where to position and integrate your subsystems in the next phase.

5. SYSTEM DEVELOPMENT & EVALUATION

In this chapter we present the construction and evaluation of the proposed vehicle systems in accordance with the architecture that was defined in Chapter 4.

The analysis includes several complementary studies, starting from CAD design and development, the total wheel torque when applying some case studies and last of all numerical simulations. These studies were conducted in comparative case studies for the case-study design to show whether or not a conventional wheel can be used with the IWM system and whether it is in effect viable to fit into a specific vehicle concept from here on.

The CAD models developed in this chapter serve as the geometric basis for the subsequent analyses. At the same time, in the case of the IWM, they allow the evaluation of the actual available space for electronic and electrical components. This supports both qualitative and quantitative assessment of the proposed configurations.

5.1 CAD Based System Development

In this section we describe the process to produce CAD models that are simplified to depict the major vehicle subsystems. It is not the intention to replicate a detailed or final design, because the development project is still in the early stage where that would not be appropriate. Rather, geometries should be as realistic and consistent as possible in order to perform system-level analysis and comparison of two configurations, determine as early as possible the initial architecture for the vehicle and narrow down the results.

The modeling approach follows a bottom-up method that is, we treat the wheel assembly primarily as a reference. This decision is due to its critical influence on ground interaction and on the integration of propulsion and braking systems.

5.1.1 Design Approach and Reference Selection

The design begins with the selection of commercial parameters of rim and tire, namely, setting the main constraints of the wheel assembly. By following this approach all the later designs will follow the real components along with dimensions which can be realistically achieved.

The project team has handed us the wheel model to be used, see Figure 19 in Section 3.4. It was from this wheel catalog that the necessary dimensions were determined and the design process began. The CAD model is constructed with the aid of the dimensions and references in the catalog, and is based on real proportions which do not make any random size or packaging assumptions.

The wheel dimensions found directly affect the space available for braking components as well as structural members and IWM-integrated parts.

5.1.2 Wheel and Rim Definition

Wheel dimensions, e.g., diameter, width, and rim size define the internal volume available for component integration. These dimensions serve as a reliable reference to assess the feasibility of the IWM and for comparative study with the conventional system. The CAD model includes a simplified representation of the tire and rim, focusing on the dimensions that are relevant for system-level analysis. Features like tread patterns or manufacturing details are intentionally omitted because most of them are not relevant if the scope of this inquiry were not to be examined.

Figure 36 shows the CAD model of the chosen wheel, including the shape of the tire along with the rim. As is mentioned, both the rim and the tire have real dimensions. The tread pattern of the tire is a custom design and is inserted only for the sake of colour. The same holds true for rim spokes. In most rims used in heavy vehicles, these are covered for structural purposes primarily due to the loads they have to withstand. Here the design is open but that is purely aesthetic.

Fig. 36. Rim and Tyre CAD

However, a structural analysis will be carried out later to determine whether the rim is in fact supported by the loads applied by the vehicle, even without being fully covered from a structural perspective. On the other hand, figures 37 and 38 show cross-section views of the rim and tire including their main dimensions and measurements.

These views help to better understand the available space, as well as the rim thickness that has been defined. The thickness value has been set based on engineering judgment, since exact industry data was not available.

With these dimensions, a solid basis is established for continuing with the subsequent design stages.

For more detailed information on the designs and dimensions, Appendix C in the Appendices document can be consulted, where all the detailed drawings are provided.

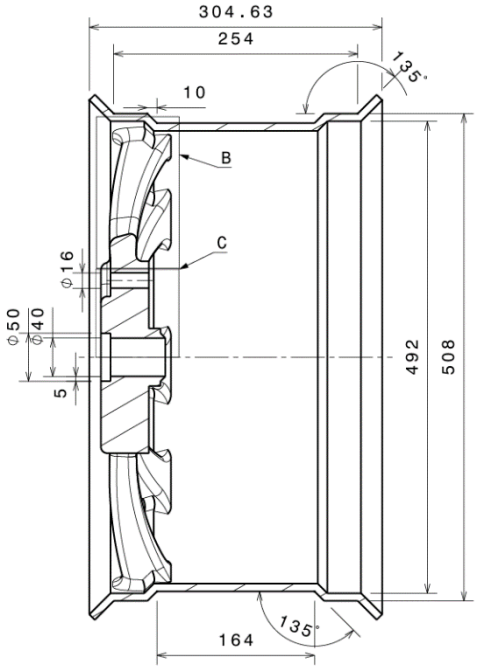

Fig. 37. Sectional view of the wheel rim showing internal packaging volume

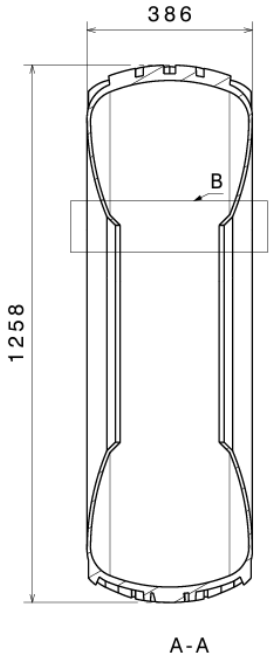

Fig. 38. Sectional view of the wheel tyre showing internal packaging volume

The internal volume defined by the rim diameter directly limits the maximum allowable size of braking and propulsion components.

The resulting geometry serves as the reference for the development of both the conventional wheel-end system and the in-wheel motor configuration presented in the following sections.

5.1.3 Conventional Wheel-End Design

Based on the wheel geometry defined in the previous section, a conventional wheel-end configuration was developed as a reference for comparison.

Figures 39 and 40 show the designed geometry.

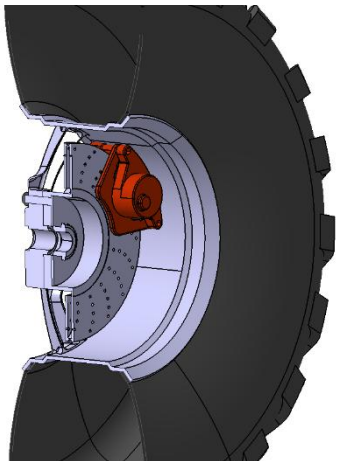

Fig. 40. Sectional view of the conventional wheel-end illustrating internal packaging

Fig. 39. Conventional wheel-end configuration with disc brake assembly

The design comprises a typical braking structure, a brake disc, brake caliper, and brake pads, all integrated within the available space defined by the rim geometry. As a result of the rim having an internal diameter, the brake components dimensions are limited; with such limited dimensions the size of the brake disc can be minimized.

In order to determine the size of the disc, Equation 3 is applied. It is often used in vehicle dynamics and brake engineering to find the biggest possible disc diameter and that the design and development process will not be terminated [51].

$$\varnothing_{max} = \varnothing_{max\,Rim} - 4" \quad \text{Eq. 3}$$

Using this general formula, it is determined that the maximum available diameter for the brake disc is 16".

The caliper is positioned to ensure proper contact with the brake disc while maintaining geometric compatibility with the wheel assembly.

Figure 41 shows two views of the brake disc and caliper geometry used in the conventional wheel-end configuration.

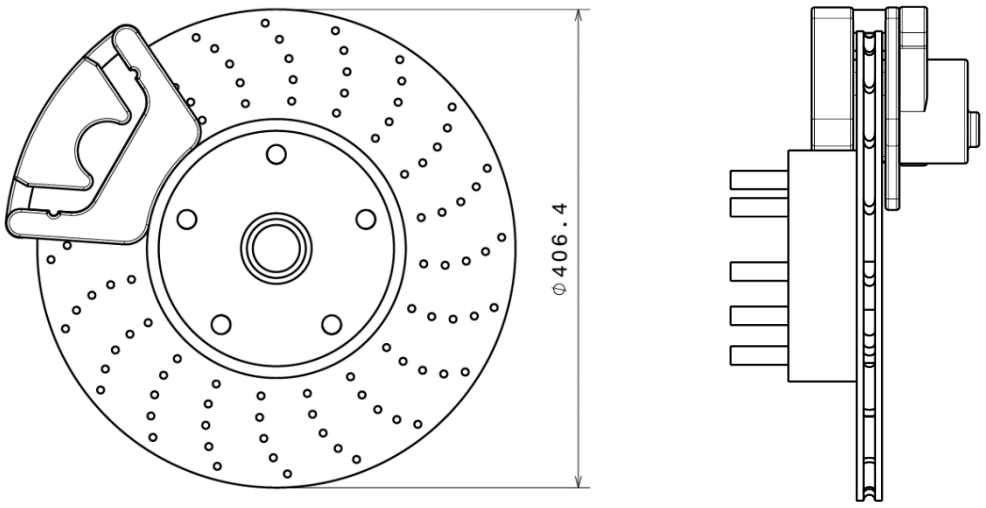

Fig. 41. Orthogonal views of the brake disc and caliper used in the conventional wheel-end configuration

The CAD model is deliberately simplified, omitting secondary features since they are not needed for the braking simulation. But since this design allows heat dissipation, the brake disc has been designed as a ventilated and drilled disc, due to the increased thermal performance of this type of geometry.

It is the most conventional solution as well as the reference case for comparison with the in-wheel motor configuration. The model is also deliberately simplified to represent some important geometric features useful for the analysis, and therefore used to compare the simulation results for both configurations.

5.1.4 IWM Conceptual Design

The definition of the wheel geometry in the previous sections makes it possible to develop the conceptual IWM configuration based on the existing geometric constraints.

Due to the limited availability of public information since most IWM systems are still in prototyping or research stages the present design is developed using an engineering-based approach, relying on the information that is currently available to gain a general understanding of how these systems are being designed today.

The focus of this model is on the mechanical integration of the system and its interaction with the braking components, as these aspects are relevant for the subsequent simulation analysis. Electrical and electronic systems, as well as the hydraulic components of the braking system, are considered outside the scope of this study.

5.1.4.1 Design Approach and Constraints

The design is based on the geometric constraints of the chosen wheel rim, matching a realistic size and the alignment of the wheel assembly. The rim geometry defines the maximum internal volume available to accommodate the IWM system. Due to this constraint, the design is space-driven and attempts to utilize all available volume. A minimal clearance is maintained between the outer rotor housing and the inner surface of the rim, representing a near-limit packaging condition.

This arrangement is a conceptual upper-bound design. In a practical implementation, additional factors including manufacturability, thermal management, and component protection would reduce the usable space inside the wheel. Consequently, the actual system would probably have smaller external and internal dimensions, restricting the size of the integrated components, and it would have implications on the integration of braking and electronic subsystems.

5.1.4.2 System Architecture Definition

Based on the dimensions and geometric constraints defined by the previously selected rim design, the model represents a simplified configuration focused on the mechanical integration of the main functional components within the wheel assembly.

Figure 42 shows how the IWM assembly fits inside the rim. Figure 43 presents the IWM design itself, where the different components that make up the system will be detailed in the following sections.

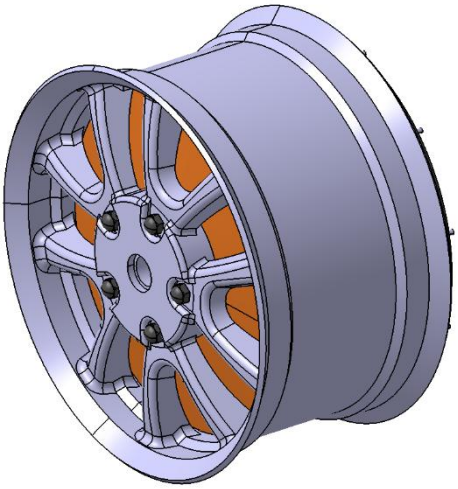

Fig. 42. General Assembly IWM Overview

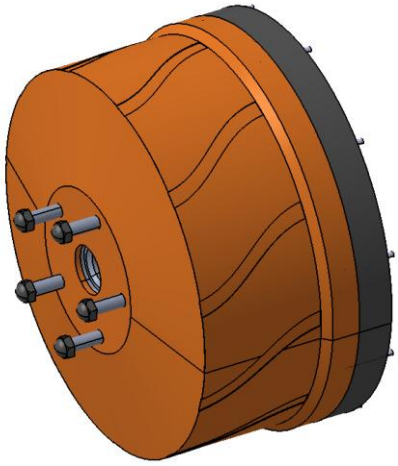

Fig. 43. IWM assembly overview

Figure 44 shows an exploded view of the IWM to illustrate its main components and their relative positioning.

The tire and rim are not shown as the focus is on the internal elements of the IWM. The individual components are not labelled or specified in that figure. Technical drawings included in the appendices are referenced for exact dimensions and full component specifications.

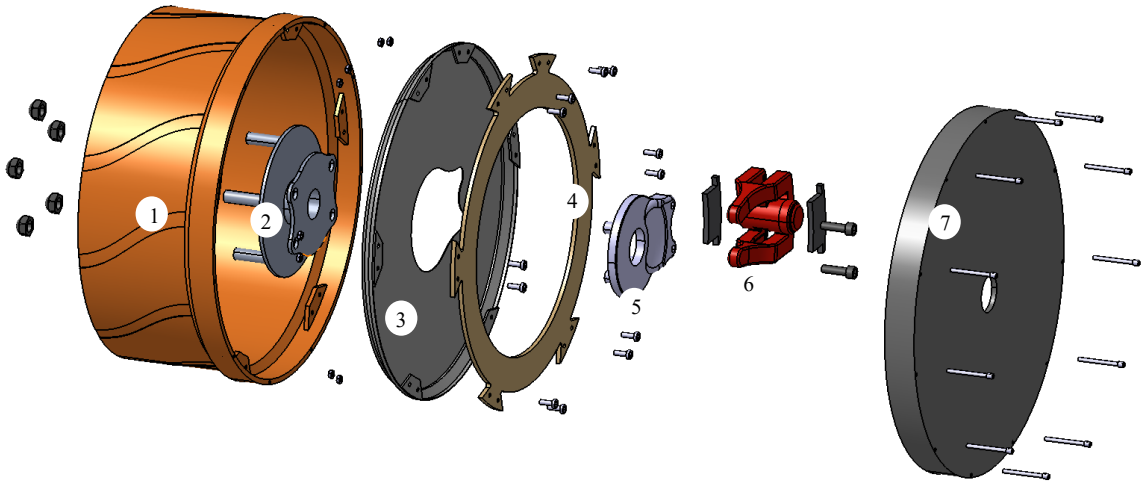

Fig. 44. Exploded view of the IWM assembly

The main components that make up the assembly, as shown in Figure 44 and identified by their corresponding numbers, are listed in Table 13.

NUMBER	DESCRIPTION
1	Outer rotor housing
2	Bearing
3	Protective cover
4	Brake disk
5	Brake support
6	Caliper and brake pads
7	Rotor lid

Table 13. Main Components of the IWM assembly

The rotor is the rotating part of the motor and the brake disc is attached to the housing. The outer part of the bearing is connected with the rim as well as the rotor to rotate them together. The inner side of the bearing is fixed and can act as support for the motor's electronics.

Through these, it can also be connected to the brake caliper support. The purpose of this overview is to provide a very basic overview of the key components and clarify the overall system architecture. Hence, their components outline the main functional structure of the IWM system which provide a synergy between propulsion and braking in the wheel volume available.

Figure 45 provides a cross-sectional view depicting the internal arrangement and function of this wheel, as well as the allocation of functional volumes in the wheel itself. Two main regions can be identified: region 1, which is intended to house the electrical and electronic components of the motor, and region 2, which corresponds to the mechanical area where the braking system is located.

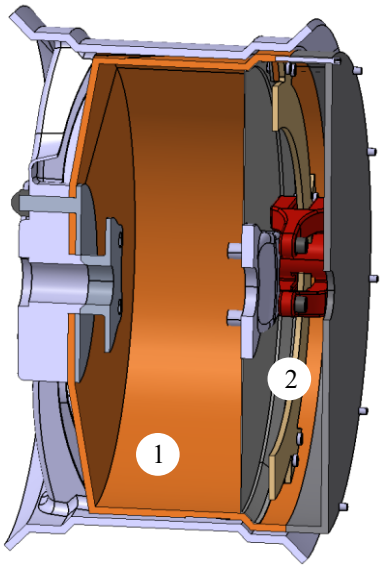

Fig. 45. Sectional view of the IWM assembly

Figure 46 shows a sectional view with some of the main dimensions of the model, as well as the clearance considered between the rotor and the inner surface of the rim. This distance is assumed to be the minimum possible, given that the model has been sized close to its maximum dimensions. In a real manufacturing process, it would likely be necessary to allow for a larger clearance.

With these dimensions, it is easier to understand the available space for the electrical and electronic area that would house the propulsion system.

The presented architecture highlights the packaging constraints associated with integrating the in-wheel motor system. The available volume inside the rim must be shared between propulsion and braking components, resulting in a highly compact configuration.

The minimal radial clearance between the rotor and the inner surface of the rim represents a limit-case condition assumed in this conceptual design. Such tight packaging has direct implications for thermal performance, manufacturability, and component integration.

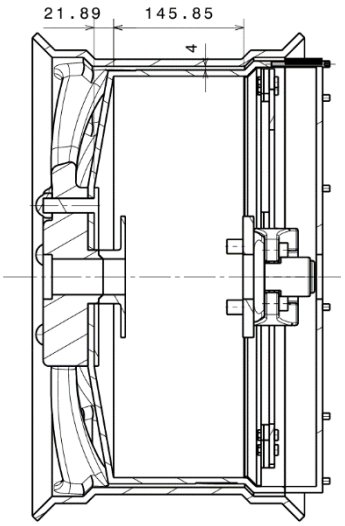

Fig. 46. Sectional drawing of the IWM

The identification of functional zones and component placement provides a geometric basis for the following analytical and numerical evaluations. In particular, the packaging constraints identified in this section will be considered together with the torque requirements calculated in the next section, allowing a first assessment of the system's feasibility.

This configuration can therefore be seen as a boundary-case scenario for packaging feasibility.

5.1.5 Vehicle Layout Integration

While not the entire main aim of this research, we spent enough time to develop a simplified vehicle layout for the dimensional parameters that were derived during the time in which to benchmark and also the IWM simulations are running or active.

We want this model to be a global geometrical representation of the vehicle architecture, showing the way in which the different subsystems described above, including the wheel assemblies, will be integrated into a coherent structure.

The layout is constructed using the main dimensions obtained from the benchmarking analysis, to give consistent size of the vehicles. The inclusion of wheel assemblies with their actual dimensions allows for a more accurate representation of the spatial constraints affecting the overall architecture. The frame rails' colours, represents the type of material that the chassis would be made of.

The resulting CAD model shown in the figure 47, represents a simplified chassis structure integrated with the wheel systems. The model focuses on capturing the main geometric relationships in order to make easier to understand how the proposed dimensions could look like

in a 3D model rather than detailed structural design because in this early-stage phases it is not realistic and worth it.

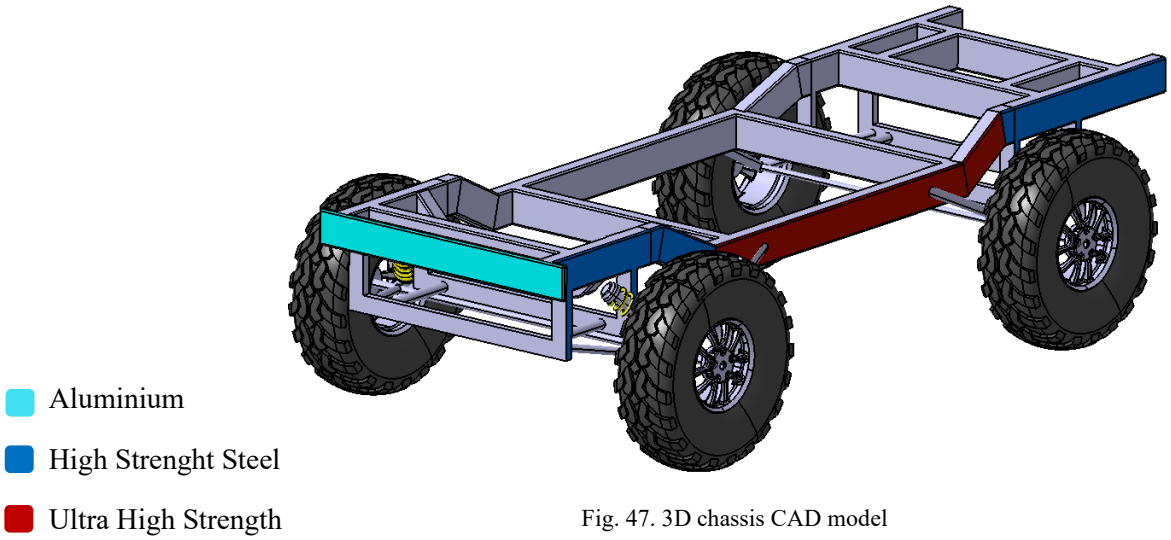

Fig. 47. 3D chassis CAD model

It should be noted that this model does not correspond to a detailed chassis design. Instead, it serves as a conceptual representation intended to support the visualisation of the vehicle architecture and provide a physical context for the previously developed subsystems.

Figure 48 shows a plan view with the main overall dimensions of the vehicle, as well as its structural layout.

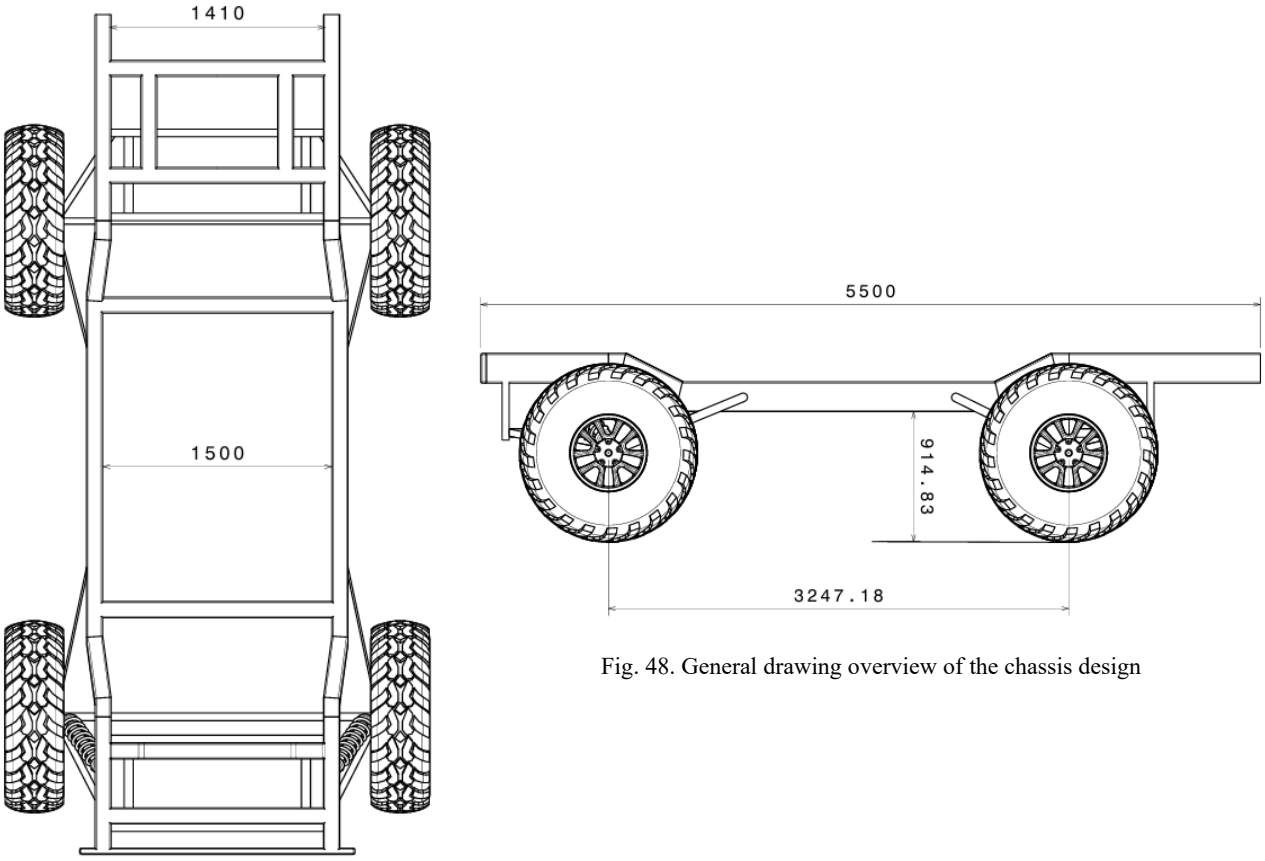

Fig. 48. General drawing overview of the chassis design

For detailed dimensions and further geometric specifications of the vehicle layout, reference is made to the technical drawings provided in the appendices. This vehicle-level integration completes the CAD-based development presented in this chapter, providing a consistent geometric basis for the designs that will be evaluated analytically and numerically in the following sections.

Together, the CAD models developed in this chapter establish the geometric and architectural foundation required for the subsequent feasibility assessment of the proposed IWM concept.

5.2 Wheel Torque Requirement Estimation

This section presents the estimation of the wheel torque demand under extreme operating conditions representative of the defined mission profile. The objective is to determine the maximum tractive effort required at wheel level to assess whether an in-wheel motor configuration can realistically satisfy these demands. Although primarily used for IWM feasibility, torque results are drivetrain-independent and therefore relevant for alternative propulsion concepts

The analysis is based on first-order longitudinal vehicle dynamics equations commonly used in transmission and mobility studies. Several sever scenarios are considered, including high-grade climbing, low-speed launch on steep slopes, and reduced wheel-ground contact conditions.

5.2.1 Modelling Approach and Baseline Definition

In order to estimate the wheel torque demand under severe operating conditions, a first-order longitudinal vehicle model is adopted. The vehicle is modelled as a rigid body subjected to forces acting along the direction of motion.

The goal of this model is to be able to know which tractive force to overcome the resistive forces during uphill driving and launch activities. Figure 49 shows how the forces act on the vehicle as it enters an inclined area of surface (wheeled level). The simplified free-body diagram illustrated in Figure 50 will be used for calculation of the study cases and the forces are included in the analysis. These include the gravitational force, rolling resistance, aerodynamic drag, and inertial forces when the vehicle accelerates. In this case, it is considered also the pressure forces of motion at lower levels in order to keep the vehicle pointing in the direction; and if it should accelerate the system with little force to be able to overcome the gravitational force, the force acting on the vehicle that acts on the air or the roll of the vehicle in the same direction will not be considered.

So, we have to define the total tractive force demand as the sum of rolling resistance, grade resistance, aerodynamic drag, and inertial components.

For a relatively conservative sizing mechanism, the mass of the vehicle is assumed to be maximized in its gross weight (GVW) mode and air density is constant. At this stage, transient effects of load-transfer are not considered as our target is to calculate initial torque.

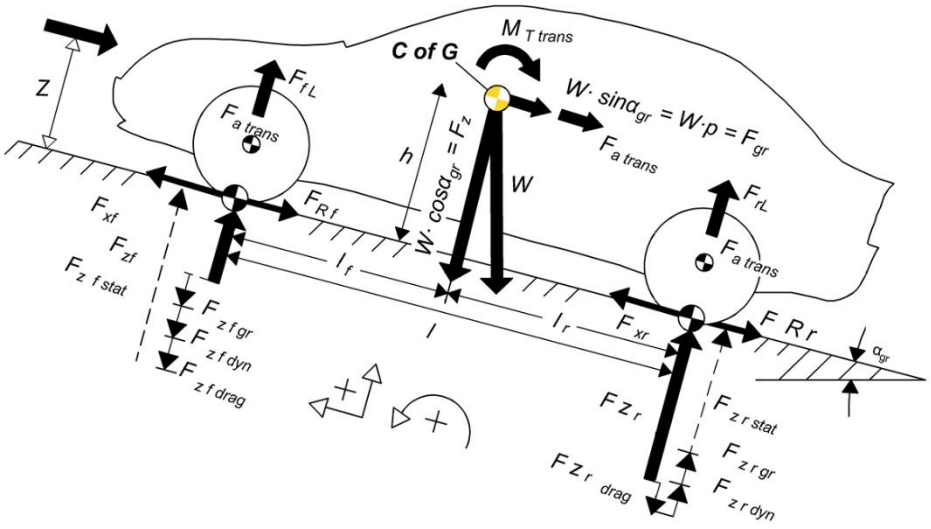

Fig. 49. Free Body Diagram of the forces acting on the vehicle

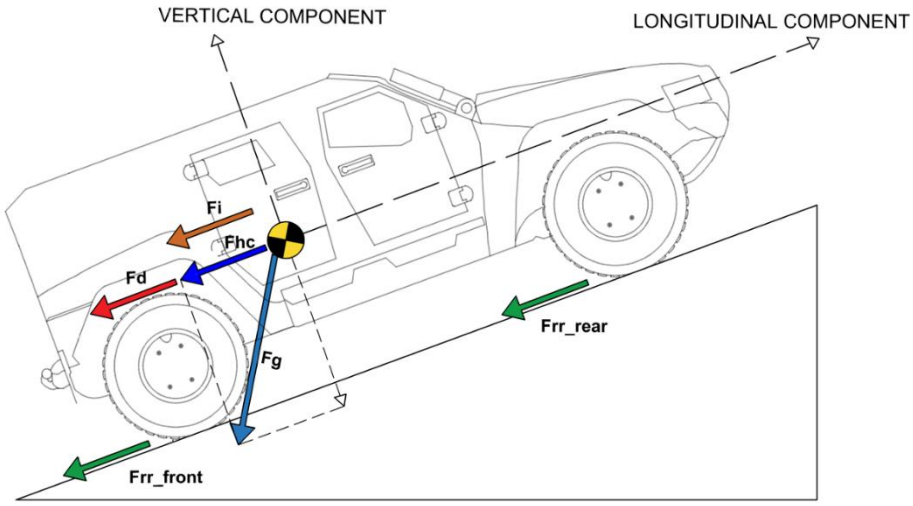

Fig. 50. Simplified Free Body Diagram of the vehicle on an inclined plane

Baseline parameter values are defined based on benchmarking results and literature references. These parameters serve as the reference configuration for the subsequent operating scenarios and sensitivity analysis.

5.2.2 Governing Equations

To carry out this study, first-order longitudinal vehicle dynamics equations are used, commonly applied in transmission and mobility calculations.
Our objective is to calculate the total theoretical traction force required in certain complex and demanding off-road situations and, in this way, also determine the theoretical torque that each wheel should deliver to overcome those conditions.
Equation 3 shows the formula for calculating this total traction force, which depends on the resistive forces opposing motion in each specific study case or scenario, as well as on the dynamic tire radius. On the other hand, Equation 4 shows how the torque to be delivered by each wheel will be calculated once the total value has been obtained.

$$T_{Total\ wheels} = F_R \cdot R_{dyn} \quad \text{Eq. 3}$$

$$T_{wheel} = \frac{T_{total\ wheels}}{N^{\underline{o}}_{wheels\ in\ contact}} \quad \text{Eq. 4}$$

Where F_R represents the resistive forces that must be determined and that will vary depending on the study case.

Thus, the dynamic radius specified in the Michelin catalog mentioned above will be used, and this value will be considered for the calculations. However, if it were necessary to calculate it, Equation 5 shown below would be used:

$$R_{dyn} = \frac{(A \cdot \frac{Rasp}{100} + \frac{R}{2} \cdot (25{,}4)}{1000}\ (mm) \quad \text{Eq. 5}$$

Where A is the tire width, R_{asp} is the tire aspect ratio, and R is the tire radius. However, as previously mentioned, it is not necessary to use this expression, since the catalog taken as reference for the calculations specifies a value of 578 mm.

It is now important to define which types of forces will be considered in the calculation of the resistive force. Equation 6 presents all the possible forces that may act in the study cases that will be analyzed later.

$$F_R = F_{rr} + F_d + F_{hc} + F_i \quad \text{Eq. 6}$$

Where F_{rr} is the rolling resistance force, F_d is the aerodynamic drag force, F_{hc} is the hill-climbing force, and finally, F_i is the inertial force.

Equations 7, 8, 9, and 10 presented below show how these forces are calculated and the parameters involved in each of their respective expressions.

$$F_{rr} = \mu_R \cdot m \cdot g \cdot cos\ (\alpha) \quad \text{Eq. 7}$$

$$F_d = \frac{1}{2} \cdot v^2 \cdot \rho_{air} \cdot C_x \cdot A_f \quad \text{Eq. 8}$$

$$F_{hc} = m \cdot g \cdot sin\ (\alpha) \quad \text{Eq. 9}$$

$$F_i = m \cdot a \quad \text{Eq. 10}$$

These equations are sufficient to calculate the wheel torque required to overcome the scenarios that will be studied and specified later.

5.2.3 Studied operating scenarios

5.2.3.1 Parameter selection rationale

Once the necessary equations to perform the calculations have been defined, it is important to establish the parameters that will be considered in the study, explain how they are selected, and justify the reasons for their selection.
The first and one of the most important parameters is the rolling resistance coefficient. Rolling resistance is the resistive force acting on a wheel when it is rolling. So the significance of this

resistance depends on many factors that are simultaneous, which in general cannot be clearly separated. The most common causes for rolling resistance acting on a moving wheel are tire deformation, friction between the tire and the road surface, aerodynamic friction around the wheel, and road surface deformation [52]. Figure 51 shows the rolling resistance force diagram of the wheel.

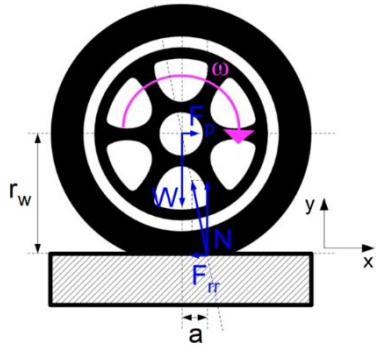

Fig. 51. Rolling resistance wheel forces diagram [52]

As stated above, this coefficient depends on many factors. We can see in Figures 52 and 53 the variation in the coefficient and the rolling resistance force as a function of the vehicle speed and the tire load.

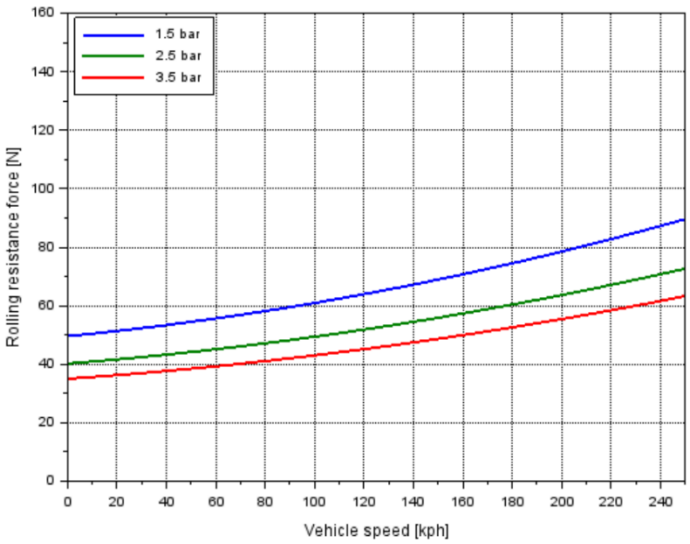

Fig. 52. Rolling resistance force variation depending on vehicle speed [52]

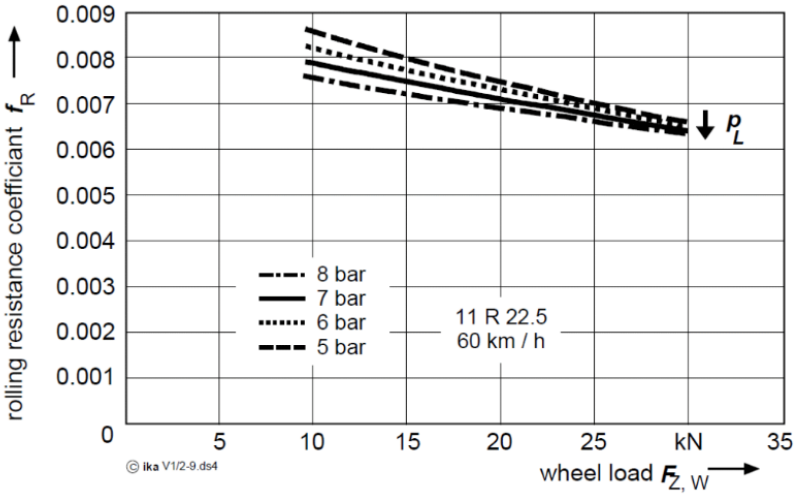

Fig. 53. Rolling resistance coefficient variation depending on wheel load and wheel pressure [52]

Since such specific data are not available, a reference coefficient will be assumed based on the terrain condition, using values obtained from low-speed studies, as shown in Table 14.

Pavement Type	*Rolling Resistance Coefficient*
Good asphalt or concrete pavement	0.01 - 0.018
General asphalt or concrete pavement	0.018 - 0.02
Gravel road	0.02 - 0.025
Good gravel road	0.025 - 0.030
Pebble potholes pavement	0.035 - 0.050
Pressed dirt road (dry)	0.025 - 0.035
Pressed dirt road (rainy)	0.050 - 0.150
Muddy dirt road	0.1 - 0.25
Dry sand	0.1 -0.3
Wet sand	0.060 -0.150
Icy roads	0.015 - 0.030
Compacts sky track	0.030 - 0.050

Table 14.Rolling resistance coefficient of a vehicle at low speed on a given road [52]

Therefore, the coefficient selected to perform the study and simulate highly unfavorable conditions will be 0.25, representing a muddy dirt terrain.

Another parameter to be considered, in this case for the calculation of the aerodynamic force, is the drag coefficient. This resistance coefficient is mainly governed by the vehicle's body architecture and surface finish. Figure 54 shows the correlation of the drag coefficient as a function of vehicle speed for different types of vehicles.

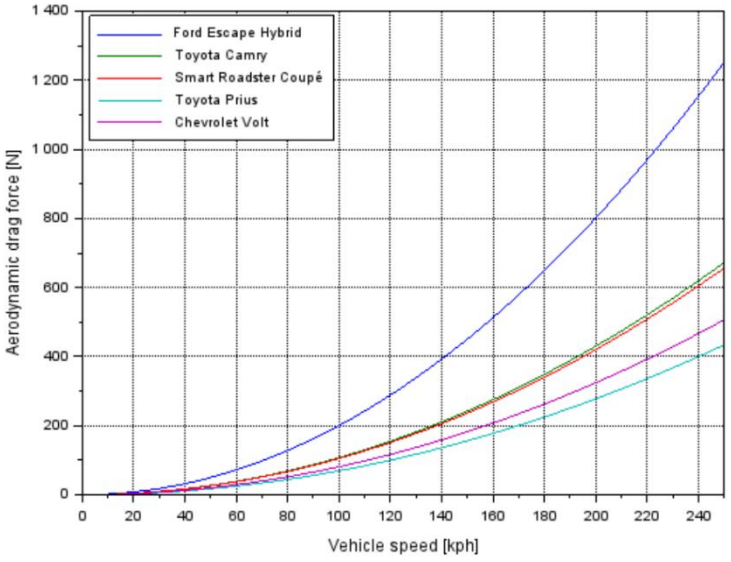

Fig. 54. Aerodynamic drag force for several vehicles [77]

As shown in Figure 54, at low vehicle speeds the force generated by aerodynamic drag is very small and varies only slightly. Nevertheless, it will still be considered in the analysis.
Estimating a reliable drag coefficient is not easy, as quite a few car manufacturers disclosed this value to their users. Table 15 lists drag coefficients of a few vehicles identified based on extensive literature and a search of available data sets.

Model	*Drag coefficient*	*Source*
Jeep Wrangler TJ	0.55-0.58	[53]
Land Rover Defender 2020	0.38	[54]
Toyota Hilux 2022	0.394	[55]
Hummer H2	0.64	[56]
Truck	0.6	[57]
Truck trailer	0.7	[57]

Table 15. Drag coefficient for different vehicles

As seen in Table, large military/tactical vehicles usually operate within a conservative drag coefficient range of approximately 0.6±0.2 CD. For the same reasons, we consider the conventional drag coefficient value of the calculations to be CD = 0.6 C.

The last parameter to be discussed, which determines the aerodynamic force, is the maximum frontal area of vehicles (m^2). Although the vehicle is often supplied by the manufacturer, a reference grid can be computed for this (corresponding with Figure 55 below).

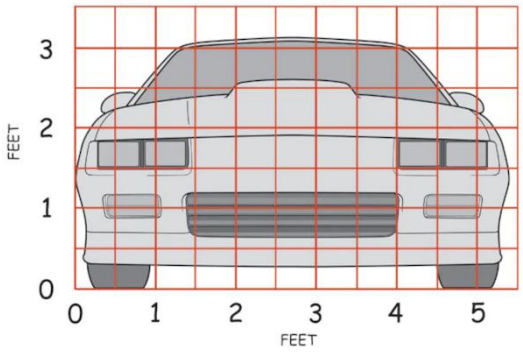

Fig. 55. vehicle frontal area approximation [77]

In this study, we will use the formula estimated approximately. However, the vehicle's architecture and dimensions are not known yet since we're still very early in the process. Consequently, the selection of these different dimensions based on the measurement from benchmarking is given only by the comparison.
Equation 11 shows how this frontal area can be theoretically calculated.

$$A_f = B \cdot H \cdot C_s \qquad \text{Eq. 11}$$

Where B is the vehicle width, H is the vehicle height, and Cs is a shape factor that corrects for gaps, exposed wheels, and geometric details that are not captured by a simple rectangular projection.
This value is theoretical and used as an approximation. However, practical engineering sources recommend values in the range of 0.85–1.00 for large off-road vehicles, 4×4 vehicles, or armored vehicles, reflecting their boxy geometry and flat surfaces.
For this study, a baseline value of Cs=0.95 will be adopted [58].

The final parameter to be defined is the vehicle acceleration. Due to the early stage of the project, it is not yet possible to determine the expected acceleration performance of the vehicle.
Finding reliable acceleration data for comparable vehicles is challenging. However, some reference data have been found. For example, VPK-233136 "Tigr" accelerates from 0 to 100 km/h in approximately 23 seconds [59] or UAZ-452 Ambulance, which accelerates from 0 to 100 km/h in approximately 34 seconds [60]. Thus, when considering the speed of the VPK reference vehicle and setting the target speed, the average acceleration of the vehicle is determined using equation 12 and will also be used for the subsequent calculations.

$$a = \frac{\Delta v}{t} \qquad \text{Eq. 12}$$

$$a = \frac{100\frac{km}{h} \cdot \frac{1h}{3600s} \cdot \frac{1000m}{1km}}{23s} = 1{,}21\ m/s^2$$

The value of acceleration used in the calculation will be 1.21 m/s2.

Lastly, it should be noted that, after setting the parameters, a sensitivity analysis will be performed during the calculations by varying their values by ±5%, ±10%, and ±20%. It enables graphical consideration of their influence on the resulting forces and whether small percentage variations produce significant changes in the calculated force values for the scenarios under study.

5.2.3.2 Studied Scenarios

Selection of the evaluation scenarios is done to get to the most critical possible scenario and for realistic, not purely theory. The scenarios are designed to provide characteristics, which correspond to real-world processes.

- ***Case 1***

Case 1 is the calculation of the required wheel torque to overcome a 60% slope gradient starting from the slope base at the rate of 4 m/s shown in Fig 56.

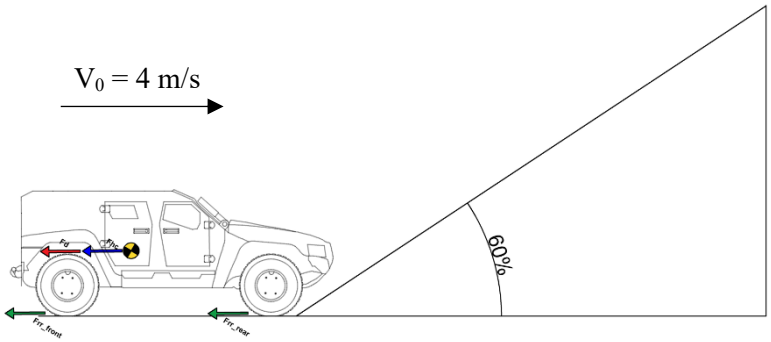

Fig. 56. Case 1 Torque Requirement Study Condition

- ***Case 2***

Case 2 consists of overcoming a slope with a lower gradient, in this case 30%, starting from the base of the incline with a higher initial speed of 11 m/s, as it shows the figure 57.

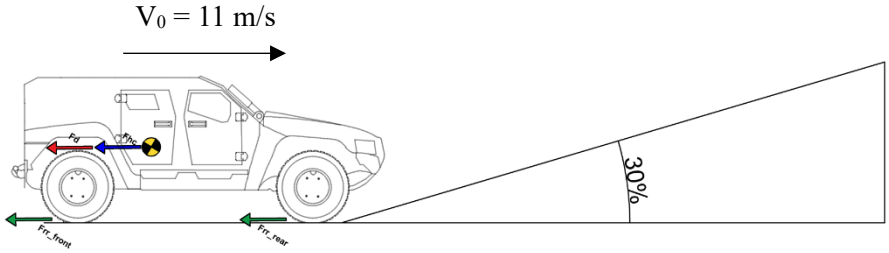

Fig. 57. Case 2 Torque Requirement Study Condition

- ***Case 3***

Case 3 evaluates the torque required when the vehicle starts from rest on a 60% slope and must initiate motion under these conditions and successfully overcome the incline, as it is shown in the figure 58.

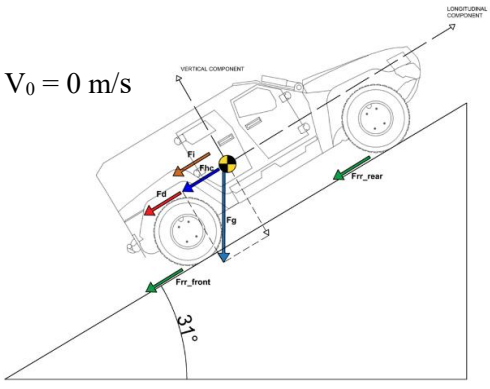

Fig. 58. Case 3 Torque Requirement Study Condition

- ***Case 4***

Case 4 compares conditions from Case 2 and Case 3. The vehicle is on a 30% slope, but in these conditions, two of those four wheels are suspended in that position, so it has to start moving from this position. It means only two wheels deliver the needed torque to overcome the situation that exists here. Figure 59 gives an example of a vehicle facing such a situation. Recall that it is an extreme case and not what the vehicle will typically experience in the majority of all operating situations.

Fig. 59. Case 4 Torque Requirement Study Condition

5.2.4 Results

This section presents the calculation procedure for each of the defined cases, as well as the corresponding results.

- ***Case 1***

Table 16 presents the data used for the calculation of this case.

DATA	
Mass (kg)	8000
Gravity (m/s^2)	9,81
Rdyn (mm)	578
Slope α (%)	60
μR	0,25
ρair (kg/m^3)	1,204
Af (m^2)	4,83
C_S	0,95
C_X	0,6
Velocity (m/s)	4

Table 16. Case 1 – Torque Calculation Data

$$F_d = \frac{1}{2} \cdot v^2 \cdot \rho_{air} \cdot C_X \cdot A_f$$

$$F_d = \frac{1}{2} \cdot 4^2 \cdot 1{,}204 \cdot 0{,}6 \cdot (4{,}83 \cdot 0{,}95)$$

$$F_d = \mathbf{26{,}52\ N}$$

$$F_R = F_{rr} + F_d + F_{hc}$$

$$F_{rr} = \mu_R \cdot m \cdot g \cdot \cos(\alpha)$$

$$F_{rr} = 0{,}25 \cdot 8000 \cdot 9{,}81 \cdot \cos\left(atan\frac{60}{100}\right)$$

$$F_{rr} = \mathbf{16824{,}01\ N}$$

$$F_{hc} = m \cdot g \cdot \sin(\alpha)$$

$$F_{hc} = 8000 \cdot 9{,}81 \cdot \sin\left(atan\frac{60}{100}\right)$$

$$F_{hc} = \mathbf{40377{,}63\ N}$$

$$T_{wheels} = F_R \cdot R_{dyn}$$

$$T_{wheels} = (16824{,}01 + 26{,}52 + 40377{,}63) \cdot 0{,}578 = \mathbf{33077{,}87\ N \cdot m}$$

$$T_{1\ wheel} = \frac{T_{total\ wheels}}{N^{o}_{wheels\ in\ contact}} = \frac{33077{,}87}{4} = \mathbf{8269{,}47\ N \cdot m}$$

As can be observed from the calculation results, the total theoretical torque that the system should be capable of delivering to the wheels in order to overcome the conditions defined in Case 1 is 33.077 kN·m.

- ***Case 2***

Table 17 presents the data used for the calculation of this case.

DATA	
Mass (kg)	8000
Gravity (m/s2)	9,81
Rdyn (mm)	578
Slope α (%)	30
μR	0,25
ρair (kg/m3)	1,204
Af (m2)	4,83
Cs	0,95
Cx	0,6
Velocity (m/s)	11

Table 17. Case 2 – Torque Calculation Data

$$F_R = F_{rr} + F_d + F_{hc}$$

$$F_{rr} = \mu_R \cdot m \cdot g \cdot \cos(\alpha)$$

$$F_{rr} = 0{,}25 \cdot 8000 \cdot 9{,}81 \cdot \cos\left(atan\frac{30}{100}\right)$$

$$F_{rr} = \mathbf{18792{,}55\ N}$$

$$F_d = \frac{1}{2} \cdot v^2 \cdot \rho_{air} \cdot C_X \cdot A_f$$

$$F_d = \frac{1}{2} \cdot 11^2 \cdot 1{,}204 \cdot 0{,}6 \cdot (4{,}83 \cdot 0{,}95)$$

$$F_d = \mathbf{189{,}99\ N}$$

$$F_{hc} = m \cdot g \cdot \sin(\alpha)$$

$$F_{hc} = 8000 \cdot 9{,}81 \cdot \sin\left(atan\frac{30}{100}\right)$$

$$F_{hc} = \mathbf{22551{,}06\ N}$$

$$T_{wheels} = F_R \cdot R_{dyn}$$

$$T_{wheels} = (18792{,}55 + 189{,}99 + 22551{,}06) \cdot 0{,}578 = \mathbf{24006{,}42\ N \cdot m}$$

$$T_{1\ wheel} = \frac{T_{total\ wheels}}{N^{o}_{wheels\ in\ contact}} = \frac{24006{,}42}{4} = \mathbf{6001{,}61\ N \cdot m\ N}$$

As the results clearly show, while the aerodynamic drag force and rolling resistance increase when this condition takes place, the hill climbing force due to the huge vehicle mass is far greater than the other forces. But when reducing the slope angle, this component is very small and there is no need to torque wheels. As described at the start of Section 5.3, we carry out a sensitivity analysis to evaluate the effect of vehicle speed and drag coefficient in the resistive force related to aerodynamic drag. The graph of Figure 60 shows on the one hand the variation in aerodynamic force as a function of vehicle speed while keeping drag coefficient at the same value (Cx). Additionally, the graph in Figure 61 shows how the drag coefficient (Cx) changes independently of an aerodynamic force.

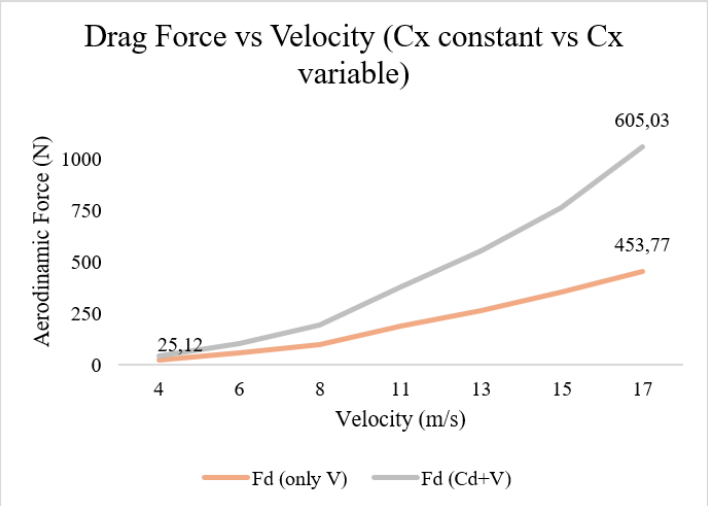

Fig. 61. Drag Force as a Function of Vehicle Speed

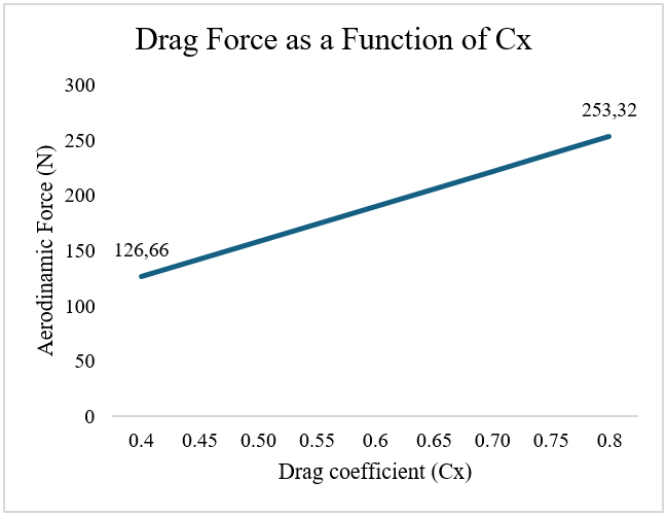

Fig. 60. Drag Force vs. Drag Coefficient (Cx)

Vehicle speed has a much greater effect than the drag coefficient, which supports the aerodynamic force formulation. However, with the drag coefficient varying from 0.4 to 0.8, the resistive force nearly doubles. When the vehicle speed is increased from 4 to 17 m/s, the aerodynamic force rises by a factor of about 17.

The force generated when both the vehicle speed and the drag coefficient are increased simultaneously can be up to 35 times greater than the lowest values of both variables. This suggests that at low vehicle speeds, the aerodynamic force is practically negligible compared to other resistive forces. However, at higher speeds, reducing the drag coefficient (Cx) becomes increasingly important, especially for electric vehicles. Hence, its optimization may represent an interesting line of investigation for future aerodynamic studies.

- ***Case 3***

DATA	
Mass (kg)	8000
Gravity (m/s2)	9,81
Rdyn (mm)	578
Slope α (%)	60
μR	0,25
ρair (kg/m3)	1,204
Af (m2)	4,83
Cs	0,9
Cx	0,6
Velocity (m/s)	11
Acceleration (m/s^2)	1,2

Table 18. Case 3 – Torque Calculation Data

$$F_R = F_{rr} + F_i + F_{hc}$$

$$F_{rr} = \mu_R \cdot m \cdot g \cdot \cos(\alpha)$$

$$F_{rr} = 0{,}25 \cdot 8000 \cdot 9{,}81 \cdot \cos\left(atan\frac{60}{100}\right)$$

$$F_{rr} = \mathbf{16824{,}01\ N}$$

$$F_i = m \cdot a$$

$$F_i = 8000 \cdot 1{,}2$$

$$F_d = \mathbf{9600\ N}$$

$$F_{hc} = m \cdot g \cdot \sin(\alpha)$$

$$F_{hc} = 8000 \cdot 9{,}81 \cdot \sin\left(atan\frac{60}{100}\right)$$

$$F_{hc} = \mathbf{40377{,}63\ N}$$

$$T_{wheels} = F_R \cdot R_{dyn}$$

$$T_{wheels} = (16824{,}01 + 9600 + 40377{,}63) \cdot 0{,}578 = \mathbf{38611{,}35\ N \cdot m}$$

$$T_{1\ wheel} = \frac{T_{total\ wheels}}{N^{o}_{wheels\ in\ contact}} = \frac{38611{,}35}{4} = \mathbf{9652{,}84\ N \cdot m}$$

As seen, this is indeed the most demanding torque requirement that has been examined so far as starting from the bottom of a slope with such extreme nature with a heavy vehicle demands a very high torque output.

We use the plotted graph in Figure 62; the rolling resistance force parameter F_{rr} is different from surface like asphalt and dry sand when the rolling resistance coefficient is changed.

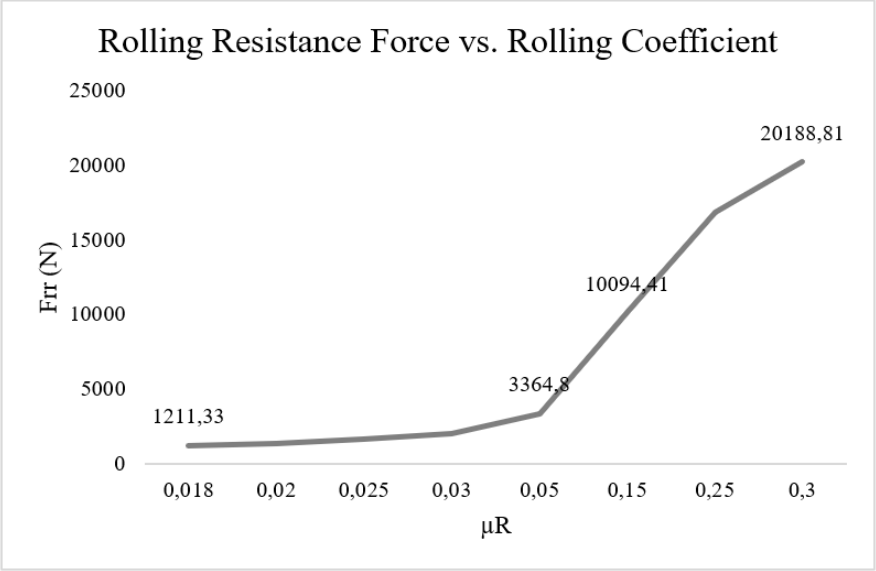

Fig. 62. Variation of rolling resistance force with µR

As you can see from the curve, the roll resistance coefficient contributes heavily to this resistive force. It is also important to note that under low traction surfaces, the total resistance to motion is affected, whereas with all engine with engine and car, the vehicle would become the one in the vehicle to overcome this type of environment as well as other reasons are likely.

To give an example, even driving 60% slope on dry sand theoretically without enough torque is unrealistic. It demonstrates a huge weakness in purely analytical models and shows the need to account for traction limits, tire-terrain interaction, and practical operation limits in order to understand what the result means.

- ***Case 4***

DATA	
Mass (kg)	8000
Gravity (m/s2)	9,81
Rdyn (mm)	578
Slope α (%)	30
µR	0,25
ρair (kg/m3)	1,204
Af (m2)	4,83
Cs	0,9
Cx	0,6
Velocity (m/s)	11
Acceleration (m/s^2)	1,2

Table 19. Case 4 – Torque Calculation Data

$$F_R = F_{rr} + F_i + F_{hc}$$

$$F_{rr} = \mu_R \cdot m \cdot g \cdot \cos(\alpha)$$

$$F_{rr} = 0{,}25 \cdot 8000 \cdot 9{,}81 \cdot \cos\left(atan\frac{30}{100}\right)$$

$$F_{rr} = \mathbf{18792{,}55\ N}$$

$$F_{hc} = m \cdot g \cdot \sin(\alpha)$$

$$F_{hc} = 8000 \cdot 9{,}81 \cdot \sin\left(atan\frac{60}{100}\right)$$

$$F_{hc} = \mathbf{40377{,}63\ N}$$

$$F_i = m \cdot a$$

$$F_i = 8000 \cdot 1{,}2$$

$$F_d = \mathbf{9600\ N}$$

$$T_{wheels} = F_R \cdot R_{dyn}$$

$$T_{wheels} = (16824{,}01 + 9600 + 40377{,}63) \cdot 0{,}578 = \mathbf{29445{,}51\ N \cdot m}$$

$$T_{1\ wheel} = \frac{T_{total\ wheels}}{N^{o}_{wheels\ in\ contact}} = \frac{29445{,}51}{2} = \mathbf{14722{,}70\ N \cdot m}$$

As observed in the results, this represents the most demanding case, even though it does not involve the maximum slope gradient. The reduction in the number of wheels capable of delivering torque has a drastic impact on the required torque per wheel.
As stated above, this is a highly demanding situation and not the most common situation to find the overall torque required. Yet it is still of particular relevance in terms of performance and transmission design since it demonstrates very high values of the operating limits to which these systems can probably be forced to operate.

5.2.5 Conclusion

Table 20 summarizes the required torque results for each of the study cases developed previously.

Study Case	*Total Tractive Torque (N·m)*	*Wheel Torque Required (N·m)*
Case 1	33077,87	8269,47
Case 2	24006,42	6001,61
Case 3	38611,35	9652,84
Case 4	29445,51	14722,7

Table 20. Torque studies results

Based on the results, Case 4 is the most demanding case for torque requirement. That said, as we covered earlier in this article, this is not an actual operating scenario and hence is not the main reference for the sizing of a motor. Following this, Case 3 imposes the most demanding torque in the calculation, which is around 9,652 N·m per wheel.
This example is a 60% obstacle scenario against muddy ground: an extreme operating and operation scenario rather than most of the time real world conditions. Of note, in mud, adhesion of terrain serves as the main limiting factor, in spite of some vehicles to the same performance specifications stating that they can reach such curves.

In reality, a slope equivalent to this isn't likely to get up on low-adhesion ground, whatever the motor torque has available. Using the same 60% incline on a high-adhesion field, e.g. dry asphalt, the required torque becomes approximately 6,000 N·m per wheel. Moreover, on account of the slightly better pavement and 15% slope, we consider the required driver's torque per wheel to be approximately 2,000 N·m, assuming the approach speed used in Case 1, which is more representative of realistic operating conditions. Our results illustrate the immense change of the torque of wheel for different ground conditions and with slope and terrain, from about 2,000 N·m (moderate) up to 7,000–9,000 N·m (extreme). In terms of present in-wheel motor designs, it is available to the public the mean torque peak levels often range between 1,500 and 2,500 N·m per wheel.
In connection with present in-wheel motor designs, it is available to the public the mean torque peak levels often range between 1,500 and 2,500 N·m per wheel. For instance, the Protean PD18 is reported to provide peak torque level of approximately 1,500 N·m [61], in contrast, the peak torque is reported to be about 2,500 N·m under short-duration using the Protean PM18 model [61].

If one compares the commercially available torque characteristics to the theoretical criteria for the described in this work, we can see that for moderate operation conditions with good adhesion and moderate slopes, the torque requirements are probably within ranges usable by current in-wheel motors. However, for severe off-road scenarios that involve steep gradients and low-adhesion terrain, the required torque levels could greatly exceed the capabilities of the current hub motor prototypes. The gap pointed to an important shortcoming of the pure direct-drive in-wheel architectures as they target the most extreme performance requirements.

5.3 Numerical Simulations

This section contains the numerical simulation to experiment the proposed wheel structure. Structural, fluid and thermal evaluations are conducted to investigate aspects like mechanical integrity, heat dissipation and flow behavior, against the traditional wheel idea and the IWM setup.

5.3.1 Rim Structural Simulation

5.3.1.1 Objective

As explained in Section 5.1, the CAD design of the rim has been developed based on catalog dimensions of the selected wheel. Although the main dimensions are realistic, the detailed design and geometry are custom. For this reason, as in any design and development phase—even at a conceptual level it is necessary to carry out a structural analysis under maximum load conditions to evaluate whether the model can withstand the loads applied by the vehicle.

For this purpose, a structural analysis of the rim is performed, and the results are evaluated to determine whether the proposed design is capable of supporting the applied loads and could therefore be considered valid for use.

5.3.1.2 Model setup

This section describes the module used, the geometry, the simplifications applied (if any) and the materials considered

First, it should be noted that the analysis is carried out using the Static Structural module in ANSYS. First, it should be noted that the analysis is carried out using the Static Structural module in ANSYS. This module allows analyzing stress and deformations under non-transient mechanical conditions. It is the sort of analysis that is relatively simple, but gives pretty direct information on if the design can take the load of the heavy vehicle.

Fig. 63. Static Structural analysis geometry

Figure 63 shows the geometry employed in the analysis. No geometric simplifications are made as this is not an extremely demanding job of the structural behavior study in this case. The purpose of this study is to compare the rim with its original design to find it as realistic as possible.

To proceed with it, ASTM A572 Grade 50 steel is used as a material in the ground. It is a strong steel which mainly needs to be used in rims for heavy vehicles. Some of its general properties are:

- Young's Modulus = 200 Gpa
- Density = 7,8 g cm^3
- Poisson's Ratio = 0,39
- Coeff of termal expansión = $1{,}2 \cdot 10^{-5}\ K^{-1}$

On the other hand, since the goal is to evaluate whether the material can withstand the applied loads, it is important to determine the safety factor. This could be calculated manually using the material limits and its mechanical properties. However, ANSYS allows this to be obtained directly within the simulation.

To do this, additional material data needs to be defined. In this case, since the analysis is only performed on the rim, this specific definition is not required for the other materials used in the remaining models.

It is necessary to define the Weibull S–N fatigue strength curve. For this purpose, two theoretical values obtained from experimental data are used as a reference [62].

The values extracted from the study are:

$$S_1 = 220{,}10\ MPa\ \ en\ N_1 = 10^3$$

$$S_2 = 131{,}72\ MPa\ \ en\ N_2 = 10^6$$

The equation used to calculate the stress values as a function of the number of cycles N is given in Equation 13, shown below:

$$S = a \cdot N^{b} \qquad \text{Eq. 13}$$

Using the initial data from the study, the factors *a* and *b* can be calculated.

We start by calculating the slope *b* using:

$$b = \frac{\log\left(\frac{S_2}{S_1}\right)}{\log\left(\frac{N_2}{N_1}\right)}$$

We substitute the values:

$$b = \frac{\log\left(\frac{131,72}{220,10}\right)}{\log\left(\frac{10^6}{10^3}\right)}$$

$$b = \frac{-0,22}{3} = \text{-0,0743}$$

Now, to determine the values of the constant a, we use the values from the study:

Given S= 220,10 y N=10^3

$$220,10 = a \cdot (10^3)^{-0,0743}$$

We rearrange the equation:

$$a = \frac{220,10}{0,599} = 367,5$$

Therefore, the final equation is:

$$S = 367,5 \cdot N^{-0,0743}$$

With this equation, we can substitute any value of cycles NNN to obtain the corresponding stress values S. These values are then used in ANSYS to define the S–N curve, shown in Figure 65.

Figure 64 presents the strain-life parameters, which are also required for the software to calculate the safety factor based on the simulation results.

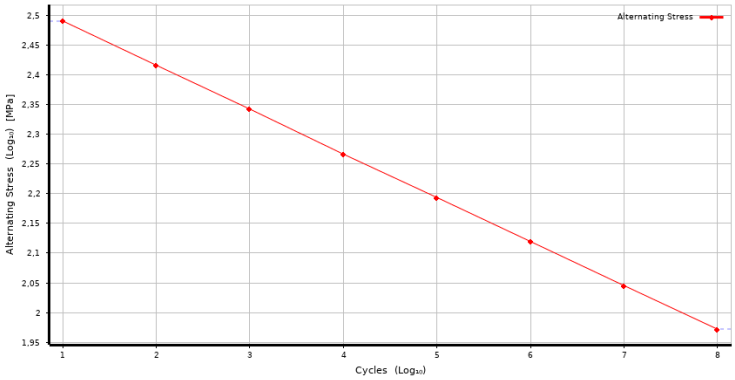

Fig. 65. S-N ASTM A572 Grade 50 curve

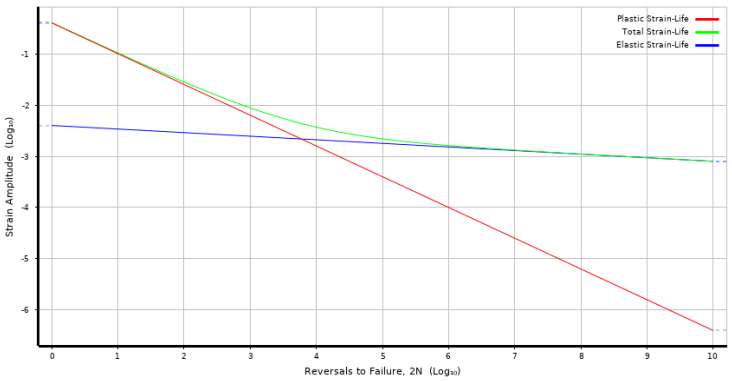

Fig. 64. Strain-Life ASTM A572 Grade 50 curve

This additional calculation and value are only required for the rim material in this study. It is included to show that, even though this is an academic and conceptual project, an effort has been made to keep the analysis as accurate as possible in order to obtain reliable results.

5.3.1.3 Boundary conditions

Our boundary conditions or applied loads are defined in the setup. In this case the estimated vehicle mass is around 8000 kg which is about 2000 kg per wheel but because the batteries are usually located at the rear of the vehicle we will assume that the rear wheel will have a larger load that is 2100 kg.

Based on this value the vertical load on the rim is 20,601 N, as shown in Figure 67. Also the tire pressure has to be considered. The value of this was derived according to the catalog above where, depending upon the type of terrain, the tire pressure is 8.6 bar.

Therefore, this is the pressure at the rim-tire contact area (Figure 66).

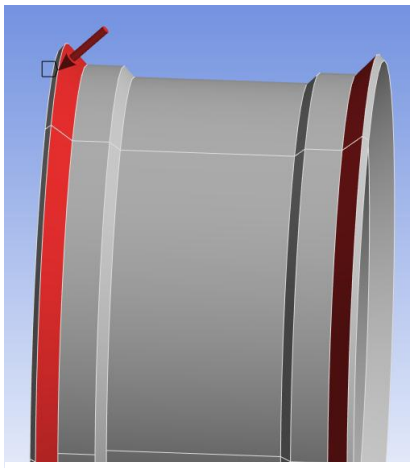

Fig. 66. Pressure applied in the Static Structural simulation

Fig. 67. “Vertical load applied during the Static Structural simulation

These are the loads acting on the rim and represent the most severe conditions considered to evaluate whether the designed model can withstand them.

5.3.1.4 Numerical Results

After the boundary conditions and loadings were specified, we performed the simulation to investigate how the rim responds structurally. The total deformation of the rim in the presence of the applied load can be presented in Figure 68. The greatest deformation is around 0.045 mm that is considered negligible given the general geometry. The post-processing stage visually intensifies the deformation for the sake of clarity, enhancing the deformation pattern.

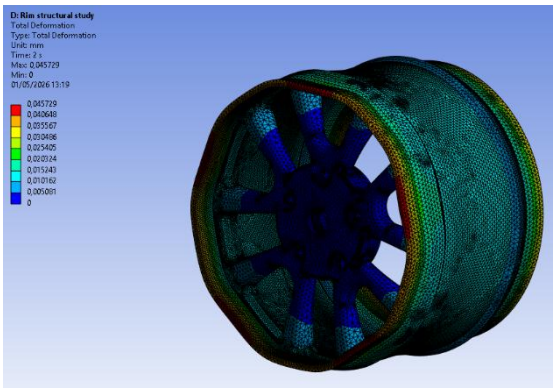

Fig. 68. Static Structural – Rim Deformation Result

The von Mises stress distributions (Figure 69) are employed to see its beginning of yielding in the material. The material elastically responds when the von Mises stress is lower than the material yield strength, otherwise it will undergo plastic deformation.

The maximum stress (approx. 36 MPa) produced in this case is much smaller than the material yield strength. That is, the rim has only elastic behaviour under the specific loading. This result is further supported by the safety factor distribution shown in Figure 70, from which we get at least 2.57. However, we should be very careful regarding values around 2 in structural analysis such that a value between that of 2 and 4 should be accepted as conservative and would be ideal, and very well suited to structural applications [63].

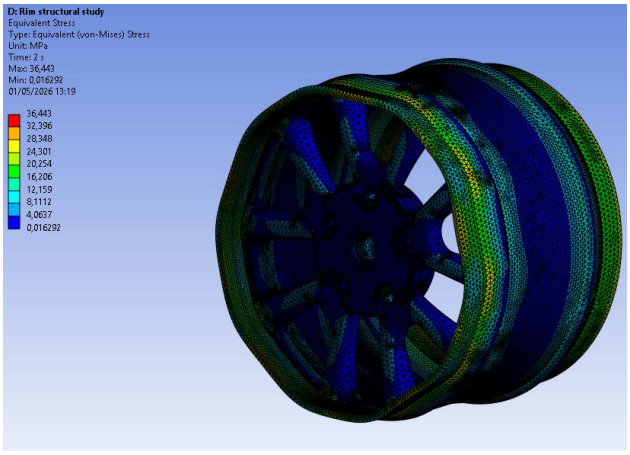

Fig. 69. Equivalent Stress – Static Structural Analysis

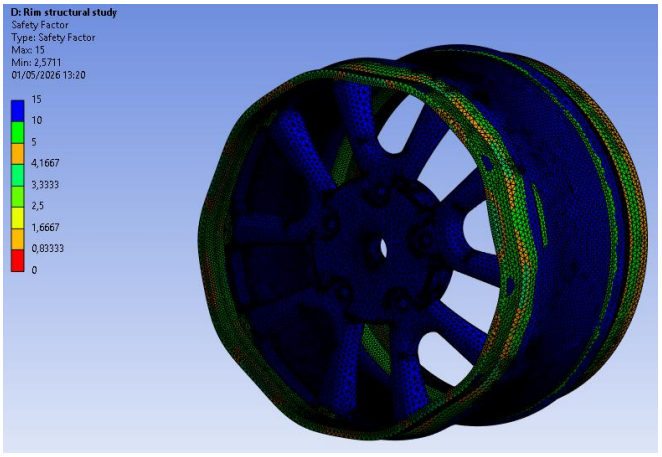

Fig. 70. "Safety Factor – Static Structural Analysis

According to the above-known characteristics, it can then be said that the rim design has been proved to be structurally sufficient for the assumed loading conditions. Although a theoretical model, the model exhibits enough mechanical strength and is able to sustain the anticipated loads for the intended prototype. After this initial validation, the rim model for use in the following analyses of the above study is considered acceptable.

5.3.2 Airflow Analysis (CFD)

5.3.2.1 Objective

The goal of this study is to observe the airflow behaviour in and around the wheel assembly in a qualitative way and identify the distinction between the traditional wheel-end arrangement and the in-wheel motor (IWM) system.

This study aims to perform an airflow assessment of the extent of its penetration in inner portions of the wheel with a view to determine its effect on convective cooling. Findings are employed for defining the boundary conditions which are adopted in the following thermal analysis.

5.3.2.2 Model Setup

The airflow dynamics around the wheel assemblies for both conventional and IWM configurations were quantified using ANSYS Fluent to create a basic CFD model. The ANSYS Fluent model is represented in the workspace of the Project Schematic and it is the two different studies for the IWM configuration and the conventional system that take place. The geometries of the IWM and the conventional model are presented in Figures 73 and 72 for this study. It is worth mentioning that although the geometries are simplified: holes are fewer, internal components have been removed (in the case of IWM) and the caliper removed in the conventional system. These simplifications were taken to reduce the complexity of models and make for a more

manageable mesh which would reduce computation time. Even with these simplified models simulation times remain quite high, around 10–12 hours.

A three-dimensional flow domain was defined around the wheel assembly to simulate the airflow conditions during vehicle motion. The domain size was selected to minimize boundary effects while maintaining a manageable computational cost.

As shown in Figure 74, the flow domain is the rectangular region where the analysis is carried out, representing, for example, the test section of a wind tunnel. The 3D wheel model is integrated into this flow domain, creating a single solid body. As it interacts with the model in later simulation steps, this setup helps analyse the flow behaviour.

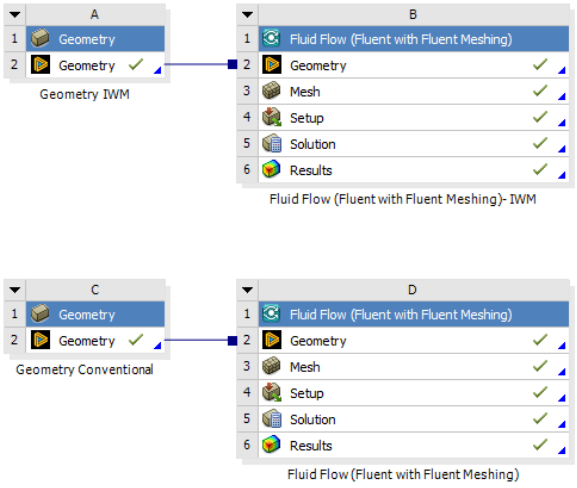

Fig. 71. CFD Analysis Workflow in ANSYS Workbench

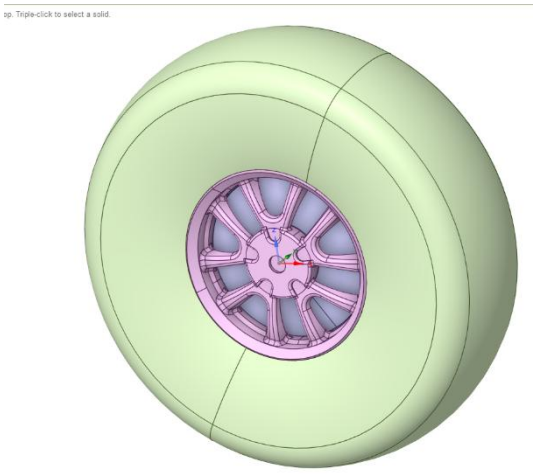

Fig. 73. Simplified IWM geometry for CFD analysis

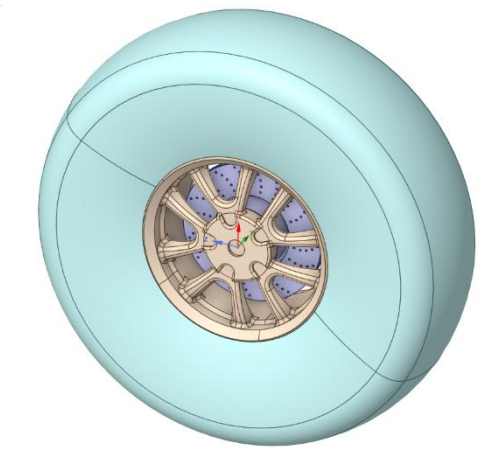

Fig. 72. Simplified conventional geometry for CFD analysis

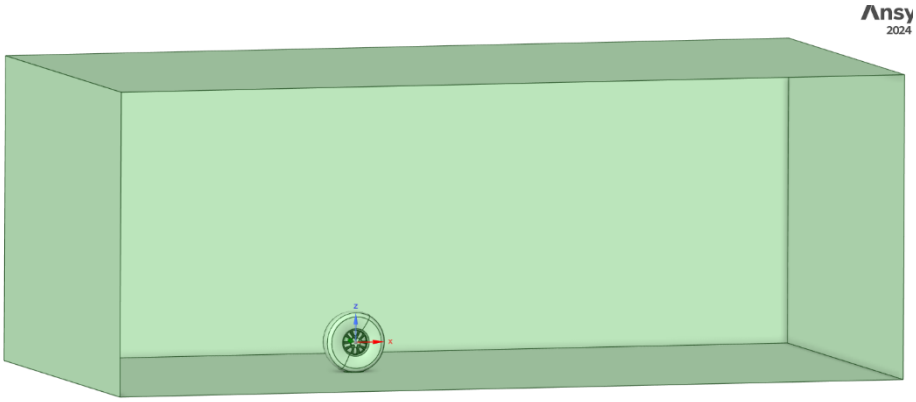

Fig. 74. Computational flow domain defined around the wheel assembly

Both configurations are modeled using the same flow domain dimensions and similar simplification criteria to ensure consistency when comparing the results.

In this chapter, as well as in the report in general, detailed simulation settings are not discussed in depth, as this information can be found in the corresponding appendices section.

5.3.2.3 Boundary Conditions

The boundary conditions are defined to describe a simplified vehicle motion in which the interaction between the airflow and the rotating wheel is modelled.

First, we formulate the surfaces of the domain to represent the various physical interactions between the airflow and the environment. Each boundary of the flow domain is assigned a specific physical condition, i.e. inlet flow, outlet flow, moving ground, and the interaction with solid surfaces.

The velocity inlet condition is utilized at the front face of the domain so that the relative airflow generated by the vehicle's motion can be simulated.

The pressure outlet condition is set at the rear of the domain, allowing the flow to exit the computational region.

A moving ground condition is used to simulate the relative motion between the vehicle and the road surface, producing more realistic flow behavior near the wheel.

The wheel is treated as a rotating surface, which ensures that the simulation will illustrate the influence of wheel rotation on the airflow.

These conditions are defined in figure 75; here the moving ground configuration is presented.

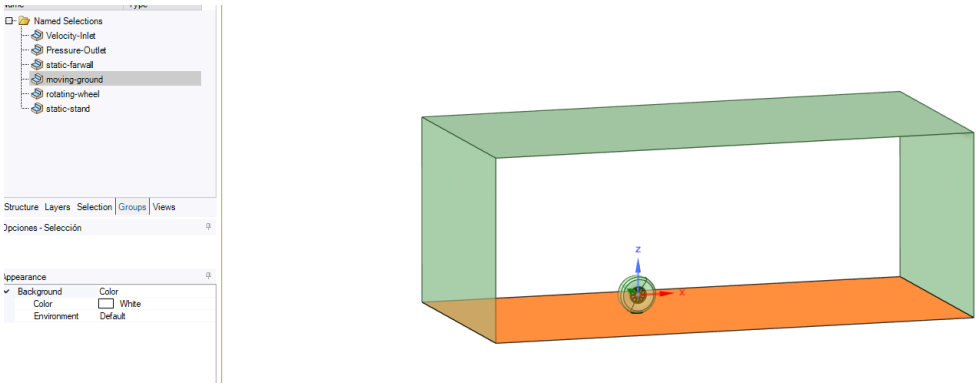

Fig. 75. Flow Domain CFD analysis

Finally, in the following steps, the mesh is generated for the entire flow domain, and the corresponding velocities are applied to each of the defined regions.

Figures 76 and 77 show the applied mesh and an example of the velocity defined for the rotating wheel, respectively.

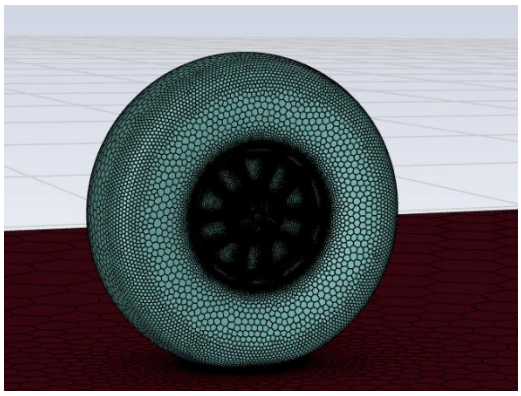

Fig. 76. IWM Mesh for CFD Analysis

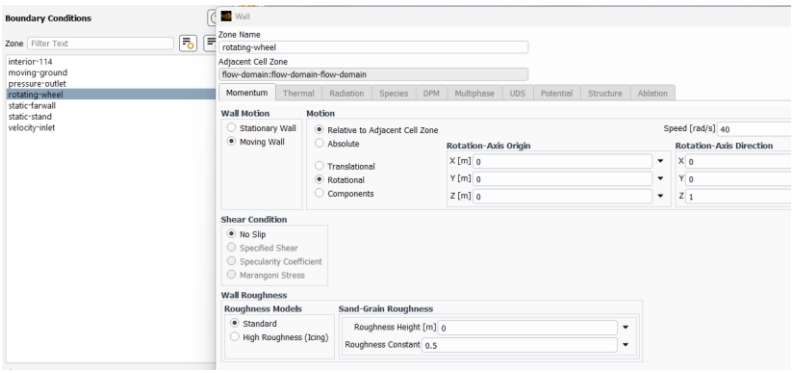

Fig. 77. Application of Velocity to the Rotating Wheel CFD Analysis

Once all the boundary conditions are defined and the mesh is generated, the simulation can be run. After the calculation is completed, the process moves to the results module.

As mentioned, these steps are carried out in exactly the same way for both models, without changing the setup. The only difference between them is the geometry used.

5.3.2.4 Results

Figure 78 shows the streamlines which serve to describe the velocity field response in this case of the IWM setup.

It demonstrates that the IWM design forms a more enclosed geometry and limits airflow to the inner dimensions of the assembly.

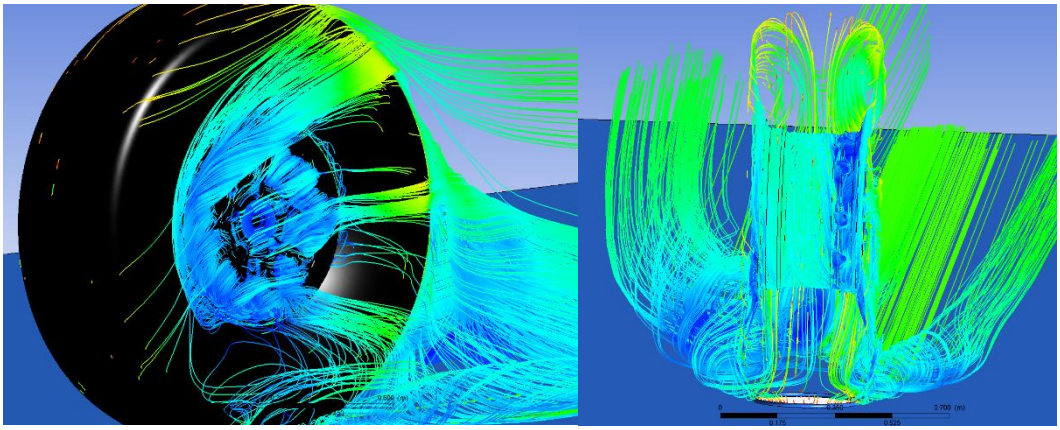

Fig. 78. Velocity streamlines in the CFD analysis of the IWM system

The flow is strictly restricted to the outside surfaces with almost no circulation in the inner space. Similarly, Figure 79 presents the equivalent outcome for the regular wheel. With the conventional wheel-end arrangement, air may pass through the inner parts of the wheel.

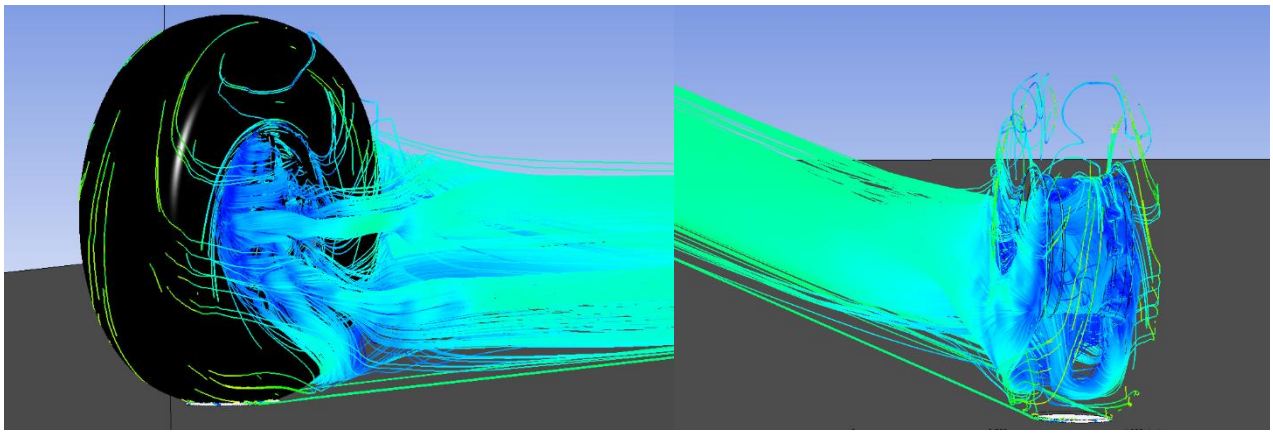

Fig. 79. Velocity streamlines in the CFD analysis of the conventional system

The open geometry opens up to air passage over the brake disc area, encouraging air penetration and the ability to provide ventilation and heat dissipation. The two configurations show one fundamentally different behaviour vis-à-vis airflow when compared side by side.

The conventional architecture allows air to pass through both significant dimensions and air through the most important areas, however, the IWM designs prevent an all-permeable internal flow within the construction which hampers heat dissipation by all-natural convection. This lower internal airflow suggests a smaller amount of convective cooling process taking place in the IWM layout. Therefore, the heat produced in the system fails to be removed as efficiently as it was when using the conventional set-up.

They support the characterization of the convective heat transfer condition which is applied during a later thermal analysis. It should be emphasised that our analysis is qualitative and based on reduced modelling assumptions. The results will allow for comparison rather than explicit quantitative predictions.

5.3.3 Thermal Simulations

5.3.3.1 Objective

Then, CFD is used to compare airflow of the IWM and conventional setups, then you take those results out and convert them into the final thermal simulation. The IWM has one of the biggest drawbacks of heat management; this step enables you to analyse it objectively. Because it is an enclosed design, keeping it cool is a major engineering challenge. This simulation directly compares heat dissipation in both systems under identical conditions, providing you with the data you need to assess if this technology actually works for your prototype.

5.3.3.2 Coupled Field Analysis

The main choice for this study is a Coupled-field analysis. This method runs a thermomechanical calculation that factors in the heat generated by physical contact. It is the best setup for simulating braking, where friction between the pads and the spinning disc creates thermal energy. Even though this model is computationally heavy, you use it because it is the most realistic way to see how both forces affect the system at the same time.

The simulation maps the frictional contact between the disc and the pads. It applies rotational speed to the system while pushing brake pressure onto the contact surfaces. You run this as a transient analysis to capture exactly how temperature and mechanical stress change over time.

Figure 80 shows the model setup, including the mesh, geometry, contacts, and loads. Unlike earlier attempts, you apply acceleration here instead of velocity. This change was made after testing to keep the solver from crashing. Applying both velocity and contact pressure in the same load step made it almost impossible for the simulation to converge. This tweak keeps solve times manageable, which were incredibly high in your first runs due to the complexity of the system.

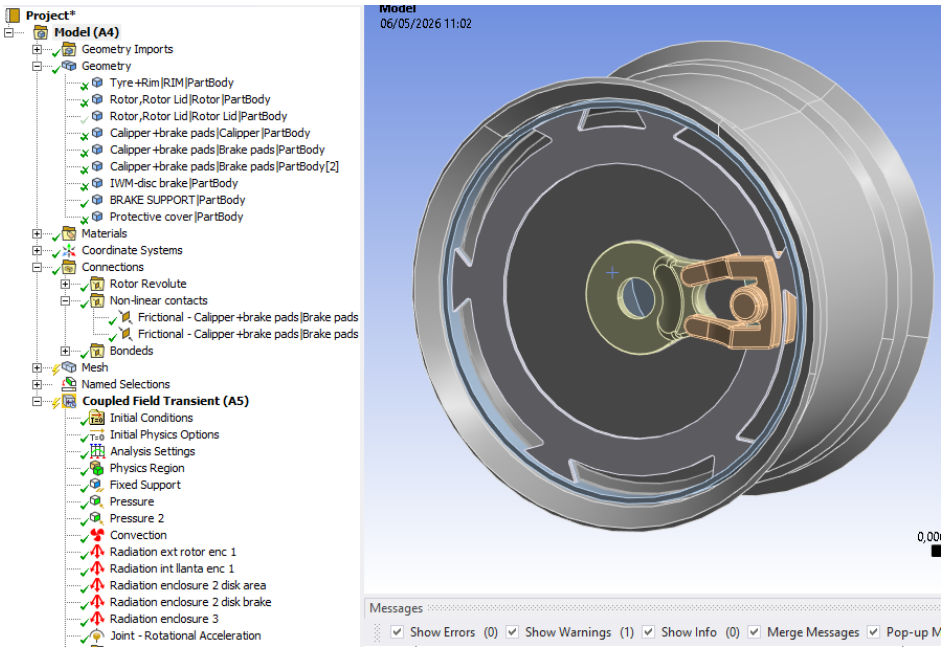

Fig. 80. Coupled thermo-mechanical setup for brake analysis

The image shows the conditions needed to simulate movement and friction realistically. To keep the model solvable, we must simplify the boundary conditions without losing accuracy. For example, you can swap velocity for acceleration. This setup lets you spin up the assembly without pressure, let it coast on inertia, and then apply the brake pressure. By doing this, you avoid running acceleration and pressure at the same time, which makes the simulation too complex.

This section is brief because, despite trying to simplify the setup, the solve times crashed my computer. Constant convergence errors and unstable contacts required a level of computing power I simply did not have.

After two weeks of testing and tweaking, it is clear that a coupled-field analysis is not feasible with my current setup. Because of this, the study shifts to a simplified thermal analysis, which is detailed in the next section. You can find the exact setup and boundary conditions in the appendices.

5.3.3.3 Thermal Analysis Strategy

Because of the technical issues with the coupled-field mode, you have to switch to a simplified thermal analysis. This approach cuts out the mechanical and friction calculations, which are the parts that drain your computing power the most. Instead, you simulate an equivalent heat effect to track the peak temperature, how it spreads, and how the system cools down.

To do this, you calculate the heat flux theoretically. This math mimics the physical setup by combining angular velocity, the friction coefficient, brake pad pressure, and the contact area. This gives you a close approximation of the heat generated by physical contact without needing a heavy coupled analysis.

Equations 14, 15, and 16 show how to calculate the heat generation rate (P). Specifically, Equation 14 defines this value using the friction force (F_f) and the linear sliding velocity (v).

$$P = F_f \cdot v \quad \text{Eq. 14}$$

Equation 15 calculates the linear velocity (v) using the angular velocity (W) and the brake pad radius (r).

$$v = w \cdot r \quad \text{Eq. 15}$$

Equation 16 then gives you the friction force (F_f) by multiplying the friction coefficient (μ) by the normal force of the caliper (F_n). To find this normal force, Equation 17 calculates the piston pressure based on the available contact area of the brake pad.

$$F_f = \mu \cdot F_n \quad \text{Eq. 16}$$

$$F_n = P \cdot A \quad \text{Eq. 17}$$

Below is the calculation for the IWM case. You would follow this exact same process for the conventional system, just swapping in its specific values.

The parameters for the IWM setup are:

- Contact Area (A) = 0,00298 m^2
- Friction Coefficient (μ) = 0,35
- Angular Velocity (W) = 40 rad/s
- Braking Pressure (P) = 8 Bar
- Mean Pad Radius = 0,185 m
-

First, you find the Friction Force (F_f) and the linear sliding velocity (v):

$$F_n = 8 \cdot 10^6\ Pa \cdot 0{,}00298\ m^2$$

$$F_n = 23840\ \text{N}$$

$$F_\text{f} = 0{,}35 \cdot 24000\ \text{N}$$

$$F_\text{f} = 8344\ \text{N}$$

$$v = 40 \frac{\text{rad}}{\text{s}} \cdot 0{,}185\ m$$

$$v = 7{,}4 \frac{\text{m}}{\text{s}}$$

With these, we can calculate the heat generation rate (P):

$$P = 8400\ \text{N} \cdot 7{,}4\ \text{m/s}$$

$$P = 61745{,}6\ \text{W}$$

This value is used to find the Heat Flux, which is the actual input you enter into Ansys to represent the heat generated by contact on the disc surface.

Because both the disc and the pads generate their own heat, you calculate the flux for each and add them together. Theoretically, the disc absorbs about 98% of the total heat due to its higher mass and volume. The individual heat generation rates for the disc and pads look like this:

$$P_{disc} = 0{,}98 \cdot\ 61745{,}6\ \text{W} = 60510{,}68\ \text{W}$$

$$P_{pad} = 0{,}02 \cdot\ 61745{,}6\ \text{W} = 1234{,}91\ \text{W}$$

Equation 18 defines the Heat Flux as the heat generation rate (P) divided by the contact area (A).

$$Q_{disc} = P_{disc/pad} \cdot\ A_{disc/pad} \qquad \text{Eq. 18}$$

By calculating each flux individually and summing them, you get the final value for the simulation.

$$\text{Q}_{\text{disc}} = \frac{60510{,}68}{0{,}0942}$$

$$\text{Q}_{\text{disc}} = 6{,}4236 \cdot 10^5\ W/m^2$$

$$\text{Q}_{\text{pad}} = \frac{1234{,}91}{0{,}00298}$$

$$\text{Q}_{\text{pad}} = 4{,}1439 \cdot 10^5\ W/m^2$$

$$\mathbf{Q_{Flux}} = \mathbf{1{,}0564 \cdot 10^6\ W/m^2}$$

This gives you the theoretical heat value that mechanical braking would generate at 8 Bar and 40 rad/s, based on the specific geometry of the parts. Essentially, this is the same value a coupled thermo-mechanical analysis would have calculated before moving on to the thermal behavior.

It is important to note that these are theoretical figures. Had the full simulation worked, the actual results might have varied. However, given the technical hurdles, this is the most accurate way to estimate the load. With this heat value ready, you can now run the first calibration in Steady-State mode to verify if the results look consistent.

5.3.3.4 Steady-State Thermal Analysis

As already mentioned, we just need to run a steady-state study and start doing the transient model first. This checks if the temperature distribution and the overall results also look reasonable instead of trying to build more complicated code. This validation step focuses only on the IWM model; if everything looks right, you then proceed with the transient analysis for both the conventional and IWM setups.

The first step is defining the materials and assigning them to the geometry. These settings stay the same for both the steady-state and transient studies. Figure 81 shows the list of the defined materials during the simulations.

The rim uses ASTM A572 Grade 50, while the IWM housing and rotor are made of AISI 4140 Alloy Steel. The brake discs and pads use specific materials detailed in the appendices field. For the other parts, the caliper is Aluminum 6061-T6, the protective cover is Phenolic, and both the brake support and bearing are AISI 4140.

Outline of Schematic A2, B2, C2, D2: Engineering Data

	A	B	C
1	Contents of Engineering Data		
2	Material		
3	AISI 1010 LOW CARBON STEEL		
4	Alloy steel AISI 4140		
5	Aluminum 6061-T6		
6	ASTM A572 Grade 50		
7	Disc Brake Material		
8	Pad Brake Material		
9	Phenolic		
10	Stainles steel 304		

Fig. 81. Material Definition for the Thermal Analysis

Once the materials are set, you can build the setup. Figure 82 shows the model structure and the geometry used. The most important thing here is the geometric simplification. To keep the computational cost low and get quick results, the rim, brake pads, caliper, and support have been left out. Also, the protective cover is modeled as a completely sealed unit to simulate airtightness. Since this is a general validation, a simplified model is enough to see if the loads and conditions work before applying them to the full transient study.

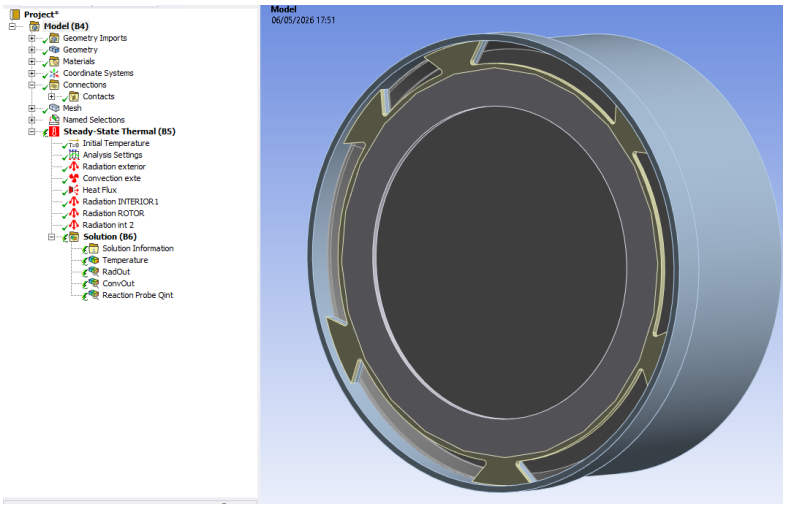

Fig. 82. Steady-State Analysis setup

Here there are connections far simpler than in the Coupled model. Since you can avoid any complex movement, just use the "bonded" contacts. This locks the parts together so they act as a single body with no sliding or gaps.

Figure 83 shows the mesh density used for the analysis. The mesh is noticeably finer around the brake disc, as this is the primary heat source and requires higher precision to capture the thermal gradients correctly.

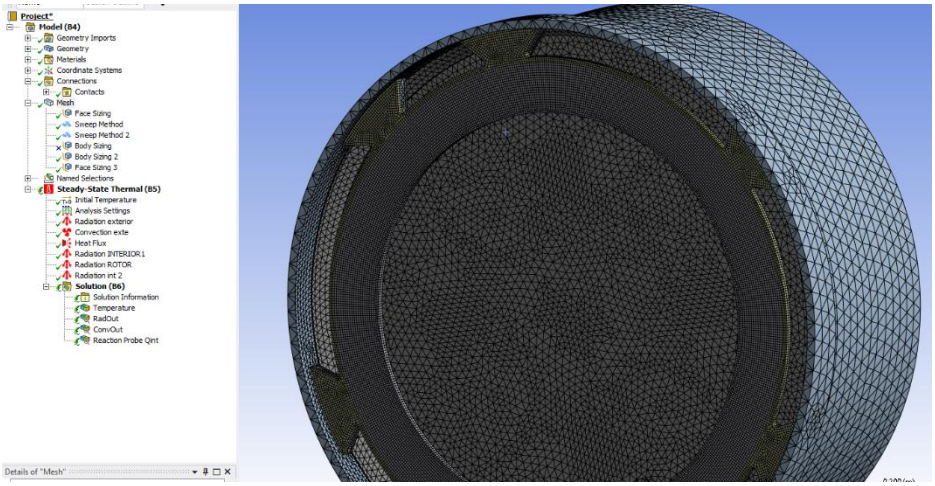

Fig. 83. Mesh for Steady-State Analysis

As shown in the figures, we applied radiation to both the outside of the rotor and the internal surfaces of the IWM. This mimics a real system where heat doesn't just move through physical contact but also radiates between parts. I used a general emissivity value of 0.65. While emissivity varies by material, we chose an average value based on "The Engineering Toolbox" [64] to keep the simulation manageable. Finally, we added external convection to the rotor housing at 17 W/m°C.

This is a very low value, but the CFD results justify it, as they showed minimal airflow hitting the outside of the rotor. In a conventional system, this number would obviously be much higher.

These radiation and convection settings are critical because they define the difference between the heat buildup in a closed IWM and an open conventional system. This is what tells Ansys how the two architectures actually behave. Lastly, Figure 68 shows how the heat flux is applied to the disc face, simulating the thermal energy generated during braking.

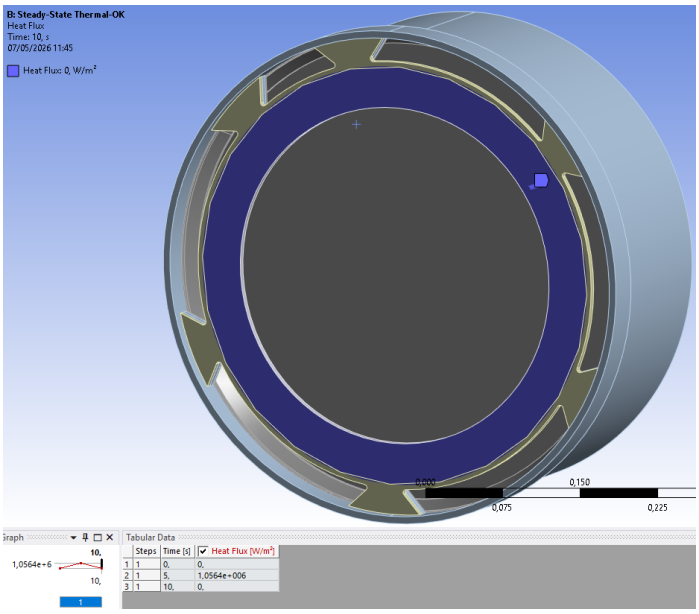

Fig. 84. Applied Heat Flux Steady-State Study

As shown in the figure 84, I applied the peak heat flux calculated in section 5.3.3.3 for 5 seconds. This simulates a continuous braking force and speed, generating a high thermal load for that duration. You can already tell the resulting temperatures will be high and somewhat unrealistic, as applying this much heat constantly doesn't happen in the real world. However, since this is a steady-state validation model, you can't vary the heat over time that happens later in the transient analysis, where the braking tests will be more realistic. For now, the goal is simply to verify that the temperature distribution is consistent and that the radiation settings work.

Once everything was set, we ran the solver. As this can be seen in Figure 85, these simulations are quite heavy and take a significant amount of time to complete.

Details of "Solution (B6)"

Adaptive Mesh Refinement	
Max Refinement Loops	1,
Refinement Depth	2,
Information	
Status	Solve Required
MAPDL Elapsed Time	14 h 35 m
MAPDL Memory Used	10,116 GB
MAPDL Result File Size	9,5281 GB
Post Processing	
Beam Section Results	No
On Demand Stress/Strain	No

Fig. 85. Steady-state solve simulation time

With simulations this long, you really can't afford many mistakes. Having to go back and tweak the setup means losing a lot of time, but that is simply the nature of FEM analysis. This is exactly why I ran the validation only on the IWM model first. Once the steady-state results are verified, I can move on to the final transient analysis. With the calculation complete, Figures 86 and 87 show the resulting temperature distribution.

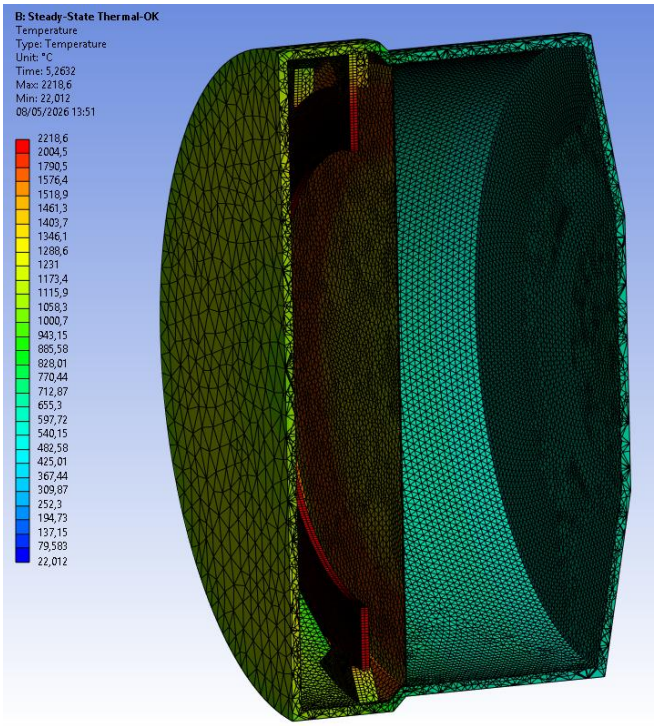

Fig. 86. Steady-State Thermal Analysis Result

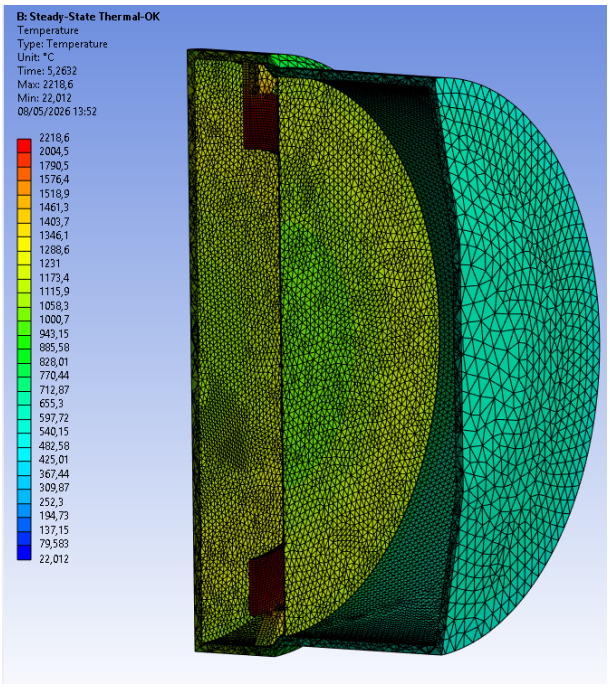

Fig. 87. Steady-State Thermal Analysis Result 2

As the figures show, the temperature values itself don't make sense exceeding 2000°C would obviously melt the materials. However, from a technical standpoint, the analysis achieved exactly what it was meant to.

Remember, we are applying a massive heat flux that simulates high-pressure braking on a rotating geometry. Because this load is applied constantly in a steady-state model, the temperatures

inevitably skyrocket. But since this was a validation study, the goal was to test if the radiation and enclosure settings were correct. The Ansys results confirm they are; you can see heat transferring through radiation to the protective cover, not just through physical contact. This proves the setup works, allowing us to move on to the transient analysis, where we can vary the heat over time to simulate realistic braking conditions.

5.3.3.5 Transient Thermal Analysis

Building on the steady-state validation, I moved to a transient thermal study to evaluate how the system behaves over time. Unlike the steady-state model, a transient analysis lets us simulate a realistic braking scenario by applying heat as a function of time.

For the IWM, I used the peak heat flux calculated in section 5.3.3.3. The conventional system follows the same calculation method, simply swapping in its specific parameters. Figures 88 and 89 show the setup structure used for this transient analysis.

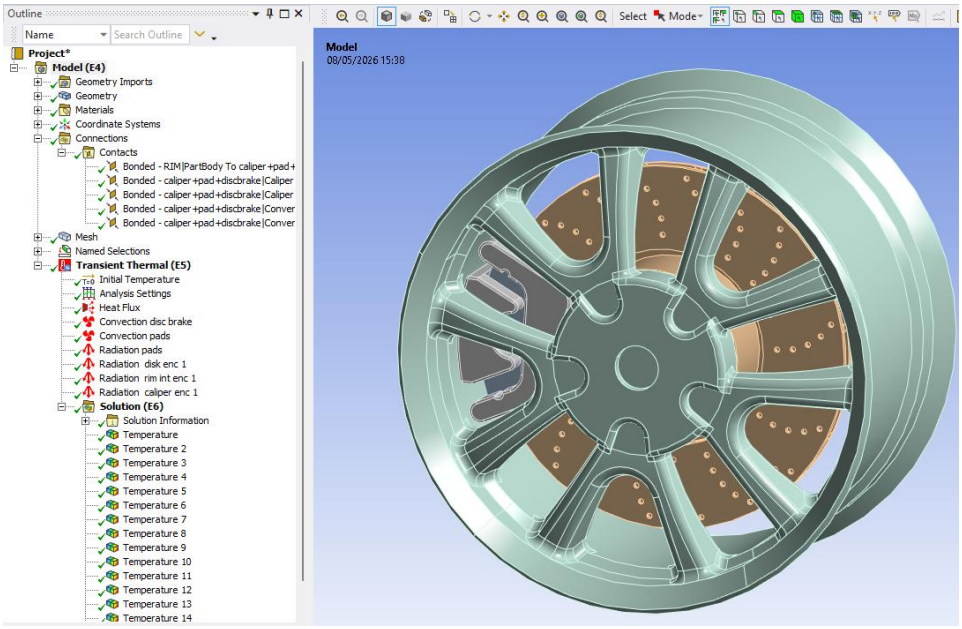

Fig. 88. Transient Thermal Analysis – Conventional Wheel Setup

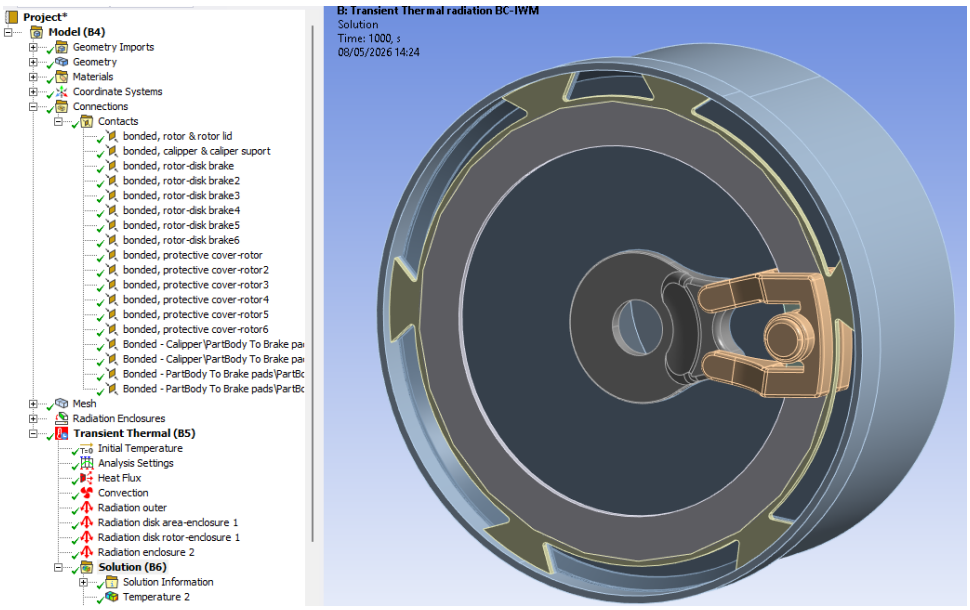

Fig. 89. Transient Thermal Analysis – IWM Setup

As the pictures showed, the main differences are the contacts. The IWM has many more parts and we need to know connections between them. The conventional system is much simpler and the only contacts required are the brake disc, rim, caliper, and pads.

It is worth noting that the conventional system has higher convection. Since more of its components are exposed to direct airflow, it dissipates heat more effectively. The most important feature of this transient simulation, however, is the ability to apply heat as a function of time.

To make this realistic, we simulated a standard automotive braking test. These tests, used for both official homologation and internal manufacturer trials, focus on heating the brakes repeatedly to check their efficiency under extreme thermal stress. The methodology starts with the vehicle at a steady speed; the brakes are applied until the speed drops to a specific point, then released to let the vehicle accelerate back to the starting speed. This cycle repeats several times. We have detailed the specific values for these simulation cycles in Figures 90 and 91 to make the process more visual.

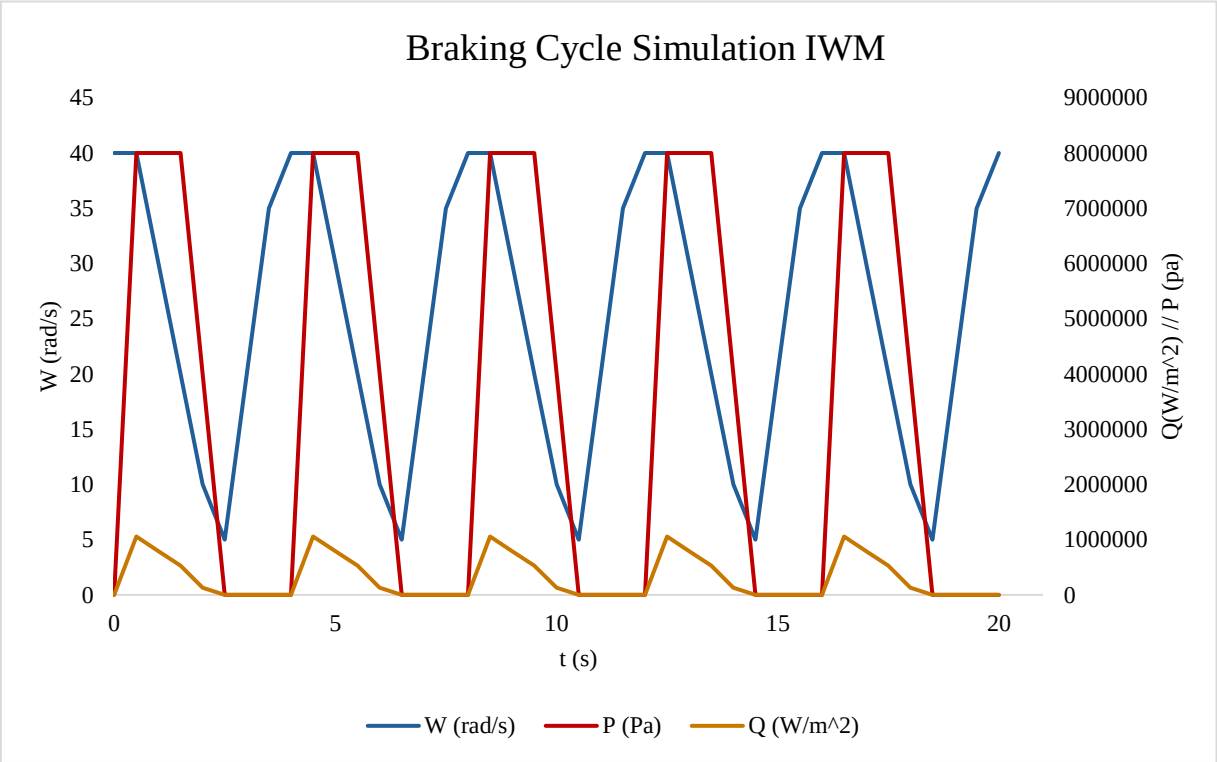

Fig. 91. Braking Cycle Simulation IWM

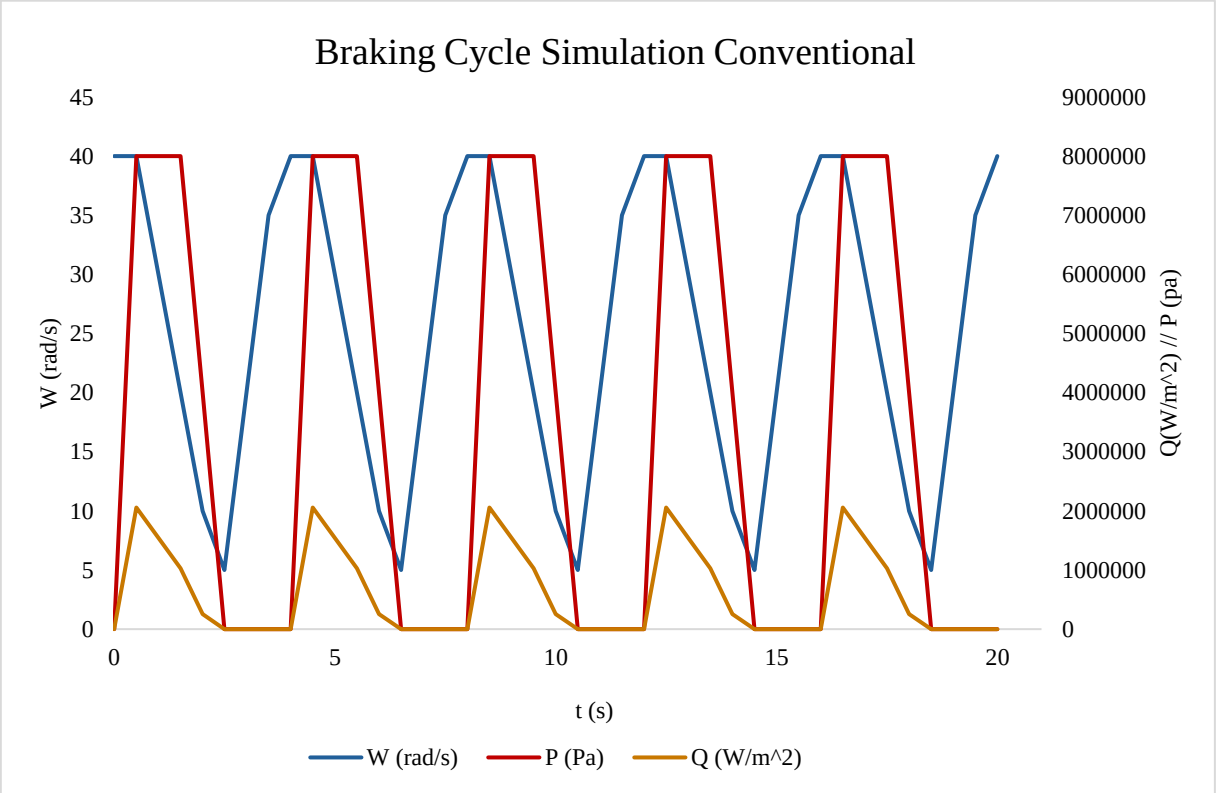

Fig. 90. Braking Cycle Simulation Conventional

The heat flux calculation for the IWM was detailed in section 5.3.3.3. The methodology for the conventional system is identical, using the following parameters:

- Contact Area (A) = 0,00723 m^2
- Friction Coefficient (μ) = 0,35
- Angular Velocity (W) = 40 rad/s
- Breaking Pressure (P) = 8 Bar
- Mean Pad Radius = 0,18414 m

As shown in the graphs, we simulated five identical braking cycles by adjusting pressure and rotational speed. When pressure is applied, the speed drops drastically, as indicated by the red and blue lines. Based on our theoretical calculations, heat generation depends on both speed and pressure, though pressure has a much larger impact. This explains why the heat spikes when the brakes are engaged and gradually tapers off as the speed decreases and friction drops.

These values were compiled into a table and imported into Ansys for the simulation. Although the conventional system generates higher total heat due to its larger contact surfaces, the real focus of this study is the cooling capacity.

Each simulation lasted 1,000 seconds. Heat was applied only during the first 18 seconds, as shown in the graphs, leaving the remaining time for the system to cool down. This allows us to compare and analyze how effectively each system dissipates heat. Once the contacts, mesh, loads, convection, and radiation were defined, both models were solved. The following sections analyze the results, starting with the visual data from Ansys and moving into a detailed comparison of cooling performance.

La Figure 92 displays the simulation duration for the conventional model. You can see that steady-state simulations take significantly more computing time than transient ones. This happens because the solver must find a global thermal equilibrium across the entire model in a steady state. This process demands more computational power when you involve multiple boundary conditions and heat transfer mechanisms.

In contrast, the transient analysis moves forward in time increments, which leads to more stable and efficient convergence. With these parameters set and the system solved, you can now examine the results.

Details of "Solution (E6)"

Adaptive Mesh Refinement	
Max Refinement Loops	1,
Refinement Depth	2,
Information	
Status	Done
MAPDL Elapsed Time	2 h 30 m
MAPDL Memory Used	21,214 GB
MAPDL Result File Size	10,74 GB
Post Processing	
Beam Section Results	No

Fig. 92. Transient Thermal Analysis Solution Time

Figures 93 and 94 show the initial moment when the system reaches its peak heat value for both models.

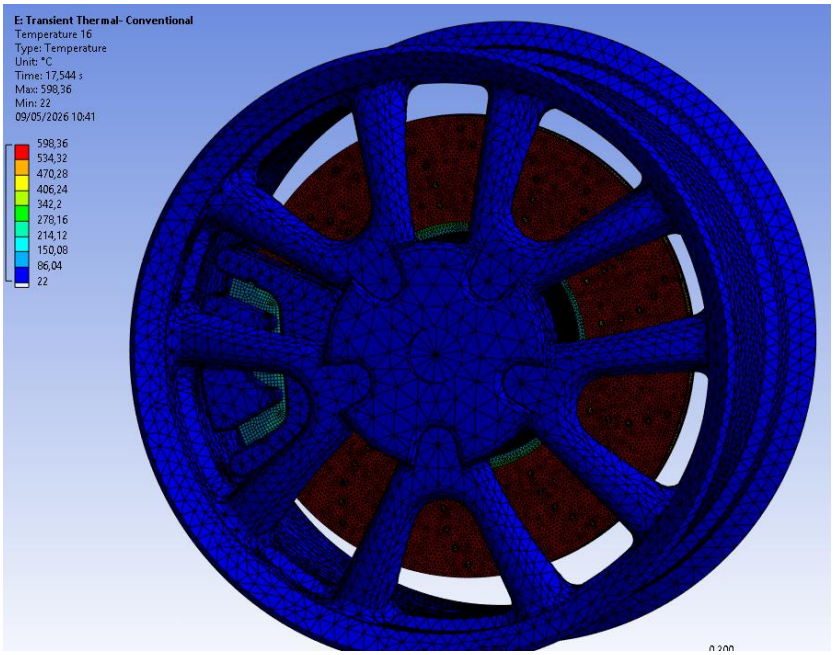

Fig. 93. Transient Thermal Analysis Conventional System Result

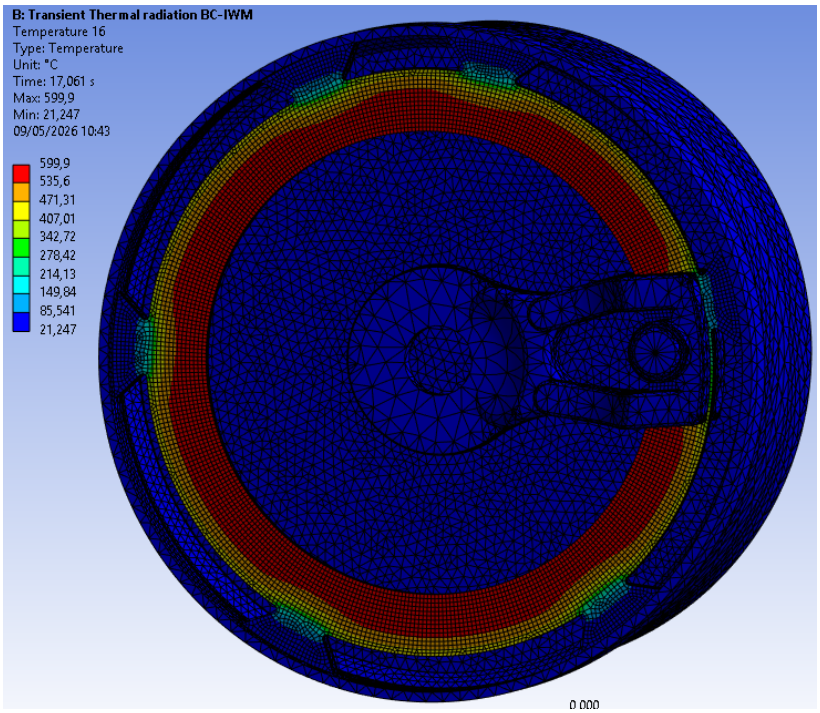

Fig. 94. Transient Thermal Analysis IWM Result

Those images are captured at the moment when both systems reach their highest temperatures. These temperatures are only temporary. This time it is the IWM and its peak value at 599.9°C whereas there is a high value for the more conventional one at 598.36°C.

Even then you might think they are almost the same, it is the difference in temperature which represents a large change. Note that the heat flux from the conventional system is nearly double what the IWM system can produce because of different brake discs and pads configuration.

Despite the conventional system generating twice as much heat during braking, it reaches the same maximum temperature as the IWM. This clearly demonstrates the superior cooling performance of the conventional design.

Figures 80 and 81 show the systems after 500 seconds. Here, you can see how the temperature evolves and spreads to other components through direct contact conduction and radiation.

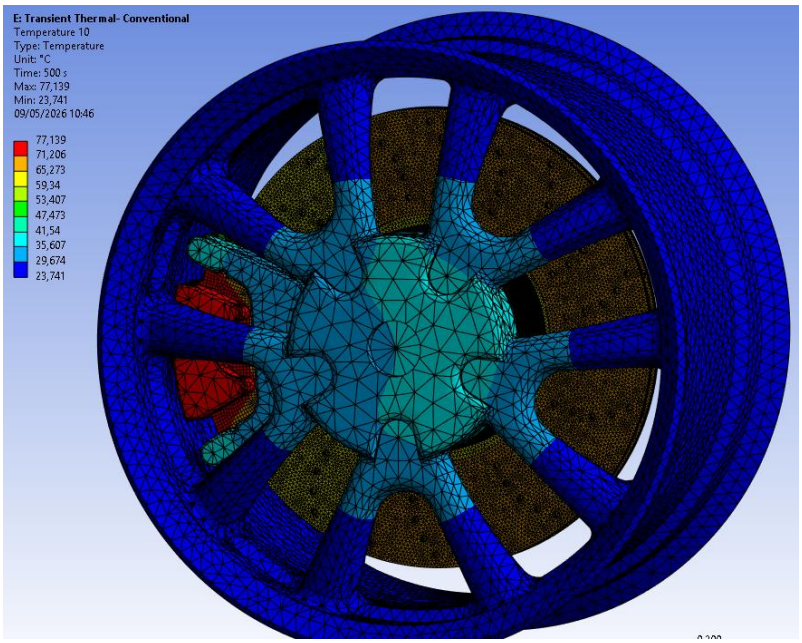

Fig. 95. Temperature Evolution after 500 s Transient Thermal Analysis (Conventional System)

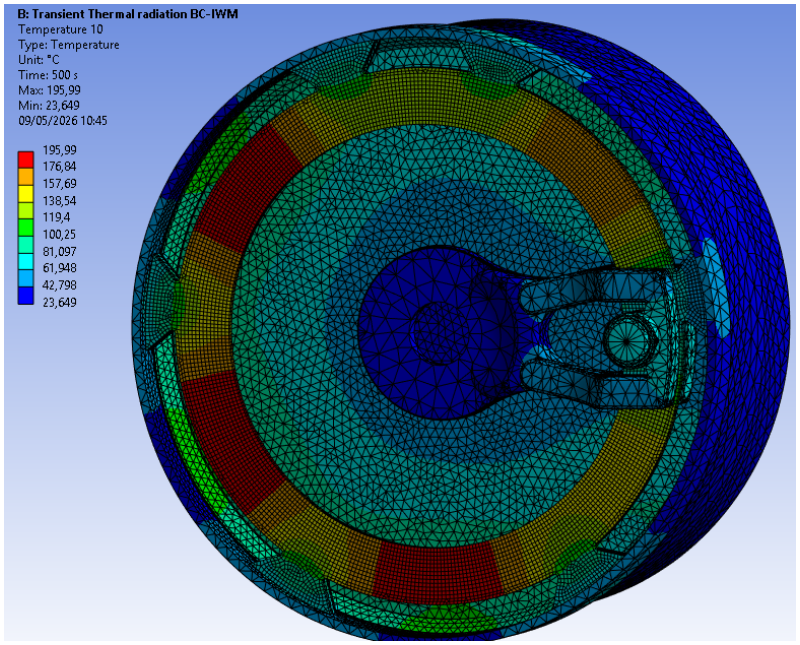

Fig. 96. Temperature Evolution after 500 s Transient Thermal Analysis (IWM System)

As can be seen, the braking simulation ends after 20 seconds. Beyond that point, no more heat is applied and the system is left to cool so we can analyze the temperature evolution. After 500 seconds, the maximum temperature of the IWM remains more than double that of the

conventional system. This result highlights the significant cooling problem of the IWM design in comparison to a standard one.

Figure 97 shows a visual representation of this data where all maximum temperature values are recorded over the entire simulation.

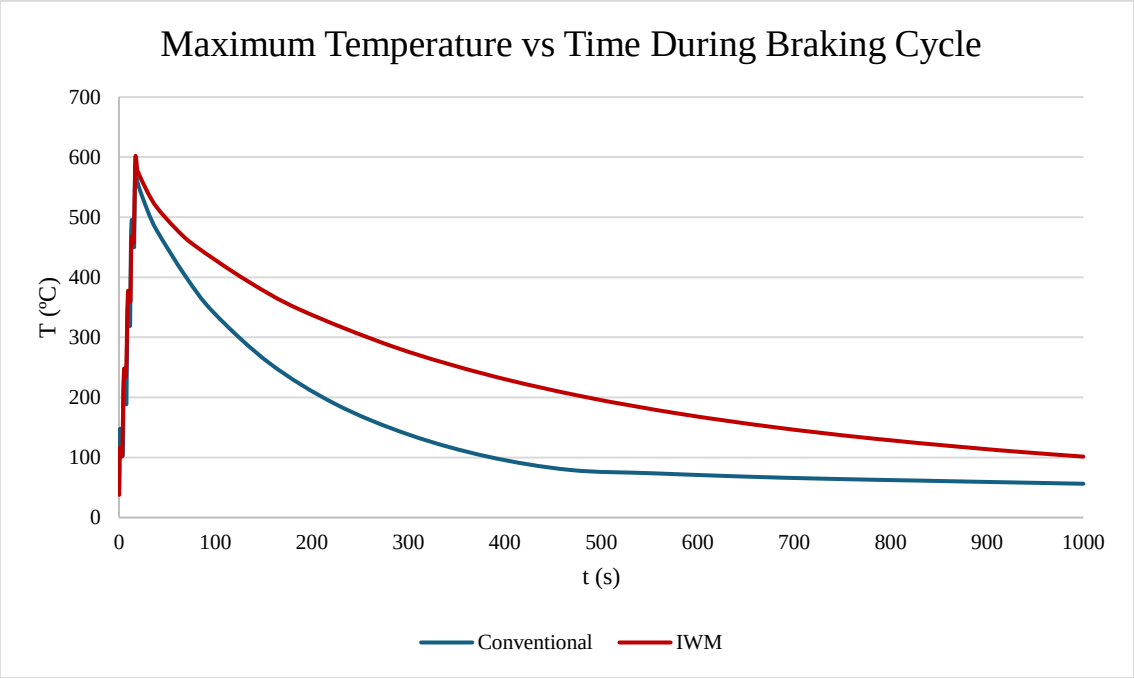

Fig. 97. Maximum temperature over time for conventional and IWM configurations

The temperatures in both configurations show that the temperature hits high by nearly the same time in the braking cycle. However, there is a huge difference in the cooling behaviour. In the same conditions, the existing system reduces the temperature to approximately 50°C, whereas in the case of IWM there is still about 100°C. This behavior confirms the low cooling ability of the IWM configuration that hence calls for a specialized system, but even with a more sophisticated one.

5.4 IWM Feasibility Assessment

Based on the various analyses throughout this chapter, we can now assess the actual feasibility of the In-Wheel Motor (IWM) concept.

From a packaging standpoint, the space inside the wheel is extremely tight. As shown in Section 5.1.4.2, we only have about 16–20 cm to work with. This is a "best-case" estimate that doesn't even account for power electronics or cooling hardware, which would crowd the volume even further. When you look at performance, the torque requirements for this vehicle are remarkably high. Meeting these demands with a direct-drive IWM is a massive hurdle, a reality also reflected in current industrial trends.

The CFD results gave us a clear look at airflow behavior, showing that the IWM naturally struggles with cooling compared to a conventional setup. The thermal analysis later confirmed this, with the IWM hitting much higher operating temperatures. When you combine these thermal issues with the packaging and torque constraints, it’s clear that implementing a full IWM system at this stage presents more challenges than practical benefits.

5.5 Discussion & Alternatives

Once the results from the studies used to assess the feasibility of the IWM have been obtained, it can be seen that, based on the available information and the results, it would not be the most suitable system for the intended prototype at this stage.

For this reason, two alternative configurations are analyzed below at a technical and theoretical level, which could better fit the requirements and be more viable for the prototype.

It should be clearly stated that these options are evaluated at a conceptual level, based on available data and public information. With them further developed, applied to the vehicle prototype after the basic structure of the vehicle is set out, it would still need more studies and analyses to refine them and characterize how they translate and work well.

5.5.1 Option 1 - In-Wheel Motor with Reduction

The first option after accepting that the IWM is not the most viable one has been realized is to keep the concept of an in-wheel motor but include a transmission or reduction system.

In this setting, the motor is still integrated within the wheel, but a mechanical reduction gearbox is introduced from both motor to wheel. This way the motor could drive faster at the wheel while also increasing the force applied to the wheel through a mechanical reduction stage between the two.

Such in-wheel motors with reduction gearboxes typically combine high-speed electric motors with internal gear systems, usually based on planetary gears. Such systems allow the motor to run at higher speeds, but reduce the output rotational speed to enable the wheel to get more torque [65].

For example, a motor operating at high rotational speeds can deliver significant torque at the wheel after the reduction stage, improving low-speed performance and traction.

Fig. 98. Schematic representation of a geared in-wheel motor with planetary reduction

The advantages of this configuration compared to the conventional IWM studied is that the electric motor needs less torque than it demands. That means that components are smaller and thus the motor can be made more efficient. With higher rotational speeds, that will make the motor more efficient.

Moreover, these systems offer higher torque at low speeds which is especially needed in vehicles with high traction or very high load capacity as is the case of the prototype we tried [66].

This particular IWM configuration will ensure also a simpler and lighter design, thanks to the gearbox to compensate for torque.

As any system it has drawbacks of course. The fact that we introduce a gearbox makes this system more complicated and adds mechanical components means it may need to have higher maintenance to minimize efficiency losses [66].

Moreover, having both motor and gearbox inside the wheel would increase the unsprung mass. Although in a heavy vehicle it is less important, it does impact vehicle dynamics and long-term durability [67].

In this configuration, the gearbox also generates more heat because of friction losses. Consequently, thermal management can be challenging, and this creates space and temperature limits also for the wheel's limited space.

As much of a consideration by our study is the torque limitations in direct-drive IWM. But the recent section results show that on top of the torque limitations there are also thermal management and packaging constraints.

The introduction of a gearbox does not solve these problems and may even make them worse with more complexity, heat generation, and space requirements in the wheel assembly.

Thus, for now, we cannot confirm this system can actually achieve for this purpose the high wheel torque requirement in Section 5.2. Not completely solving the limitations noted in the feasibility analysis of an in-wheel motor.

For this reason, a third propulsion system will be considered in the following section.

5.5.2 Option 2 – Quad Motor Distributed

Based on the limitations identified in the IWM concept and the previous analysis of geared IWMs, this section explores a more conventional electric propulsion architecture.

This alternative is based on distributed electric propulsion systems. Unlike the IWM concept, the motors are positioned outside the wheel assembly and connected to the wheels via short transmission shafts. This is the most widely used architecture in electric cars today, and is now the most popular one - the most reliable, robust and mature. The setup requires electric drive units that harness the motor and power systems and that are provided by a single-speed transmission. Rather than mount the motor inside of the wheel on the frame of an already existing vehicle, a motor is mounted and sent to the wheels using torque-carrying short driveshafts.

Electric motors produce impressive torque even at low speeds, so multi-speed gearboxes are unnecessary. Since these motors run at very high RPMs, you need a fixed reduction gear to tune the motor speed to the wheel, so the ratio is between 8:1 and 10:1 that would let you keep it moving around efficiently at both low and high speeds. Figure 99 shows the general layout of a standard electric drive unit [68].

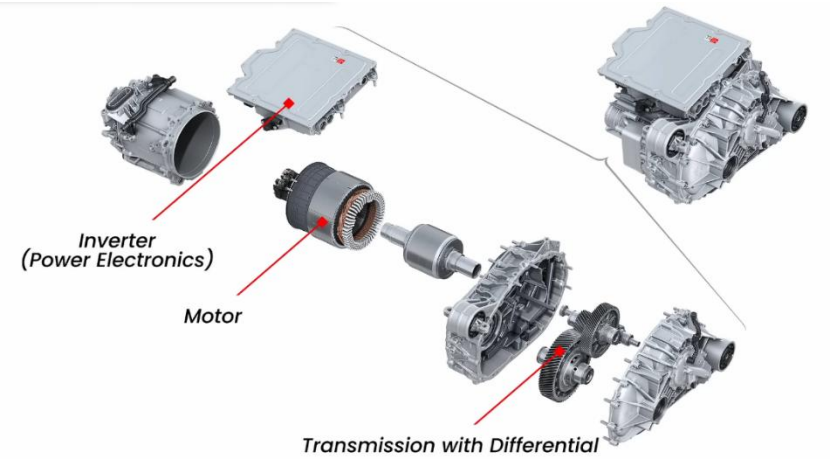

Fig. 99. Layout of a standard electric drive unit

Setting up a propulsion system for the vehicle will be determined with many configurations based on number and placement of motors. The vehicle control, performance and overall complexity will be affected by each configuration as well.

The simplest setup is to run in one motor that normally resides on the rear axle as shown in figure 100. Here torque is transmitted to both wheels via mechanical differential. This is a cheap and simple mechanical solution, however torque control is not used on each wheel.

Fig. 100. Single motor electric drivetrain configuration

The simplest setup is to run in one motor that normally resides on the rear axle as shown in figure 100. Here torque is transmitted to both wheels via mechanical differential. This is a cheap and simple mechanical solution, however torque control is not used on each wheel. The second solution is dual-motor setup: one motor per axle. With such a situation there is no need for a mechanical link between the front and back axles and it creates independence in torque distribution between them.

This setup greatly improves traction control as torque can be dynamically adjusted based on the grip available at each axle. Figure 101 provides this layout.

Fig. 101. Dual motor electric drivetrain configuration

The third and advanced setup employs three motors (one on the front axle and two on the back axle). For this configuration, front wheels are independently operated while the front axle remains on the standard differential.

This structure helps improve performance (and hence partial torque vectoring ability) on the axle with independent motors for each wheel. Figure 102 shows this setup.

Fig. 102. Three-motor electric drivetrain configuration

Finally, the most advanced configuration has one motor per wheel. The corresponding motor is connected to it by an independent reduction gear and driveshaft. The entire control is handed with torque vectoring for all the wheels. The vehicle's overall stability, traction, and dynamic performance increase dramatically.

Each motor is moving rapidly with high rotational speeds and is coupled with a reduction system (typically 9:1) to supply a much greater torque on the wheels. Figure 103 illustrates this four-motor configuration.

Of all the setups discussed so far, the four-motor system has the highest advantages for the intended vehicle. Independent torque control is particularly beneficial in off-road conditions and on variable terrain. Furthermore, this layout preserves the primary benefit of the IWM concept distributed propulsion while bypassing the limitations of housing the motor inside the wheel assembly.

Moving the motor out of the wheel fixes the heat issues you see in IWM setups. In an in-wheel design, the motor sits in a cramped space where heat builds up fast. By mounting it on the chassis instead, you get better airflow and much lower operating temperatures. You also separate the motor from the brakes. This stops heat from the brake discs from soaking into the motor, which is a major failure point for IWMs.

This layout gives you more room to work with. You no longer have to cram the motor, brakes, and electronics into the tiny volume inside the rim. Even with the motors moved, you still keep the ability to control torque at each wheel independently. This ensures your vehicle handles just as well as an IWM setup but without the packaging headaches.

Fig. 103. Four motor distributed electric drive configuration

Most of this layout is not good; there are a few obvious deficiencies of course. And adding gears and drive shafts introduces mechanical friction so that when using it you might suffer some efficiency on a direct-drive motor. You also need more parts. Many more parts lead to weight gain

and a more extensive assembly process and a longer maintenance list. Still, almost all engineers accept these losses. The improvement in reliability along with ease of installation of the system makes it worthwhile.

After the thermal, airflow analyses and study, it is established that the distributed electric drive architecture is more adequate in the proposed vehicle; hence the distributed electric drive is more suitable for the current vehicle. The constraints found for the IWM scheme such as limited airflow, high thermal loading and severe packaging limitation are much alleviated in this system. Accordingly, this configuration is a lower-risk and more practical alternative, that is consistent with industry solutions and gives a good prospect for a solid foundation for the development in the next evolution.

5.5.3 Final Recommendation

Our analysis shows that the IWM concept has major thermal and packaging limitations, making it impractical for the intended prototype.

Among the alternative layouts, using four electric motors is the best option. This setup lets you control each wheel independently while avoiding the integration issues that come with in-wheel designs. While it adds extra mechanical parts, it is a far more robust and practical solution that matches what the automotive industry actually uses today.

6. CONCLUSIONS

In this study, we have focussed on an early definition of the system-level architecture of an off-road electric vehicle and on whether it can be implemented in an IWM propulsion system.

To accomplish it, a benchmarking study was carried out to establish realistic parameters ranges and vehicle architecture constraints, comparing existing vehicles operating in similar conditions and with similar characteristics to our expected prototype. Based on these results, a conceptual CAD model was developed to represent conventional wheel system and IWM-based design. Furthermore, a conceptual chassis was developed based on the dimensions defined during the benchmarking process to feed into the developed wheel systems and get a first view of the proposed vehicle architecture.

In parallel, a theoretical torque calculation was performed to estimate the propulsion requirements under different operating conditions. Additionally, several simulations including CFD calculations and thermal analysis were performed to assess the behaviour of both systems.

The results show that the wheel space is extremely limited, and that integration of the electrical and electronic components of the IWM system is particularly difficult for such an advanced vehicle. The high torque requirement for an in-wheel was estimated to be 7000-8000 Nm, and this value is not achievable for the in-wheel car system given the available packaging configuration.

This CFD analysis has helped to understand the airflow on these two configurations with better definition of convection conditions for the thermal analysis ahead. The thermal profile confirms the clear disadvantages of the IWM system in heat dissipation with higher thermal loads on the conventional configuration. Meanwhile, the IWM configuration exhibits much higher operating temperatures, which does not lead to a cooling capability of the conventional configuration in comparison to the IWM system.

IWM would require a central, sophisticated thermal management system, and that would decrease the available space and make the system much more complex. Based on our findings, the implementation of the IWM system is not a solution for our proposed vehicle.

Therefore, different propulsion architectures were considered at a conceptual level. In particular, a distributed electric drive based on four independent motors was found to be a better solution: distributed propulsion leads to in-wheel system integration.

Overall, this work offers an architectural baseline for future development and a first engineering assessment that is important for future development.

7. REFERENCES

[1] Santander Research, “Europe’s automotive industry: Between transformation and competitive pressure Market situation and trends,” 2025. Accessed: Feb. 09, 2026. [Online]. Available: https://www.santander.com/content/dam/santander-com/es/contenido-paginas/sala-de-comunicacion/the-year-ahead-2025/what-challenges-is-europes-automotive.pdf

[2] “Automobile - Invention, Evolution, Impact | Britannica.” Accessed: Feb. 09, 2026. [Online]. Available: https://www.britannica.com/technology/automobile/History-of-the-automobile

[3] R. Mildner, T. Ziller, and F. Baiocchi, “Car IT Reloaded Disruption in the Car Industry.”

[4] “Automotive Industry 2025: Electrification, Software, and Supply Chain Transformation.” Accessed: Feb. 09, 2026. [Online]. Available: https://www.gminsights.com/blogs/top-challenges-in-the-automotive-industry-pre-COVID

[5] “Cars and vans - Climate Action - European Commission.” Accessed: Feb. 09, 2026. [Online]. Available: https://climate.ec.europa.eu/eu-action/transport-decarbonisation/road-transport/cars-and-vans_en

[6] “Chinese OEMs continue march of progress across Europe in 2025 | Market insight.” Accessed: Feb. 09, 2026. [Online]. Available: https://www.am-online.com/news/chinese-brands-surge-in-europe-as-tesla-loses-bev-lead

[7] “A New Era of Global Defense Spending: Key Trends and What’s Ahead - Defense Security Monitor.” Accessed: Feb. 10, 2026. [Online]. Available: https://dsm.forecastinternational.com/2025/06/13/a-new-era-of-global-defense-spending-key-trends-and-whats-ahead/

[8] J. D. Simulcik, F. E. Villalobos, and M. D. Bazilian, “Electrification of the joint force: Challenges and opportunities for competition in the Pacific and Arctic theaters,” *Electricity Journal*, vol. 38, no. 1, Feb. 2025, doi: 10.1016/j.tej.2025.107458.

[9] “Military Vehicle Electrification Market Size, Share [2026-2034].” Accessed: Feb. 10, 2026. [Online]. Available: https://www.fortunebusinessinsights.com/military-vehicle-electrification-market-115393

[10] “As Tactical EV Plans Take Shape, Army Charges Ahead Marines Stay Cautious.” Accessed: Feb. 10, 2026. [Online]. Available: https://www.nationaldefensemagazine.org/articles/2024/2/12/as-tactical-ev-plans-take-shape-army-charges-ahead-marines-stay-cautious

[11] “The Product Development Process: A Step-by-Step Guide.” Accessed: Feb. 11, 2026. [Online]. Available: https://productschool.com/blog/product-strategy/product-development-process

[12] K. T. . Ulrich and S. D. . Eppinger, *Product design and development*. McGraw-Hill/Irwin, 2012.

[13] T. Kolossváry, D. Feszty, and T. Dőry, "Systems engineering in automotive product development: A guide to initiate organisational transformation," *Journal of Open Innovation: Technology, Market, and Complexity*, vol. 9, no. 4, Dec. 2023, doi: 10.1016/j.joitmc.2023.100160.

[14] "Automotive Product Development: Stages, Case, and Consideration - Visure Solutions." Accessed: Feb. 11, 2026. [Online]. Available: https://visuresolutions.com/automotive/product-development-stages/

[15] R. Mildner, T. Ziller, and F. Baiocchi, "Car IT Reloaded Disruption in the Car Industry."

[16] M. Saravi, L. Newnes, and T. Mileham, "Optimising Performance and Cost at the Early Design Stages," *International Journal of Engineering and Technology Innovation*, vol. 3, no. 3, pp. 214–228, Jul. 2013, Accessed: Feb. 11, 2026. [Online]. Available: https://ojs.imeti.org/index.php/IJETI/article/view/111

[17] "Concept Development Guide: 9 Steps, Process & Examples (2026)." Accessed: Feb. 11, 2026. [Online]. Available: https://slickplan.com/blog/what-is-concept-development

[18] "de:hub Academy - Den Markt verstehen: Technology Push vs. Market Pull | Digital Hub Initiative - YouTube." Accessed: Feb. 12, 2026. [Online]. Available: https://www.youtube.com/watch?v=tr3iXw4aXQs

[19] "What is the difference between market-pull and technology-push innovation? / bromundlaw.com." Accessed: Feb. 12, 2026. [Online]. Available: https://bromundlaw.com/innovation/market-pull-vs-technology-push-innovation

[20] "What Is System Level Design." Accessed: Feb. 12, 2026. [Online]. Available: https://duitdesign.com/system-level-design-what-is-it.html

[21] S. Sieniutycz, "Systems design: Modeling, analysis, synthesis, and optimization," *Complexity and Complex Thermo-Economic Systems*, pp. 85–115, 2020, doi: 10.1016/b978-0-12-818594-0.00005-2.

[22] R. Abbott and R. A. Org, "Position paper for 1.1 Panel on Complex Systems Engineering Complex Systems + Systems Engineering = Complex Systems Engineering What do complex systems and systems engineering have in common?," 2006. [Online]. Available: http://www.econ.iastate.edu/tesfatsi/ace.htm,

[23] M. V Cilli and G. S. Parnell, "Systems Engineering Tradeoff Study Process Framework," 2014.

[24] K. Oizumi, A. Ito, and K. Aoyama, "Early stage model based system design under uncertainties," in *Proceedings of the Design Society: International Conference on Engineering Design*, Cambridge University Press, 2019, pp. 3621–3630. doi: 10.1017/dsi.2019.369.

[25] “A Comprehensive Guide to Product Architecture in 2026.” Accessed: Feb. 12, 2026. [Online]. Available: https://deeprojectmanager.com/product-architecture/

[26] “What is Product Architecture? | Definition & Overview.” Accessed: Feb. 12, 2026. [Online]. Available: https://www.productplan.com/glossary/product-architecture/

[27] Karl T. Urich, “The Role of Product Architecture in the Manufacturing Firm,” Cambridge, MA, WP #3483-92-MSA, 1992. Accessed: Feb. 13, 2026. [Online]. Available: https://dspace.mit.edu/bitstream/handle/1721.1/48938/roleofproductarc00ulri.pdf?sequence=1&isAllowed=y

[28] “Modular Vs Integral Design.” Accessed: Feb. 13, 2026. [Online]. Available: https://design-encyclopedia.com/?T=Modular%20Vs%20Integral%20Design

[29] “Build To Order | PDF | Outsourcing | Supply Chain.” Accessed: Feb. 13, 2026. [Online]. Available: https://es.scribd.com/document/843129171/Build-to-Order

[30] S. E. Rice *et al.*, “Product architecture strategies and effects matrices for early evaluation and selection of product architectures,” *Design Science*, vol. 10, Dec. 2024, doi: 10.1017/dsj.2024.18.

[31] S. K. Fixson, “Modularity and Commonality Research: Past Developments and Future Opportunities,” 2006.

[32] R. B. Stone, K. L. Wood, and R. H. Crawford, “A heuristic method for identifying modules for product architectures,” *Des. Stud.*, vol. 21, no. 1, pp. 5–31, Jan. 2000, doi: 10.1016/S0142-694X(99)00003-4.

[33] “ATP 4-02.13 CASUALTY EVACUATION,” 2021. [Online]. Available: https://www.armypubs.mil

[34] R. T. Jeppsson and K. Krigsvetenskapsakademien, “Kämpa för livet.”

[35] “ATP 4-02.13 CASUALTY EVACUATION,” 2021. [Online]. Available: https://www.armypubs.mil

[36] J. Y. Wong, P. Jayakumar, E. Toma, and J. Preston-Thomas, “A review of mobility metrics for next generation vehicle mobility models,” *J. Terramech.*, vol. 87, pp. 11–20, Feb. 2020, doi: 10.1016/j.jterra.2019.10.003.

[37] “Standards For The Mobility Requirements of Military Vehicles | PDF | Vehicles | Transport.” Accessed: Feb. 16, 2026. [Online]. Available: https://es.scribd.com/document/702266427/Standards-for-the-mobility-requirements-of-military-vehicles?utm_source=chatgpt.com

[38] “Giving U.S. Soldiers the Advantage of Silence | Article | The United States Army.” Accessed: Feb. 16, 2026. [Online]. Available: https://www.army.mil/article/275128/giving_u_s_soldiers_the_advantage_of_silence

[39] C. Hua *et al.*, “The Prediction Method and Application of Off-Road Mobility for Ground Vehicles: A Review,” Jan. 01, 2025, *Multidisciplinary Digital Publishing Institute (MDPI)*. doi: 10.3390/wevj16010047.

[40] C. Pizzinini, L. Langer, I. Froissart, A. Elsayed, and M. Lienkamp, “Vehicles for the Service Economy: Early-stage Vehicle Concept Designs for Vehicle-based Service,” in *Procedia CIRP*, Elsevier B.V., 2023, pp. 746–751. doi: 10.1016/j.procir.2023.01.016.

[41] “IN-WHEEL-MOTOR ELECTRIC VEHICLES AND THEIR ASSOCIATED DRIVETRAINS,” *INTERNATIONAL JOURNAL FOR TRAFFIC AND TRANSPORT ENGINEERING*, vol. 10, no. 4, Oct. 2020, doi: 10.7708/ijtte.2020.10(4).01.

[42] V. Popovici *et al.*, “A New Approach to In-Wheel Motor Solutions for Electric Vehicles,” *World Electric Vehicle Journal 2026, Vol. 17,* vol. 17, no. 2, Feb. 2026, doi: 10.3390/wevj17020087.

[43] K. Deepak, M. A. Frikha, Y. Benômar, M. El Baghdadi, and O. Hegazy, “In-Wheel Motor Drive Systems for Electric Vehicles: State of the Art, Challenges, and Future Trends,” Apr. 01, 2023, *MDPI*. doi: 10.3390/en16073121.

[44] A. El Mourabit and I. H. Baraka, “Recent Developments in Four-In-Wheel Electronic Differential Systems in Electrical Vehicles,” *Computer Sciences & Mathematics Forum 2025, Vol. 10,* vol. 10, no. 1, p. 17, Jul. 2025, doi: 10.3390/cmsf2025010017.

[45] K. Yan *et al.*, “A critical review of radial field in-wheel motors: technical progress and future trends,” *eTransportation*, vol. 22, p. 100353, Dec. 2024, doi: 10.1016/j.etran.2024.100353.

[46] “CAD (diseño asistido por ordenador) con CATIA V5| Dassault Systèmes.” Accessed: Mar. 31, 2026. [Online]. Available: https://www.3ds.com/es/products/catia/catia-v5

[47] “▷¿Qué es ANSYS? | Simulación de Ingeniería para un Diseño Preciso.” Accessed: Apr. 02, 2026. [Online]. Available: https://deingenierias.com/software/ansys-simulacion-de-ingenieria-para-un-diseno-preciso/

[48] “Static Structural.” Accessed: Apr. 29, 2026. [Online]. Available: https://ansyshelp.ansys.com/public/account/secured?returnurl=/Views/Secured/corp/v242/en/wb2_help/wb2h_structstaticAN.html

[49] “Coupled Field Transient.” Accessed: Apr. 02, 2026. [Online]. Available: https://ansyshelp.ansys.com/public/account/secured?returnurl=/Views/Secured/corp/v242/en/wb2_help/wb2h_cf_transient.html

[50] “Ansys Fluent | Fluid Simulation Software.” Accessed: Apr. 03, 2026. [Online]. Available: https://www.ansys.com/products/fluids/ansys-fluent?utm_source=chatgpt.com#tab1-2

[51] “EBC Brakes Racing – Brake Kit Wheel Fitment/Clearance Templates - EBC Brakes.” Accessed: Apr. 27, 2026. [Online]. Available: https://www.ebcbrakes.com/race-motorsport-articles/ebc-brakes-racing-brake-kit-wheel-fitment-clearance-templates/?utm_source=chatgpt.com

[52] “How to calculate rolling resistance – x-engineer.org.” Accessed: Feb. 21, 2026. [Online]. Available: https://x-engineer.org/rolling-resistance/?utm_source=chatgpt.com

[53] “Jeep Wrangler TJ Specifications 2005 - 2006 | Quadratec.” Accessed: Feb. 21, 2026. [Online]. Available: https://www.quadratec.com/c/reference/jeep-wrangler-tj-specifications-2005-2006?utm_source=chatgpt.com

[54] “All the specs on the new Land Rover Defender 2020 | Practical Motoring.” Accessed: Feb. 21, 2026. [Online]. Available: https://practicalmotoring.com.au/car-news/all-the-specs-on-the-new-land-rover-defender-2020/?utm_source=chatgpt.com

[55] “220217M-Hilux-Press-Pack”.

[56] “6.4 Fuerza de arrastre y velocidad límite - Física universitaria volumen 1 | OpenStax.” Accessed: Feb. 21, 2026. [Online]. Available: https://openstax.org/books/f%C3%ADsica-universitaria-volumen-1/pages/6-4-fuerza-de-arrastre-y-velocidad-limite

[57] C. Bayındırlı, Y. Erkan Akansu, and M. Sahir Salman, “Academic @ Paper The Determination of Aerodynamic Drag Coefficient of Truck and Trailer Model by Wind Tunnel Tests,” *Journal of Automotive Engineering and Technologies*, vol. 5, pp. 53–60, 2016, doi: 10.18245/ijaet.11754.

[58] “Air Drag Coefficients.” Accessed: Feb. 21, 2026. [Online]. Available: https://www.bgsoflex.com/airdragchart.html?utm_source=chatgpt.com

[59] “The Digital Sleuths Tracking Russia’s Weapons and War Crimes in Ukraine,” *Vice.com*, Mar. 2022, Accessed: Feb. 22, 2026. [Online]. Available: https://www.vice.com/en/article/ukraine-weapons-tracker-russian-arsenal-war-crimes/

[60] “Comunidad de Steam :: Guía :: ARMA REFORGER EVERY GROUND VEHICLE SPEED TESTED!” Accessed: Feb. 22, 2026. [Online]. Available: https://steamcommunity.com/sharedfiles/filedetails/?id=3602850591&utm_source=chatgpt.com

[61] “Protean-Pm18-HP-Datasheet-August_2025”.

[62] A. Molina, M. R. Piña-Monarrez, and J. M. Barraza-Contreras, “Weibull S-N Fatigue Strength Curve Analysis for A572 Gr. 50 Steel, Based on the True Stress—True Strain Approach,” *Applied Sciences 2020, Vol. 10,* vol. 10, no. 16, Aug. 2020, doi: 10.3390/APP10165725.

[63] “Safety Factor, Factor Of Safety, Margin Of Safety, Unity Check - What’s The Difference And Which Should You Use? - Fidelis Engineering Associates.” Accessed: May 01, 2026. [Online]. Available: https://www.fidelisfea.com/post/safety-factor-factor-of-safety-margin-of-safety-unity-check-whats-the-difference-and-which-should-you-use

[64] “Emissivity Coefficients of Common Materials: Data & Reference Guide.” Accessed: May 07, 2026. [Online]. Available: https://www.engineeringtoolbox.com/emissivity-coefficients-d_447.html

[65] “Geared Hub Motors vs Direct Drive Hub Motors | Himiway Bikes.” Accessed: May 02, 2026. [Online]. Available: https://himiwaybike.com/blogs/news/e-bike-geared-hub-motors-vs-direct-drive-hub-motors

[66] A. M. Fathabad, X. Li, J. Cheng, and Y.-J. Wu, “Data-Driven Optimization for E-Scooter System Design,” 2022, doi: 10.15760/TREC.274.

[67] “What is a Hub Motor & How Does It Work: Types, Pros & Cons-What is a Hub Motor & How Does It Work: Types, Pros & Cons.” Accessed: May 02, 2026. [Online]. Available: https://www.fukuta-motor.com.tw/en/news_i/K06/N2025071100002

[68] “Single vs Dual vs Tri vs Quad Motors | Electric vehicle Performance - YouTube.” Accessed: May 09, 2026. [Online]. Available: https://www.youtube.com/watch?v=65mp_wvGcog

[69] “Electric Vehicle Sales Review Q2 2025 Foresight to drive the industry,” 2025. [Online]. Available: www.pwc.com/structure

[70] “Drone Proliferation Dataset | CNAS.” Accessed: Feb. 10, 2026. [Online]. Available: https://www.cnas.org/publications/reports/drone-proliferation-dataset

[71] © Daniel and E. Whitney, “Definition of Product Architecture”.

[72] D. Cole, “SOT Mobility Classification: Strategic, Operational, Tactical”, doi: 10.1007/978-3-031-66968-2_10.

[73] “THE HX-MORE THAN A TRUCK.”

[74] “1 new message.” Accessed: Feb. 16, 2026. [Online]. Available: https://www.datainsightsmarket.com/reports/autonomous-military-vehicles-664158?tab=summary

[75] L. Jian, K. T. Chau, and J. Z. Jiang, “An integrated magnetic-geared permanentmagnet in-wheel motor drive for electric vehicles,” *2008 IEEE Vehicle Power and Propulsion Conference, VPPC 2008*, 2008, doi: 10.1109/VPPC.2008.4677512.

[76] “Continental and DeepDrive collaborate on braked in-wheel motor | Automotive Powertrain Technology International.” Accessed: Mar. 27, 2026. [Online]. Available: https://www.automotivepowertraintechnologyinternational.com/news/electric-motors/continental-and-deepdrive-collaborate-on-braked-in-wheel-motor.html

[77] “How to calculate aerodynamic drag force – x-engineer.org.” Accessed: Feb. 22, 2026. [Online]. Available: https://x-engineer.org/aerodynamic-drag/

DEPARTMENT OF MATERIAL AND INDUSTRIAL SCIENCE
CHALMERS UNIVERSITY OF TECHNOLOGY
Gothenburg, Sweden 2026
www.chalmers.se

CHALMERS
UNIVERSITY OF TECHNOLOGY